2015-05-05

Multi-Scale Remote Sensing Assessments of Forested Wetlands: Applications to the Everglades National Park

Emanuelle A. Feliciano
University of Miami, ema804@gmail.com

UNIVERSITY OF MIAMI

MULTI-SCALE REMOTE SENSING ASSESSMENTS OF FORESTED WETLANDS: APPLICATIONS TO THE EVERGLADES NATIONAL PARK

By

Emanuelle A. Feliciano

A DISSERTATION

Submitted to the Faculty
of the University of Miami
in partial fulfillment of the requirements for
the degree of Doctor of Philosophy

Coral Gables, Florida

May 2015

UNIVERSITY OF MIAMI

A dissertation submitted in partial fulfillment of
the requirements for the degree of
Doctor of Philosophy

MULTI-SCALE REMOTE SENSING ASSESSMENTS OF FORESTED WETLANDS: APPLICATIONS TO THE EVERGLADES NATIONAL PARK

Emanuelle A. Feliciano

Approved:

_____
Shimon Wdowinski, Ph.D.
Research Associate Professor of
Marine Geology and Geophysics

_____
Falk Amelung, Ph.D.
Professor of Marine Geology
and Geophysics

_____
Timothy H. Dixon, Ph.D.
Professor of Geophysics
University of South Florida

_____
M. Brian Blake, Ph.D.
Dean of the Graduate School

_____
Matthew D. Potts, Ph.D.
Assistant Professor of Environmental
Science Policy and Management
University of California Berkeley

FELICIANO, EMANUELLE A. (Ph.D., Marine Geology and Geophysics)
Multi-Scale Remote Sensing Assessments of Forested Wetlands: Applications to the Everglades National Park (May 2015)

Abstract of a dissertation at the University of Miami.

Dissertation supervised by Research Associate Professor Shimon Wdowinski.
No. of pages in text. (103)

Wetlands are regions that are covered permanently or seasonally with water and/or have saturated soils for long periods of time. They provide benefits to human society, including flow regulation, storm protection, aquifer recharge, sediment and nutrient retention, energy production, conservation of fauna and flora, recreation and tourism, and are a natural laboratory for research and education. Wetland ecosystems are under severe pressure due to anthropogenic activities and climate change. There is an urgent need to conserve, restore and monitor wetlands at all scales (local to global). Wetlands are difficult to monitor, due to their large area and limited accessibility. High-resolution remote sensing technology represents a useful tool to quantify forests structural parameters such as vegetation structure (canopy height) and above-ground biomass (AGB) from regional up to global scales and to establish a baseline for present and future ecosystem comparisons. Quantifying vegetation structure and AGB is important to establish a monitoring database. Recent advances in remote sensing present an enormous opportunity to characterize wetland vegetation cover and structure. Studies have successfully used optical satellite, data such as Landsat 7 Enhanced Thematic Mapper Plus (ETM+), to estimate and classify wetland vegetation cover. However, wetland forest characterization requires also the quantification of forest canopy height,

which cannot be obtained from optical remote sensing observations. A large-scale characterization of forested wetland vertical structure is possible using active remote sensing sensors from (1) air- or spaceborne LiDAR/Laser Scanning or (2) spaceborne Synthetic Aperture Radar (SAR) systems such as the Shuttle Radar Topography Mission (SRTM) and TerraSAR-X add-on for Digital Elevation Measurement (TanDEM-X). However, these techniques depend on plot-level AGB estimations for validation and calibration purposes. Emerging remote sensing techniques such as Terrestrial Laser/LiDAR Scanning (TLS) can be used in wetland environments for accurately estimating AGB at the tree- and plot-levels.

The Everglades National Park (ENP) wetland ecosystem presents a useful study area as it is largely protected from development. However, historical changes in its water flow have stressed the system. The ENP is home to a vast amount of unique endangered and native species (fauna and flora) that are being threatened by (1) deprivation of the freshwater inflow into the park and (2) the dominance of exotic and invasive species. The main objective of this study is to provide quantitative canopy height and AGB estimates for four wetland forest ecosystems: mangrove, rockland pine, bald cypress and tropical hardwood hammock, all located within the boundaries of the ENP. I produce canopy height and AGB maps using three techniques, TLS/LiDAR Scanning, Airborne Laser/LiDAR Scanning, and single-pass Polarimetric-Interferometric Synthetic Aperture Radar (Pol-InSAR) TanDEM-X data. Furthermore, I provide uncertainty estimations for the calculated parameters. I was able to successfully use TLS to estimate vegetation volume and AGB in addition to its related uncertainty. This dissertation provides the first TLS study ever reported in a wetland environment. Airborne LiDAR and TanDEM-X

data were successfully used to estimate canopy height in the mangrove forests with an R^2 = 0.85 and RMSE = 1.96 m. An important conclusion of this dissertation reveals that the integration of remote sensing techniques at multiple scales is fundamental and necessary for wetland forestry studies.

Acknowledgments

First and foremost I would like to thank my advisor Dr. Shimon Wdowinski for his invaluable support on professional and personal challenges throughout my doctoral studies. Dr. Matthew Potts provided important feedback from his forestry and ecology expertise, in addition of reviewing and providing comments on my doctoral manuscripts and dissertation. Dr. Falk Amelung and Dr. Timothy Dixon were an essential part of my studies, providing suggestions, feedback and guidance on the remote sensing aspect of my dissertation. I'm very thankful to Dr. Temilola Fatoyinbo, who gave me the opportunity to work in two NASA Goddard internships, which were vital for making progress and finishing my studies. Dr. Seung-Kuk Lee (NASA Goddard) was vital on the processing aspect of Pol-InSAR data and provided comments on my dissertation. I'm very grateful to UNAVCO, which provided equipment, personnel and support throughout all of my studies. Dr. David Phillips and Brendan Hodge, from UNAVCO, were essential in the completion of my ground-based LiDAR fieldwork. Dr. Roni Avissar was very helpful as he was the helicopter pilot of my Everglades aerial photography campaign.

I'm very thankful to the National Science Foundation (NSF) for providing funding for three years through the Graduate Research Fellowship Program under Grant No. DG1E-0951782. Additionally, I would to thank Dr. Fernando Miralles-Wihelm, who was the Principal Investigator of the NASA WaterSCAPES project No. NNX10AQ13A, which provided funding in the beginning of my doctoral studies and NASA internships. The Florida Coastal Everglades-Long Term Ecological Research (FCE-LTER: Grant No. DEB-1237517) provided boats for my Everglades research. I'm very grateful to the

National Center of Airborne Laser Mapping (NCALM) for providing Airborne LiDAR data and the Digital Globe Foundation (DGF) for providing World-View 2 satellite data.

Dr. David Lagomasino, which at the time was finishing his doctoral studies at Florida International University, was essential in the completion of the fieldwork logistics as he was in charge of driving the boat to the Everglades National Park. In addition, Dr. Lagomasino helped me in every aspect of the fieldwork. I'm very grateful to him as always said yes to everything and was always present when I needed him the most. Estefania Sandoval, Dr. Stephanie Long, Lillian Marrero, Camilo Arias, Jan Henrik, Marco Bagnardi, Yan Liang, and Christina Plattner also provided essential help in my Everglades fieldwork. I'm very thankful to Dr. Batuhan Osmanoglu, who more than a colleague, I consider him a friend, which helped me professionally and personally. Dr. Fernando Greene was essential on finishing my doctoral studies when I was having personal challenges. Additionally, he and his family provided professional and personal guidance. I would like to thank all of my friends in the Geodesy Lab (Anieri Morales, Talib Oliver, Yoangel Torres, Dario Solano, Emre Havazli, Heresh Fattahi), which provided a great college atmosphere for professional and personal discussions. In addition, I would like to thank my RSMAS MGG and non-MGG friends (Viviana Diaz, Jara Schnyder, Ergin Karaca, Kelly Jackson, Pierpaolo Marchesini, Kimberly Galvez, Jan Henrik, Juan Pinales, Alexis Denton) for providing a friendly work environment which I certainly will miss.

Lastly, but most important I would like to thank my family as without their support, the completion of my doctoral studies was going to be impossible. I dedicate my dissertation to my mother (Mary Ann Bonilla), my father (Rufino Feliciano), my brothers

(Christian Feliciano and Xavier Feliciano), my sisters (Melissa Feliciano and Paola Feliciano), my nieces (Nathalia Feliciano and Mercedes Rosario) and my nephew (Emanuel Rosario).

TABLE OF CONTENTS

Page

List of Figures xi

List of Tables xiii

Acronyms xiv

Chapter 1: Introduction 1

1.1. Wetlands 1

1.2. Everglades Wetland Ecosystem Overview 2

1.3. Everglades National Park 4

1.3.1. Everglades National Park Vegetation 5

1.4. Monitoring and Measuring Wetland Vegetation Structure 7

1.5. Objectives and Dissertation Synopsis 9

Chapter 2: Methodology 11

2.1. Terrestrial Laser/LiDAR Scanning (TLS) 11

2.1.1. Plot-Level Vegetation Structure Parameters and their Uncertainties 13

2.2. Airborne Laser/LiDAR Scanning (Airborne LiDAR) 15

2.3. Interferometric Synthetic Aperture Radar (InSAR) 19

2.3.1. TanDEM-X 22

2.3.2. TanDEM-X Data Processing 23

Chapter 3: Assessing Mangrove Above-Ground Biomass and Structure using Terrestrial Laser Scanning: A Case Study in the Everglades National Park 28

3.1. Summary 28

3.2. Overview 28

3.3. Study Area 32

3.4. Methods 33

3.4.1. Terrestrial Laser Scanner Data Collection 33

3.4.2. TLS Data Processing 36

3.4.3. TLS Data Post-Processing (Tree Volume Geometry Modelling) 36

3.4.3.1. Volume and AGB Estimation of Main Stem 38

3.4.3.2. Volume and AGB Estimation of Prop Roots (*R. mangle*) 40

3.4.4. Canopy Correction 42

3.4.5. Mangrove Allometry from TLS Data 43

3.4.6. Mangrove Allometry Comparison 44

3.5. Uncertainty Analysis 44

3.5.1. Parameter Uncertainties 45

3.5.1.1. TLS Measurement Errors 45

3.5.1.2. Geometrical Parameters 45

3.5.1.3. Wood Specific Density 45

3.5.1.4. Canopy Correction 46

3.5.2. Estimation of Uncertainty Propagation 46

3.6. Results 47

3.6.1. AGB Estimation and Allocation 47

3.6.2. AGB Uncertainty 49

3.7. Discussion 51

3.7.1. Mangrove Allometry from TLS Data 51

3.7.2. Mangrove Allometry Comparison 52

3.7.3 TLS Data Analysis 53

3.8. Conclusion 54

Chapter: 4: Estimating Mangrove Canopy Height and Above-Ground Biomass in Everglades National Park with Airborne LiDAR and TanDEM-X Data 56

4.1. Summary 56

4.2. Overview 57

4.3. Study Area 58

4.4. Datasets and Methods 59

4.4.1. Ground Measurements 60

4.4.1.1. Terrestrial Laser Scanning 60

4.4.2. Airborne Measurements 62

4.4.2.1. Airborne Laser Scanning 62

4.4.3. Space-based Measurements 63

4.4.3.1. WorldView-2 Mangrove Cover Map 63

4.4.3.2. TanDEM-X Data 65

4.6. Multi-Scale Canopy Height Data Calibration Results 66

4.6.1. Airborne LiDAR vs. TanDEM-X Canopy Height Validation along the Shark River Slough 66

4.6.2. Everglades National Park Mangrove Digital Canopy Model 68

4.6.3. Above-Ground Biomass 69

4.7. Discussion 71

4.7.1.Mangrove Canopy Height and Biomass 71

4.8. Conclusion 74

Chapter 5: Assessing the Vegetation Structure of Non-Mangrove Vegetation Communities in the Everglades National Park using Multi-Spatial Remote Sensing Techniques 76

5.1. Overview 76

5.2. Study Area 77

5.2.1. Rockland Pine 78

5.2.2 Bald Cypress and Tropical Hardwood Hammocks 79

5.3. Methods 80

5.3.1. Datasets 80

5.3.1.1. TLS Data 80

5.3.1.2. Airborne LiDAR Data 81

5.3.1.3. TanDEM-X Data 82

5.3.2. Data Processing 82

5.3.2.1. TLS Data Processing 82

5.3.2.1.1. Stem Volume and AGB Estimation 83

5.3.2.2. Airborne LiDAR Data Processing 83

5.3.2.3. TanDEM-X Data Processing 86

5.4. Airborne LiDAR and TanDEM-X Canopy Height Results 86

5.4.1. Airborne LiDAR vs. TanDEM-X Canopy Height Comparison in the Rockland Pine, Hammock and Bald Cypress Sites 86

5.5. Above-Ground Biomass Examples 90

5.6 Canopy Height Implications 90

Chapter 6: Conclusions 92

6.1. Future Directions 94

Bibliography 96

List of Figures

Figure 1.1: Greater Everglades Ecosystem extent. 3

Figure 1.2: Everglades Ecosystem historic water flow. 4

Figure 1.3: Current status of Everglades ecosystem. 5

Figure 1.4: Everglades National Park vegetation map. 7

Figure 1.5: Everglades National Park location within South Florida. 9

Figure 2.1: Leica C10 TLS specifications. 12

Figure 2.2: TLS point cloud in mangrove site. 13

Figure 2.3: Schematic illustration of Airborne LiDAR system. 16

Figure 2.4: Schematic illustration of Airborne LiDAR waveform. 17

Figure 2.5: Airborne LiDAR mangrove surveying area. 18

Figure 2.6: ALS pine, cypress and hammock surveying area. 19

Figure 2.7: Schematic illustration of repeat-pass InSAR. 21

Figure 2.8: Schematic illustration of single-pass InSAR. 22

Figure 2.9: Artistic rendering of TDX and TSX satellites. 23

Figure 2.10: Random Volume over Ground model illustration. 24

Figure 3.1: TLS mangrove surveying sites within the ENP. 32

Figure 3.2: Leica C10 TLS photograph in ENP mangrove site. 34

Figure 3.3: Schematic of TLS logistics for mangrove surveying. 35

Figure 3.4: Black mangrove photograph versus TLS point cloud. 35

Figure 3.5: Tree stem volume modeling. 37

Figure 3.6: Prop root volume modeling. 37

Figure 3.7: Mangrove stem volume estimation example. 39

Figure 3.8: Mangrove prop root volume estimation example. 41

Figure 3.9: TLS-based mangrove allometry. 43

Figure 4.1: Study area: ENP mangrove forests. 59

Figure 4.2: 50 x 50 m TLS SRS-6 mangrove plot. 61

Figure 4.3: 50 x 50 m SRS-6 plot showing DBH measurements. 61

Figure 4.4: ALS-based DCM for SRS mangrove forests. 62

Figure 4.5: WorldView-2 mangrove classification and validation. 64

Figure 4.6: ENP helicopter photography. 64

Figure 4.7: TDX processing (coherence, phase, forest height inversion). 66

Figure 4.8: ALS-derived versus TanDEM-X-derived DCMs in SRS. 67

Figure 4.9: ALS H100 versus TanDEM-X canopy height results. 68

Figure 4.10: ENP TanDEM-X-based mangrove DCM. 69

Figure 4.11: ENP AGB map based on TDX and global AGB equation. 71

Figure 4.12: Simard et al. (2006) versus Feliciano et al. (2015) DCMs. 73

Figure 4.13: Simard et al. (2006) ENP AGB map. 74

Figure 5.1: Study area: ENP pine, cypress and hammock sites. 78

Figure 5.2: Leica C10 TLS photograph in ENP cypress site. 81

Figure 5.3: Bald Cypress site DCM. 84

Figure 5.4: Rockland pine and hammock site ALS DCM. 85

Figure 5.5: Rockland pine and hammock site TDX DCM. 87

Figure 5.6: ALS 10 m vs. TDX 10 m hammock forest DCM. 88

Figure 5.7: Hammock forest ALS H100 vs TDX forest height plot. 89

Figure 5.8: AGB estimation examples with pine and cypress trees. 90

List of Tables

Table 2.1: Leica C10 TLS specifications. 12

Table 2.2: Optech Gemini ALS system specifications. 19

Table 3.1: Red mangrove canopy-stem-root volume-AGB estimations. 48

Table 3.2: TLS-based mangrove allometry versus published allometry. 49

Table 3.3: TLS uncertainty for three ENP mangrove species. 50

Table 3.4: AGB uncertainty estimates for the three mangrove species. 51

Table 4.1: TDX data used for mangrove canopy height. 65

Table 5.1: TDX data used for pine, cypress, hammock canopy height. 82

Acronyms

AGB	Above-Ground Biomass
ALS	Airborne LiDAR/Laser Scanning
ALTM	Airborne Laser Terrain Mapper
BGB	Below-Ground Biomass
CC	Carbon Concentration
CEPP	Central Everglades Planning Project
CERP	Comprehensive Everglades Restoration Plan
DBH	Diameter at Breast Height
DCM	Digital Canopy Model
DEM	Digital Elevation Model
DSM	Digital Surface Model
DTM	Digital Terrain Model
ENP	Everglades National Park
FCE-LTER	Florida Coastal Everglades–Long Term Ecological Research Network
InSAR	Interferometric Synthetic Aperture Radar
LiDAR	Light Detection and Ranging
NAD83	North American Datum of 1983
NCALM	National Center for Airborne Laser Mapping
NSF	National Science Foundation
Pol-InSAR	Polarimetric–Interferometric Synthetic Aperture Radar
RMSE	Root Mean Square Error
RVoG	Random Volume over Ground Model

SAR	Synthetic Aperture Radar
SRS	Shark River Slough
SRTM	Shuttle Radar Topography Mission
TDX	TerraSAR-X add-on for Digital Elevation Measurement/TanDEM-X
TLS	Terrestrial Laser/LiDAR Scanning
TSX	TerraSAR-X
UTM	Universal Transverse Mercator Coordinate System
WSD	Wood Specific Density

Chapter 1: Introduction

1.1. Wetlands

Wetlands are regions that are covered permanently or seasonally with water and/or have saturated soils for long periods of time. Hydrophytic plants are widespread in wetlands. They are able to live under water or in saturated soils as either emergent plants (rooted in soils), submerged plants (beneath water surface), floating plants (leaves and stems on water surface), or shrubs and large woody trees (mangroves). Since wetlands encompass marine and terrestrial habitats, they support the life of various faunal species such as mammals, monotremes, birds, reptiles, amphibians, fish, insects and arthropods. Wetlands provide numerous benefits to human society, including aquifer recharge, flow regulation, storm protection, sediment and nutrient retention, energy production, conservation of fauna and flora, recreation and tourism, and as a place for research and education (Davies et al., 1993; Mitchell, 2001). Due to the extraordinary biodiversity and ecosystem goods and services of wetlands, they are categorized as biomes with high productivity (Davies et al., 1993; Gibbs, 2000). Wetland environments sequester and store high amounts of carbon due to their anoxic and wet conditions (Mitsch et al., 2013). In fact, although wetlands only cover approximately 5-8% of the world's terrestrial area (Mitsch and Gosselink, 2007), they sequester approximately 12% (830 Tg/year) of the total carbon dioxide (7000 Tg/year) emitted from fossil fuel combustion (Mitsch et al., 2013). However, wetland ecosystems are under severe pressure due to anthropogenic activities and climate change (Erwin, 2009).

The need to conserve, restore and monitor wetlands at a regional and global scale is well recognized, e.g. as evidenced by the RAMSAR convention. The RAMSAR convention was established in the 1970's. Its main goal is to conserve wetlands though local, national and international cooperation. Almost 90% of the United Nation member nations participate in this initiative, including the U.S. Wetland area has decreased by 53% in the U.S. since the 1780s due to dredging, draining and filling (Gibbs, 2000). Currently, there are a total of 2186 RAMSAR sites, (168 countries), designated Wetlands of International Importance. The U.S. has a total of 35 RAMSAR sites including the only subtropical wetland in the U.S., Everglades National Park (ENP) located in South Florida.

1.2. Everglades Wetland Ecosystem Overview

The ENP represents what remains of the historic Greater Everglades Ecosystem (Figure 1.1). The Everglades ecosystem is relatively young in geological terms (5,000 years), although the underlying limestone rocks were formed roughly 2 million years ago. Historically, it extended from Lake Okeechobee (Figure 1.1) south to Florida Bay, encompassing a total of 16 counties. Today, mostly due to anthropogenic activities, only 50% of the original landscape and water flow dynamics (Figure 1.2) remain (Davies et al., 1993). However, ENP continues to provide habitat to various endangered species such as the American crocodile, the West Indian manatee, the Florida panther and the wood stork. Federal and state restoration initiatives such as the Comprehensive Everglades Restoration Plan (CERP, 2000) and the Central Everglades Planning Project (CEPP, 2011) have been created in order to restore the flow of water and stabilize the

ecosystems within and adjacent to the ENP. Additionally, it provides water to approximately 8 million Floridians.

Figure 1.1 Extent of the historic Greater Everglades Ecosystem (red line) and Florida and state protected lands and waters (yellow line). *(Figure provided by the Everglades Foundation).*

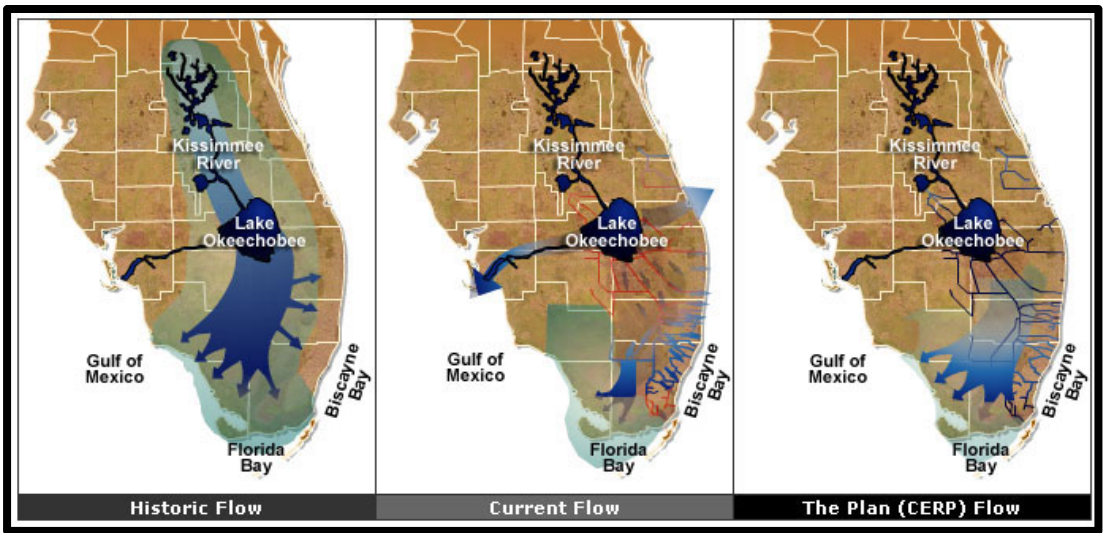

Figure 1.2 Greater Everglades Ecosystem historic water flow in comparison with the current water flow and the proposed Comprehensive Everglades Restoration Plan water flow. *(Figure provided by the Everglades Restoration Plan).*

1.3. Everglades National Park

On December 6th of 1947 the U.S. government acquired 1.5 million acres of land to be designated as the ENP (Figure 1.3). In addition of being a designated National Park and a RAMSAR site, the ENP is a World Heritage Site and a Biosphere Reserve. The ENP is home to a large number of unique endangered and native species (fauna and flora) that are being impacted by (1) the deprivation of the freshwater inflow into the park, (2) the dominance of exotic and invasive species and (3) rising sea level. One of the key objectives of the Everglades restoration plan involves the conservation of primary vegetation ecosystems, as they have suffered severe consequences by water diversion, agriculture, land clearing, population growth and urban development (Fröhlich and Mettenleiter, 2004). In order to monitor the current status and future recovery of the various vegetation ecosystems, it is imperative to assess and quantify vegetation species changes, including vegetation structural changes such as canopy height and above-ground biomass (AGB)/carbon as a function of time.

Figure 1.3 Land cover map of south Florida showing the current status of the Everglades ecosystem. The black and yellow lines mark the locations of the ENP and the Greater Everglades Ecosystem, respectively. *(Figure provided by the Everglades Foundation).*

1.3.1. Everglades National Park Vegetation

The ENP is home to several types of wetland plant communities. The last comprehensive mapping of the ENP conducted by University of Georgia's Center of

Remote Sensing and Mapping Science took place approximately two decades ago (Welch et al., 1999). The most abundant vegetation types found were: mangrove, scrub, savanna (rockland pine, cypress, palm), hammock, marsh, and sawgrass (Figure 1.4). Of all of these, mangroves are the largest in terms of area and are estimated to cover an area of 144,447 ha in the ENP (Simard et al., 2006), much more than the bald cypress, slash pine and hammock forests. These plant communities (mainly the mangrove forests) provide a variety of ecosystem services as they link terrestrial and aquatic eco-environments (Fatoyinbo et al., 2008) harbor unique biodiversity, provide storm protection (Donato et al., 2011) and sequester carbon (Giri et al., 2011). Of these ecosystem services, carbon sequestration might be the most important in the long term as the carbon stock of these coastal ecosystems forms a vital part of the carbon cycle in coastal regions and ranks among the most productive ecosystems in the world (Fatoyinbo et al., 2008; Giri et al., 2011). CO^2 release from wetlands due to anthropogenic or natural causes may have significant effects on global warming. Mangroves, however, are very fragile and sensitive to change, because they are affected by devastating storm winds and surges (Florida: Andrew 1992 and Wilma 2005), anthropogenic activities (e.g. coastal projects, agriculture and tourism) and global climate change (sea level rise) (Giri et al., 2011).

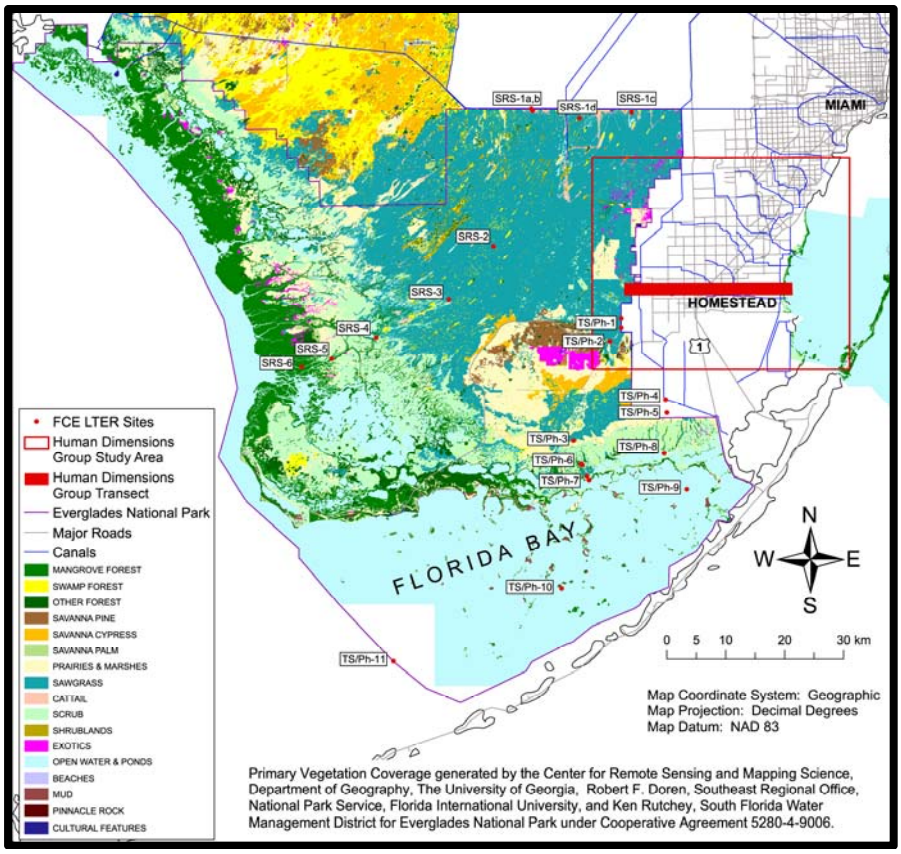

Figure 1.4 Everglades National Park vegetation map created by the Center for Remote Sensing and Mapping Science, University of Georgia (Welch et al., 1999).

Hence, a major part of this dissertation is devoted to assessing the current conditions of mangroves in the ENP. I also studied the other wetland forest ecosystems in order to compare freshwater plant communities with saltwater plant communities and to have a general idea of their current status.

1.4. Monitoring and Measuring Wetland Vegetation Structure

High-resolution remote sensing technology represents a useful tool to study large forested areas such as wetlands and to quantify forests structural parameters such as vegetation structure (canopy height) and AGB from regional up to global scales. Understanding both vegetation parameters is vital if a monitoring database is to be

established, especially on mangroves forests as they provide beneficial ecosystems goods and services. Remote sensing can be potentially used to establish a framework for present and future ecosystem comparison.

Recent advances in remote sensing sensors and techniques present an enormous opportunity to characterize wetland vegetation land cover and structure. Previous studies have successfully used optical satellite data such as Landsat 7 Enhanced Thematic Mapper Plus (ETM+) to estimate and classify mangrove cover (Fatoyinbo et al., 2008; Giri et al., 2011). However, it is now possible to study the vertical structure of mangrove forests using active multi-spatial remote sensing sensors from (1) air- or spaceborne LiDAR/Laser Scanning or (2) spaceborne Synthetic Aperture Radar (SAR) systems such as Shuttle Radar Topography Mission (SRTM) (Simard et al., 2006; Fatoyinbo et al., 2008) and TerraSAR-X add-on for Digital Elevation Measurement (TanDEM-X) (Kugler et al., 2013; Sadeghi et al., 2014). The main product of an Airborne LiDAR system is a 3-D point cloud with (x, y, z) coordinates, where x and y correspond to horizontal location and z to height. For forestry studies, accurate canopy height maps or Digital Canopy Models (DCM) can be derived using Airborne LiDAR data. However, the acquisition of Airborne LiDAR data is expensive for small regions, an enormous disadvantage when compared with space-based remote sensing sensors such as SRTM or TanDEM-X. The TanDEM-X mission represents a great opportunity to estimate the structure of the world's forests, such as mangrove canopy height, using Interferometric SAR (InSAR) or Polarimetric–InSAR (Pol-InSAR) data (Kugler et al., 2013; Sadeghi et al., 2014). The TanDEM-X mission has the advantage of not having temporal decorrelation (Krieger et al., 2007), an important element in the processing of a DCM derived from SAR data.

1.5. Objectives and Dissertation Synopsis

The main objective of this study is providing quantitative canopy height and AGB estimates of four wetland forest ecosystems: mangroves, slash pines, bald cypresses and hammocks, all located within the boundaries of the ENP (Figure 1.5). In my thesis, I produce canopy height and AGB maps using three techniques, Terrestrial Laser/LiDAR Scanning (TLS), Airborne Laser/LiDAR Scanning (Airborne LiDAR), and single-pass bistatic Pol-InSAR. Furthermore I also provide sensitivity and uncertainty analyses of the calculated parameters for each sensor and for each forested wetland environment.

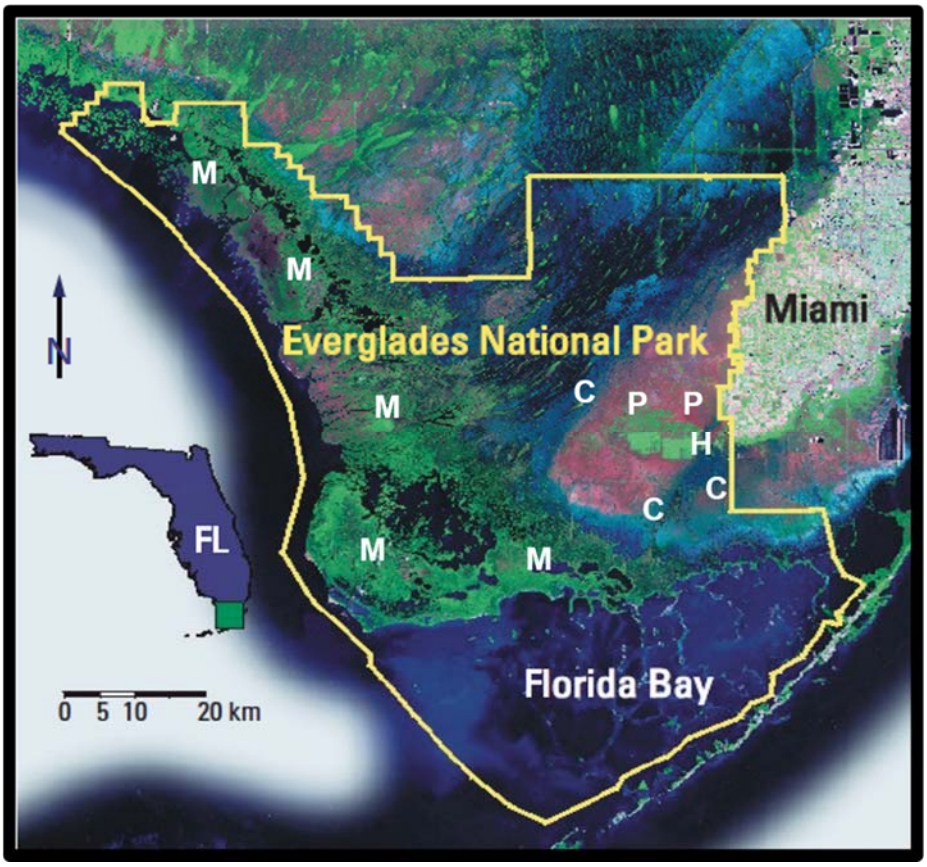

Figure 1.5 ENP location map within the South Florida Peninsula. Vegetation communities for this study include: M = Mangrove, C = Bald Cypress, P = Slash Pine and H = Hammock.

This dissertation comprises this introductory chapter and five additional chapters briefly summarize below.

Chapter 2 provides an overview of the main three remote sensing datasets and sensors (TLS, Airborne LiDAR, TanDEM-X) used in this dissertation and their application to quantify vegetation structure and biomass. Additionally, there is a brief overview of SAR InSAR and two methods of SAR data acquisitions (single-pass InSAR and repeat-pass InSAR).

Chapter 3 describes the use of TLS to estimate mangrove stem volume, prop root volume and AGB in three sites located inside the ENP. Detailed explanations of the TLS processing and TLS-based allometric equations generation are presented.

Chapter 4 covers the use of TLS, Airborne LiDAR and TanDEM-X (Pol-InSAR) to quantify canopy height and AGB across the entire ENP mangrove forests. A comparison with a previous study is also presented.

Chapter 5 describes the use of TLS, Airborne LiDAR and TanDEM-X (Pol-InSAR) to quantify canopy height and AGB across three other vegetation ecosystems in the ENP (rockland pines, bald cypresses and hammocks).

Chapter 6 presents the finding and conclusions of this Dissertation in two parts: an overview and summary of the dissertation and recommendations to enhance future related work.

Chapter 2: Methodology

The monitoring and estimation of vertical structure and AGB in large extent forested wetlands largely relies on the use of airborne and space-based remote sensing techniques. Space-based SAR represents a great opportunity to estimate forest height over very large areas using InSAR and Pol-InSAR techniques. However, these technologies depend on plot-level estimations for calibration. Emerging remote sensing techniques such as TLS present a new way to conduct ground-based measurements in wetland environments and overcome challenges of traditional forestry surveys (Feliciano et al., 2014). In this thesis, I investigated the use of TLS with the goals of providing better AGB estimates at the plot-level for Airborne LiDAR and InSAR calibrations. The Airborne LiDAR served as a validation and comparison dataset for the TanDEM-X data. The following sub-sections introduce the instruments and sensors used in my thesis.

2.1. Terrestrial Laser/LiDAR Scanning (TLS)

TLS or ground-based LiDAR is a remote sensing tool that is being widely used in many fields such as: geology, archeology, geodesy, criminology, engineering and forestry. The main advantage of a TLS is its ability to image the 3-D structure, range and coordinates (x, y, z) of any given object with high accuracy and resolution (mm level). TLS is a range measurement instrument that scan objects within a range of up to ~1000 meters by deflecting and reflecting a laser beam to an object using mirrors (Fröhlich and Mettenleiter, 2004). For this thesis, I used a compact and lightweight Leica ScanStation C10 TLS (Figure 2.1), which exceeds the minimum requirements suggested for a forestry study (Maas et al., 2008). These requirements are: a minimum data acquisition range of

50 meters; a scanning rate of 10,000 points per second for field-time efficiency; an hemispheric field of view for data acquisition flexibility; and a spot size of 10 millimeters to allow for adequate measurements of stem diameter. A summary of the Leica ScanStation C10 internal (Figure 2.1) and technical specifications (Table 2.1) is provided below.

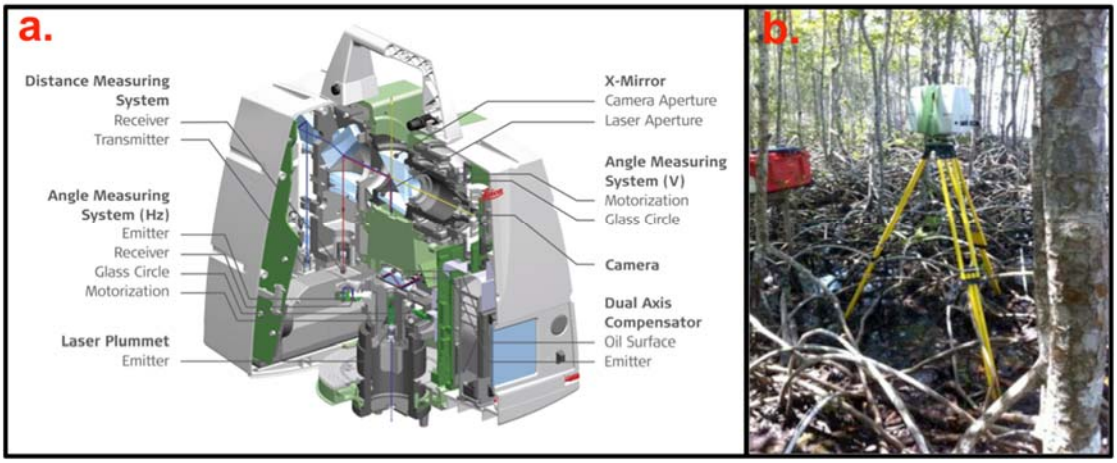

Figure 2.1 a) Leica ScanStation C10 internal design and specifications *(Figure 2.1 a provided by Leica - http://hds.leica-geosystems.com/en/Leica-ScanStation-C10_79411.htm)* b) Leica ScanStation C10 TLS in partially inundated mangrove site.

Leica ScanStation C10 TLS Specifications	
Laser Class	3R (eye safe)
Field-of-view	Horizontal (360°) Vertical (270°)
Range	300 m
Scan Resolution	Spot Size (7 mm), Point Spacing (<1 mm)
Scan rate	50,000 points per second
Weight	0.4 kg
Wavelength	Green Laser (532 nm)
Special Features	Integrated Camera, Touch Display

Table 2.1 Leica ScanStation C10 TLS technical specifications.

TLS has been used to estimate vegetation parameters such as DBH (diameter at breast height) (Hopkinson et al., 2004; Watt and Donoghue, 2005) and stem density (Maas et al., 2008; Liang et al., 2012). This dissertation reports the first use of TLS in a forested wetland ecosystem. The TLS data are used to calculate tree volume using geometrical surfaces known as frustums (Chapter 3). My approach for obtaining AGB was to multiply the TLS-derived tree volume by species-specific wood specific density (WSD). Additionally, high-resolution photography was acquired with the TLS after each scan to help with the identification of species. (Figure 2.2.). Feliciano et al. (2014) describes in detail the use and processing of TLS data in the ENP mangroves.

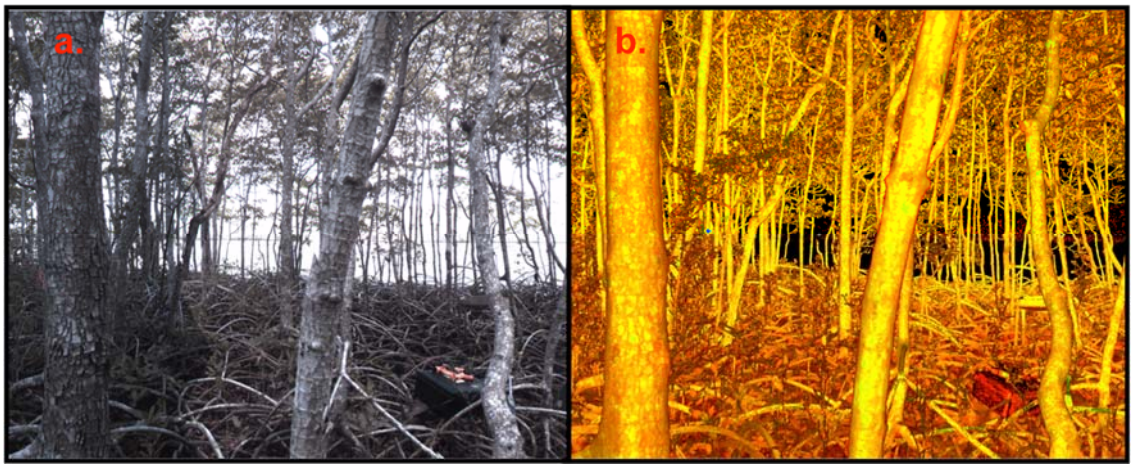

Figure 2.2 a) Photograph of the same area scanned in figure 2.2. b. b) TLS 3-D point cloud in intermediate mangrove site (SRS-5).

2.1.1. Plot-Level Vegetation Structure Parameters and their Uncertainties

AGB is a vital measurement used to predict the carbon stock of forest ecosystems. As important as AGB is, uncertainties related to its calculations have not been studied in great detail. Uncertainties of AGB estimations at the plot level (ground) and the regional level (airborne and spaceborne remote sensing) are important as they are ultimately propagated into the final AGB estimation or product. Therefore, there is a need to

quantify and address AGB estimation uncertainty. Of all sources of uncertainties, ground estimations are the most important, as airborne and spaceborne estimations rely on these measurements. The most common method used to estimate AGB of specific trees at the plot level is allometry. Allometry or allometric equation describes the relationship between one or several parameters of a specific object and its shape. In forestry, allometry relates one or more parameters (DBH or height) to the total volume or AGB of a given tree. DBH is the most common measurement used as input in allometric equations because it is easily acquired in the field. Allometric uncertainties are thus the first source of uncertainty in AGB estimates.

Chave et al. (2004) suggested four types of uncertainties that could affect AGB estimates at the plot level using allometry. These uncertainties were: (1) error related to tree parameter measurement (DBH, height, WSD) and canopy area), (2) error related to the selection of an AGB allometric equation, (3) sampling error due to the size of the plot and the (4) how representative the study plots are of the entire ecosystem. Chave et al. (2004) concluded that the choice of the allometric equation was the most important source of uncertainty. He suggested using allometric equations that included WSD as one of the inputs and were created using data from individual trees having less than 10 cm DBH, as they might represent 10% of the carbon stock. Most of the allometric equations are based on the power function $F(x) = a*x^b$, where F(x) or y is AGB, x is DBH, *a* represents the allometry coefficient and *b* represents the proportionality between cumulated variables. Ketterings et al. (2001) suggested that one method that can be used to reduce the uncertainty using allometric equations is to correct the two allometry coefficients (*a* and *b*). More generally, Ahmed et al. (2013) suggested comparing the

variation between AGB estimations from various allometric equations of same species in order to analyze the range of possibilities of ground-truth estimations.

Remote sensing technologies such as LiDAR and SAR rely on the AGB measurements estimated at ground level. These technologies are not able to directly measure AGB, but only other parameters such as canopy height that are related to AGB. Although, canopy height measurements introduce other types of uncertainty (1 m uncertainty in Airborne LiDAR surveys) (Hyyppä et al., 2004), the final AGB calibration is affected more by the uncertainty introduced from the field derived allometric relationships. Therefore, new methodologies that can substitute the allometric approach and are non-destructive are needed.

2.2. Airborne Laser/LiDAR Scanning (Airborne LiDAR)

Similar to TLS, the main product of an Airborne LiDAR survey is a 3-D point cloud with x, y and z coordinates. The LiDAR system (Figure 2.3) is mounted in an aircraft with an Inertia Measurement Unit (IMU), which gives the precise orientation of the scanner and a Global Positioning System (GPS), which gives the precise location of the scanner. The scanner emits laser pulses that are reflected from objects located on the surface of the earth. These multiple pulses or returns are recorded by the laser scanner (Figure 2.4). The advantage of Airborne LiDAR is its larger area coverage and canopy height measurements, in contrast to the below-canopy high-resolution data coverage of TLS. Airborne LiDAR data fills the scale gap between the ground- and spaceborne measurements and it is widely used to estimate vegetation canopy height with an accuracy of approximately 1 m (Hyyppä et al., 2004). A DCM can be derived with

Airborne LiDAR data by subtracting the Digital Terrain Model (DTM) created with the bare ground points (last laser returns) from the Digital Surface Model (DSM) created with the top of the canopy points (first laser returns) (Figure 2.4). The advantage of having canopy height measurements is their linear relationship with AGB (Lefsky et al., 2005). Therefore, TLS-based AGB estimates can be used to derive an AGB-Canopy height relationship with Airborne LiDAR data to expand the study area.

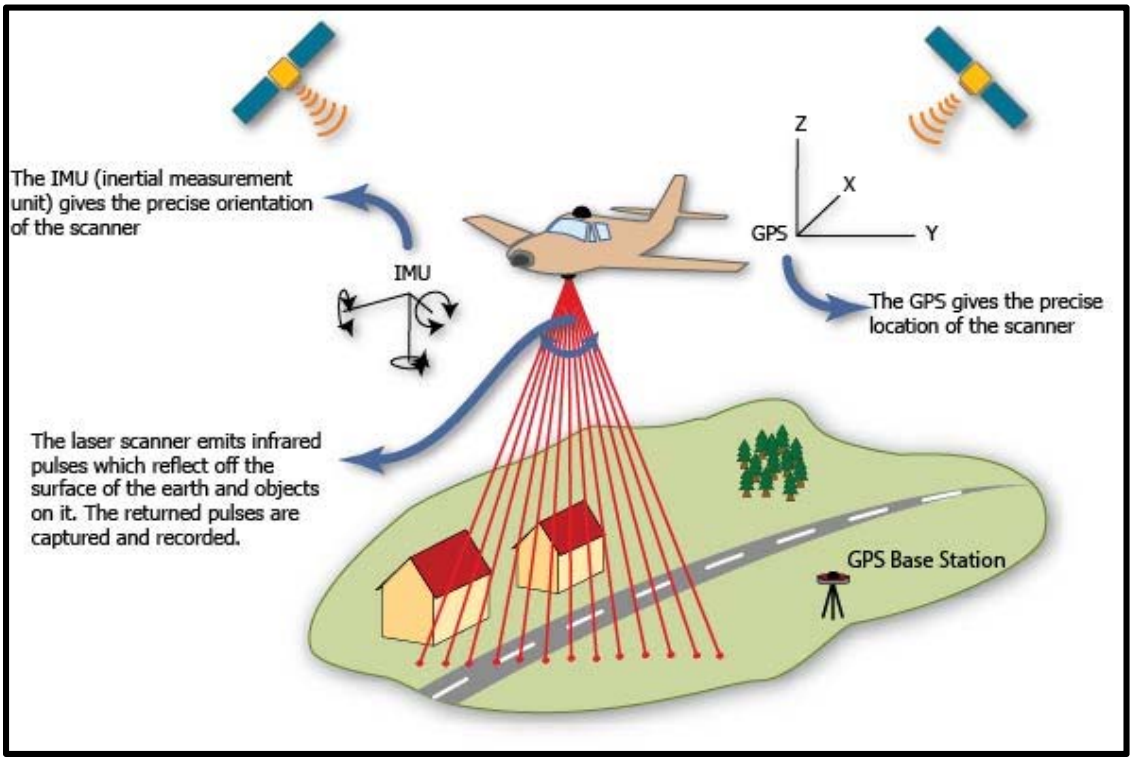

Figure 2.3 Schematic illustration of an airborne laser scanning (Airborne LiDAR) system. *(Figure provided by Geospatial Modeling and Visualization).*

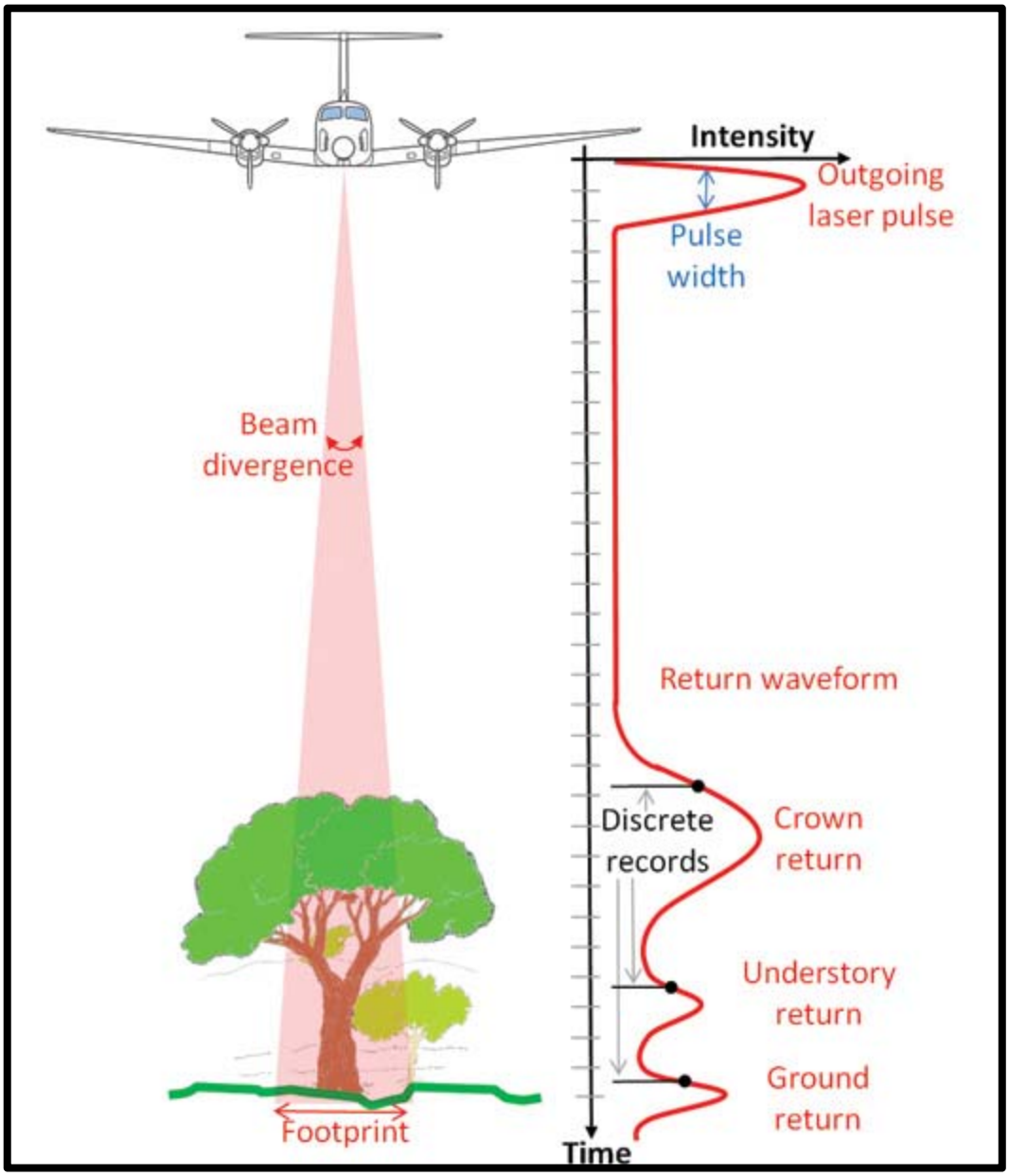

Figure 2.4 Schematic illustration of Airborne LiDAR waverform and discrete recordings for forestry studies. *(Figure provided by Imaging Notes).*

In this study Airborne LiDAR data was acquired using an Optech Gemini Airborne Laser Terrain Mapper (ALTM) operated by the National Center for Airborne Laser Mapping (NCALM) based at the University of Houston and funded by the National Science Foundation (NSF). The Airborne LiDAR survey was conducted on November

17, 2012 and comprised 3 regions (Mangrove, Cypress and Pine-Hammock) totaling 53 km^2 in area (Figures 2.5, 2.6). Table 2.2 presents a summary of the technical specifications for this survey, including: flight altitude and speed, swath width, swath overlap, point density, laser pulse rate frequency, beam divergence, scan frequency and scan angle. DTMs, DSMs and DCMs were produced using LAStools, ENVI and ArcGIS software (Chapter 4). Additionally, as stipulated by NSF policies, these data are freely available to the general public at: http://www.opentopography.org/.

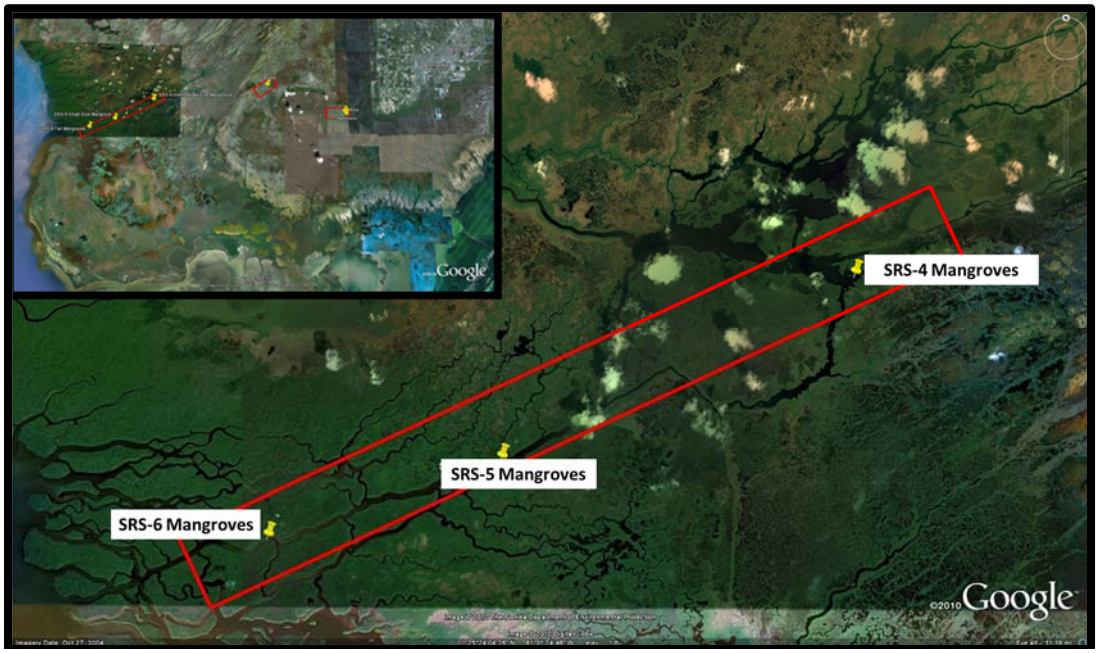

Figure 2.5 Airborne LiDAR surveyed sites in the 2012 NCALM campaign. On the top left corner, the ENP map showing the three Airborne LiDAR data acquisition regions. The main image shows a zoom-in to the Mangrove region. The yellow pins indicate my 2011 TLS surveyed sites (SRS-6: tall mangroves, SRS-5: intermediate size mangroves and SRS-4: small mangroves).

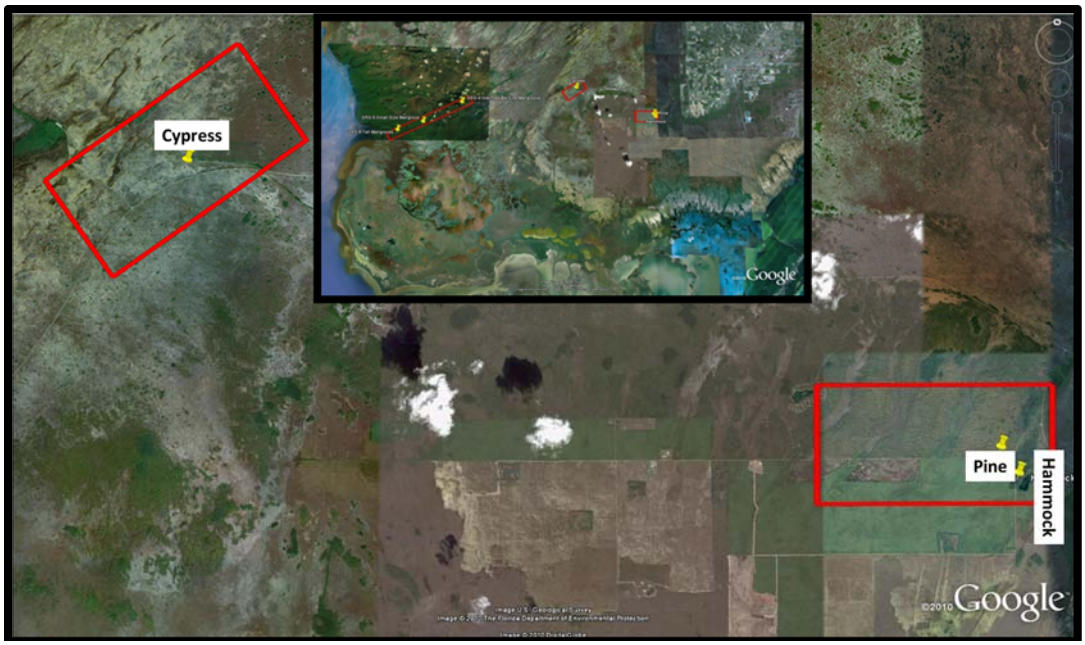

Figure 2.6 Airborne LiDAR surveyed sites in the 2012 NCALM campaign. On the top of the image, the ENP map showing the Airborne LiDAR 2012 data acquisition regions. The main image shows a zoom-in to the Cypress, Pine and Hammock (right) sites. The yellow pins indicate my 2011 TLS surveyed sites (Cypress, Pine and Hammock).

Optech Gemini ALTM Specifications	
Flight Altitude	600 m
Flight Speed	60 m/s
Swath Width	360 m
Swath Overlap	50%
Point Density	6.4 p/m^2
Laser Pulse Rate Frequency	125 kHz
Beam Divergence	0.25 mrad
Scan Frequency	45 Hz
Scan Angle	$\pm 21°$

Table 2.2 Optech Gemini ALTM specifications for Everglades National Park survey.

2.3. Interferometric Synthetic Aperture Radar (InSAR)

SAR is a side looking airborne or spaceborne radar system that is in constant motion and emits electromagnetic waves as pulses and receive the reflected backscatter

energy of a target. Radar systems are able to acquire data during day or night as they emit their own energy and their wavelength penetrates the atmosphere, including clouds. Additionally, radar sensors operate at different regions of the microwave spectrum (X-band [3.1 cm], C-band [5.6 cm], L-band [23 cm] or P-band [70 cm]), suitable for different applications such as the generation of digital elevation models (DEM) (Ferretti et al., 1999; Jacobsen, 2003), forest structure characterization (Hajnsek et al., 2009; Kugler et al., 2013; Sadeghi et al., 2014) detection of volcanic activity (Amelung et al., 2000), land subsidence (Amelung et al., 1999; Dixon et al., 2006) and water level changes (Wdowinski et al., 2008) among others. SAR measurements have two main observables, amplitude and phase. An amplitude image represents the strength of the backscattered energy. The phase represents a fraction of one single SAR wavelength. The phase of the returned signal is measured by a SAR system. Phase measurements are the basis of the InSAR technique, which detects phase changes between two SAR acquisitions to create an interferogram.

The two main InSAR data acquisition methods are repeat-pass (two-pass) and single-pass bistatic acquisition. The most common InSAR acquisition method used to quantify changes and deformation in the Earth (e.g. earthquakes, volcanic activity, subsidence, water level changes) is the repeat-pass, where a specific satellite acquires SAR data for a specific region, at different points in time (days to weeks apart between acquisitions). For forest height applications repeat-pass InSAR (Figure 2.7) presents disadvantages due to the inherent changes between SAR acquisitions (e.g. coherence loss, temporal decorrelation, wind decorrelation) (Papathanassiou and Cloude, 2003; Santoro et al., 2007). However, single-pass bistatic InSAR acquisitions (e.g. SRTM, TanDEM-X

mission) have the advantage of acquiring two SAR images simultaneously (Figure 2.8), as one satellite emits the signal and two satellites receive the reflected signal with no temporal decorrelation (Krieger et al., 2007). Fixed-baseline InSAR collects data at the same time with two antennas (SRTM) or two satellites (TanDEM-X) fixed at a specific distance.

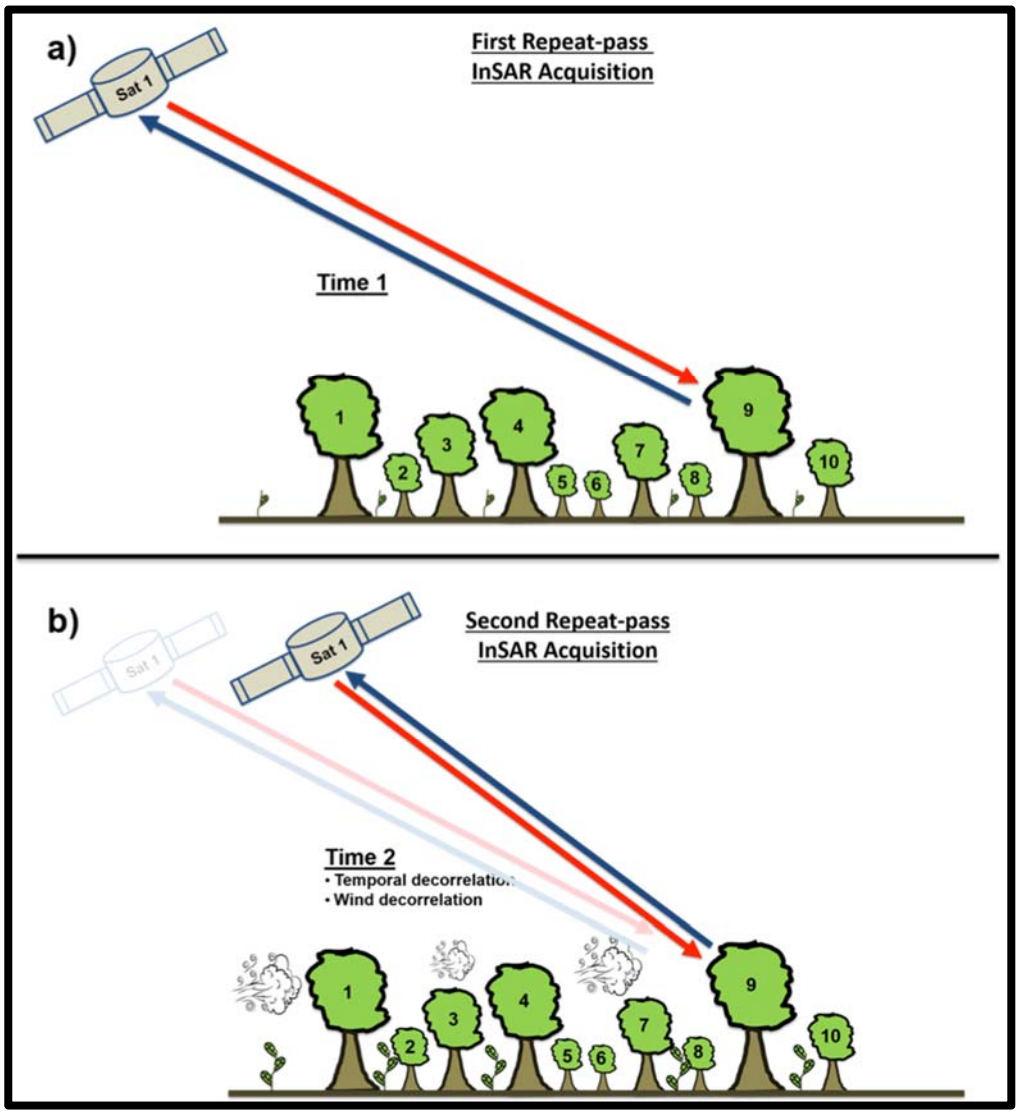

Figure 2.7 Schematic illustration of repeat-pass InSAR. a) First SAR acquisition. b) Second SAR acquisition. By the time the second SAR image is acquired temporal decorrelation and wind decorrelation are factors that introduce uncertainty for the estimation of forest strucutre.

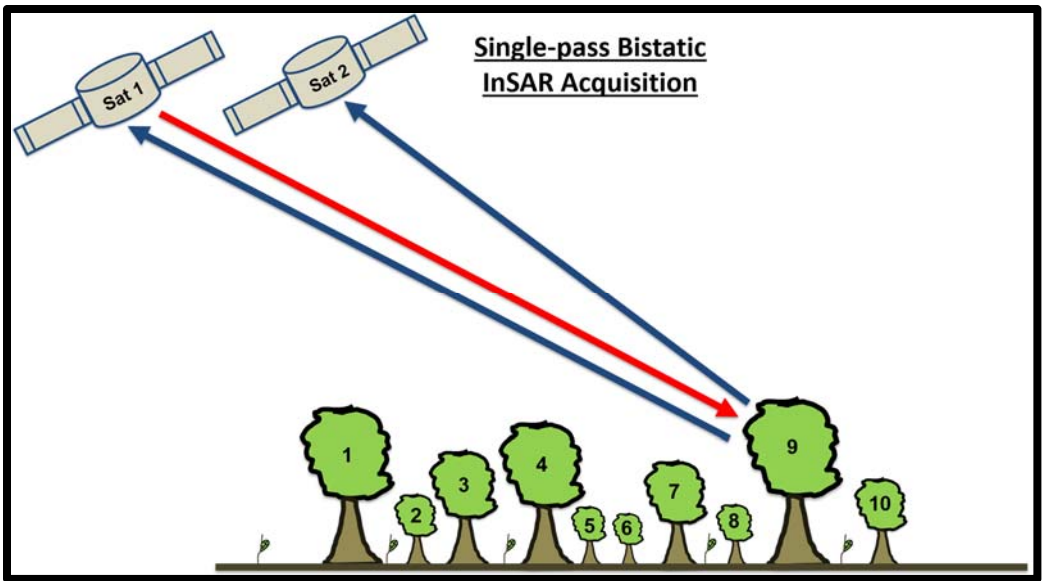

Figure 2.8 Schematic illustration of single-pass bistatic InSAR. Sattelite 1 transmits a signal and Satellite 1 and 2 receive the reflected signal. Since both signal (images) are acquired simultaneosly, temporal decorrelation is not present.

2.3.1. TanDEM-X

Surveying large wetland forests with TLS and Airborne LiDAR would be extremely expensive and would need enormous amount of resources and fieldwork. In this thesis, I evaluated the use of TanDEM-X data to study and analyze the vegetation structure of the large mangrove forests located in the western region of the Everglades and the Pine, Cypress and Hammock forests in which TLS and Airborne LiDAR data were acquired. The TanDEM-X SAR mission (Figure 2.9) was launched on June 21, 2010 with the goal of providing a worldwide high-resolution (< 2-m relative vertical accuracy and 12-m horizontal) DEM using radar interferometry with its twin satellite TerraSAR-X (Krieger et al., 2007). For comparison, the highest resolution of the current globally available DEM generated by the SRTM mission is 30 m (Kellndorfer et al., 2004). One of the potential applications of TanDEM-X is the determination of forest canopy height over large regions (Kugler et al., 2013). Simard et al. (2006) and Fatoyinbo

et al. (2008) used this concept to estimate mangrove canopy height and AGB in the ENP and Mozambique, using SRTM data.

Figure 2.9 Artistic rendering of TanDEM-X and TerraSAR-X satellites in flight formation. *(Figure provided by German Aerospace Center [DLR]).*

2.3.2. TanDEM-X Data Processing

The processing of the TanDEM-X InSAR data to obtain forest height in this dissertation is based on Pol-InSAR data, which are used to constrain a volume scattering model known as Random Volume over Ground Model (RVoG) (Figure 2.10). Pol-InSAR permits the investigation of scattering mechanisms in natural volume scatterers, such as forests, by assuming that interferometric coherence is related to the vertical distribution of scatterers. The most important observation in Pol-InSAR is the interferometric coherence $\tilde{\gamma}$ (Hajnsek et al., 2009) and it mainly consists of three decorrelation parameters:

$$\tilde{\gamma} : (\tilde{\gamma}_{Temp})(\gamma_{SNR})(\tilde{\gamma}_{Vol}) \quad \textbf{(1)}$$

where $\tilde{\gamma}_{Temp}$ is the temporal decorrelation and can be neglected in TanDEM-X data as the data is acquired almost simultaneously, γ_{SNR} is the noise decorrelation due to the noise contribution on the received signal (Hajnsek et al., 2001) and is of less importance for studying forests at standard frequencies (Hajnsek et al., 2009) and $\tilde{\gamma}_{Vol}$ is the volume decorrelation related to the vertical distribution of scatterers in the two images.

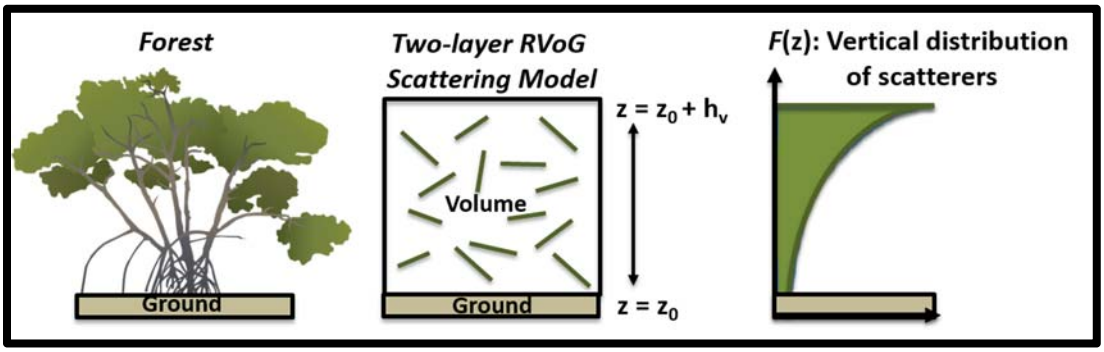

Figure 2.10. Schematic illustration of the RVoG model modified after Cloude and Papathanassiou (1998).

Volume decorrelation can be mathematically described in a normalized Fourier transformation $F(z)$:

$$\tilde{\gamma}_{Vol} = \mathrm{e}^{(\varphi_0)} \frac{\int_0^{h_v} F(z')\,\mathrm{e}^{(i\kappa_z z')} dz'}{\int_0^{h_v} F(z') dz'} \quad \textbf{(2)}$$

where φ_0 is the interferometric phase, k_Z is the effective vertical interferometric number that represents the effective spatial baseline between the satellites and h_V is the height of the volume layer. $\tilde{\gamma}_{Vol}$ has the information of the vertical structure of scatterers, thus it is the most important observable for forest parameter estimation (Cloude and

Papathanassiou, 1998; Papathanassiou and Cloude, 2001). The estimation of the vertical forest structure can be summarized in two steps: Firstly (modeling), $F(z)$ is parameterized for a limited set of physical parameters related by equation (2) to the interferometric coherence. Secondly (inverting), the inversion of the volume distribution of the coherence is used to estimate and derive the physical parameters (Hajnsek et al., 2009). $F(z)$ can be model using the RVoG model, which consists of two independent layers: a volume layer of randomly oriented vegetation scatterers and an impenetrable bottom/ground layer (Figure 2.10) (Treuhaft et al., 1996; Papathanassiou and Cloude, 2003). In the RVoG model, the volume layer is modeled by an exponential function that has a normalized volume height (Figure 2.10).

The RVoG model can be mathematically described as:

$$F(z) = \tilde{m}_V e^{(\frac{2\sigma}{\cos(\theta_0)} z)} + m_G e^{(\frac{2\sigma}{\cos(\theta_0)} h_V)} \delta(z - z_0) \quad \textbf{(3)}$$

where $\tilde{m}_V$ represents the volume scattering amplitudes, m_G represents the ground scattering amplitudes, σ is a mean extinction coefficient that describes the attenuation rate of the vegetation layer and z_0 is the ground topography. Equation (3) leads to equation (4) $\tilde{\gamma}_{Vol}$:

$$\tilde{\gamma}_{Vol} = \mathrm{e}^{(ik_z z_0)} \frac{\tilde{\gamma}_{v0} + m}{1 + m} \quad \textbf{(4)}$$

where $k_z z_0$ or φ_0 is the interferometric phase related to z_0 ground topography, m is the ground to volume amplitude ratio that accounts for the attenuation of the signal through the volume and $\tilde{\gamma}_{v0}$ is the volume decorrelation only to the vegetation layer. If temporal decorrelation is neglected and noise decorrelation is assumed to be compensated,

equation (4) can be balanced and inverted in terms of a quad-polarized fixed-baseline acquisition with six unknowns parameters (h_v, σ, m_1, m_2, m_3, ϕ_0 - ground phase) and three interferometric coherences (γ_1, γ_2, γ_3) assuming no ground response in one polarization (e.g. $m_3 = 0$) (Cloude and Papathanassiou, 1998; Cloude and Papathanassiou, 2003; Hajnsek et al., 2009).

For dual-polarized acquisitions there are only two interferometric coherences (γ_1, γ_2) for five unknowns (h_v, σ, m_1, m_2, ϕ_0). Assuming no ground contribution in one polarization (e.g. $m_2 = 0$), a balanced inversion problem can be achieved (Papathanassiou and Cloude, 2001). For a single-polarized acquisition, the Pol-InSAR inversion is unbalanced with four unknown parameters (h_V, σ, ϕ_0, m_1) and one interferometric coherence (γ_1). Even assuming no ground contribution (e.g. $m_1 = 0$), the inversion is unbalanced. It has been suggested that an external DTM can be used to reduce one unknown (e.g. ϕ_0) (Hajnsek et al., 2009). The problem is that a high resolution DTM cannot be obtained in a mangrove study area similar to the ENP, as high canopy cover and density does not allows ground laser returns. For this reason, I estimate the ground phase ϕ_0 directly from the TanDEM-X interferogram (if_{ϕ_0}), assuming that topography under mangroves is flat because of their unique environment and location close to sea water level. This assumption leaves the single-polarization (HH) inversion with two unknowns (h_V, σ) and a unique balance solution:

$$\min_{h_V,\sigma} \| \tilde{\gamma}_1 - \tilde{\gamma}_V(h_V, \sigma \mid \phi_0 = if_{\phi_0}) \| \qquad \textbf{(5)}$$

Equation (5) can be inverted to provide forest height estimates in a single TanDEM-X channel, HH in this dissertation.

Chapter 3: Assessing Mangrove Above-Ground Biomass and Structure using Terrestrial Laser Scanning: A Case Study in the Everglades National Park

3.1. Summary

Mangroves are among the ecosystems with highest potential for carbon sequestration and storage. In these ecosystems and others AGB is often used to estimate above-ground carbon content. I used a Leica-ScanStation-C10 TLS to estimate the volume and AGB of 40 mangrove trees distributed in three different mangrove sites located along Shark River Slough (SRS), in the western ENP. To estimate the volumetric shape of mangroves, I modeled stems as tapered geometrical surfaces called frustums of paraboloids and prop roots (*Rhizophora mangle*) as toroids and cylinders. AGB was estimated by multiplying the TLS-derived volume by wood specific density. My TLS method for the SRS sites resulted in AGB estimates in the range of: 3.9 ± 0.4 to 31.3 ± 3.4 kg per tree in the short mangrove (< 5 m) site, 27.4 ± 3.0 to 119.1 ± 12.9 kg per tree in the intermediate (< 13 m) site and 52.1 ± 6.7 to 1756.5 ± 189.7 kg per tree in the tall (13 – 23 m) mangrove site. My quantitative results: (1) enabled us to develop site-specific allometric relationships for tree diameter and AGB and (2) suggested that TLS is a promising alternative to destructive sampling.

3.2. Overview

Mangroves are among the ecosystems with the highest potential for carbon sequestration and storage (Donato et al., 2011; Alongi, 2012). These coastal ecosystems link terrestrial and aquatic environments; harbor unique biodiversity; provide storm protection; sequester nutrients, sediments and carbon; and provide shoreline stabilization (Alongi, 2002; Giri et al., 2011). Anthropogenic disturbances (e.g. aquaculture,

agriculture and coastal projects), and global warming (sea level rise) are threatening mangrove forests and the ecosystem services they provide (Alongi, 2002). Although mangroves are relatively simple in structure, they are variable in stature (dwarf up to tall) and play an important role as blue carbon storage systems (Mcleod et al., 2011). Of the ecosystem services they provide, carbon sequestration is among the most important. Thus, quantifying the carbon stock of these tropical and sub-tropical tidal forests is of upmost importance as they form a vital part of the carbon cycle and rank among the most productive ecosystems (Twilley et al., 1992; Jennerjahn and Ittekkot, 2002) in the world. In this paper, I take an important first step by assessing the ability of cutting edge ground-based remote sensing technology to quantify one of the two main components of carbon stock: tree-level AGB, in a mangrove ecosystem.

The carbon stock of an ecosystem is usually divided in two major reservoirs: AGB and below-ground biomass (BGB). In mangrove ecosystems and others AGB is often quantified to estimate above-ground carbon content. While estimating AGB might seem to have limited importance for mangrove ecosystems where previous studies have found that mangroves have a high BGB to AGB ratio (Saenger, 1982; Sánchez, 2005) and that most of the biomass (up to 98%) is located and stored below-ground (Donato et al., 2011); ground-based, airborne and spaceborne technologies only provide estimates of the AGB component. Nevertheless, a substantial amount of biomass is located and sequestrated above-ground, motivating the need to generate accurate estimates of AGB in mangrove ecosystems. Additionally, tree-based AGB estimates are relatively simple to transform into estimates of carbon content, by multiplying AGB by the carbon concentration (CC) of the wood. Generally, it is common and accepted to multiply by a

CC that ranges between 45% and 50% (Schlesinger and Bernhardt, 2013). For mangroves, there are reported CC values ranging from 45.9% and 47.1% (Kauffman et al., 2011), which fall on the published range for AGB conversion into above-ground carbon.

To date, the majority of published studies estimating AGB have used allometric equations, which usually relate tree size, shape, volume or AGB to tree diameter. The theoretical basis of allometry assumes that one or more parts of an organism are directly proportional to the growth or size of other tree parts. (Komiyama et al., 2008). Several studies have used allometry to estimate the AGB of mangroves. DBH has been used as a predictive variable to estimate AGB (Imbert and Rollet, 1989; Fromard et al., 1998). Crown area, number of prop roots and total tree height have been used as AGB predictors (Coronado-Molina et al., 2004). DBH and total tree height were excellent AGB predictors (R^2=0.92) in a study by Smith and Whelan (2006) . Finally, DBH and WSD were used to develop generic mangrove allometric equations that predict AGB (Chave et al., 2005; Komiyama et al., 2005).

Drawbacks of the allometric approach include the need for intensive fieldwork and vegetation harvesting to create allometric equations as well as the use of usually only one predictor variable (DBH) since other parameters (e.g. tree height and crown area) often have 10-15% field measurement errors (Fromard et al., 1998). Another drawback is the limited applicability of the derived equations to a certain forest site and specific species. However, frequently, equations derived from one mangrove forest site are applied to other sites without knowing site-specific structural characteristics. Some studies have suggested that species-specific allometric relationships can change between

regions and site conditions (e.g., Smith and Whelan, 2006). It is recommended to use site-specific allometry to predict AGB, as abiotic conditions might yield unique characteristics not captured in general allometric equations (Rivera-Monroy et al., 2013).

Due to some drawbacks of developing allometric equations to estimate AGB, new approaches for precise AGB estimations are needed. In this study, I use a state-of-the-art LiDAR-based TLS to estimate AGB. In recent years, the usage of TLS has been increasing in forestry. The main advantage of a TLS survey is its ability to capture a 3-D image of the forest structure. Several studies have shown that TLS can measure vegetation parameters such as DBH (Hopkinson et al., 2004; Watt and Donoghue, 2005), tree height (Hopkinson et al., 2004; Maas et al., 2008) leaf area index (LAI) (Clawges et al., 2007) and non-explicit parameters such as wood-to-total-tree area and leaf-to-total-tree area (Clawges et al., 2007), basal area (Tansey et al., 2009), stem density (Maas et al., 2008; Liang et al., 2012) and AGB in juvenile trees (Seidel et al., 2011). To date, no study using TLS for a forestry application has been conducted in a mangrove ecosystem.

One common method used to estimate stem AGB of trees is to acquire information on WSD and multiply it by its stem volume. Estimating volume is a challenging task due to the geometry of trees, which resemble tapered surfaces (Husch et al., 2002). Moreover, estimating mangrove tree volume is even more challenging as *Rhizophora mangle* individuals have prop roots. Several studies have reported that AGB allocation into *R. mangle* prop roots can constitute between 2-47% of the total AGB, depending on the maturity of the forest (Lugo and Snedaker, 1974; Gong and Ong, 1990; Fromard et al., 1998; Ross et al., 2001; Coronado-Molina et al., 2004). The goal of my study was two-fold. The first was to use TLS to estimate the volume, AGB, and AGB

allocation of various individuals of different mangrove species. The second goal was to compare and contrast these TLS-derived estimates to published estimates calculated using traditional allometric methods.

3.3. Study Area

My study area was located within a large mangrove forest along the southwestern coast of South Florida. The forest lies within the boundaries of the ENP (Figure 3.1) and consists mainly of three mangrove species: *Rhizophora mangle* L. (Red mangrove), *Laguncularia racemosa* (L.) C.F.Gaertn (White mangrove), and *Avicennia germinans* (L.) L. (Black mangrove). Mangrove canopy height in the region can reach up to 23 meters (Simard et al., 2006). The mangrove communities used in my study area have been extensively studied with substantial research focused on nutrient exchange, root dynamics, physiological responses and CO_2 fluxes (Rivera-Monroy et al., 2007; Barr et al., 2009; Castaneda-Moya et al., 2011).

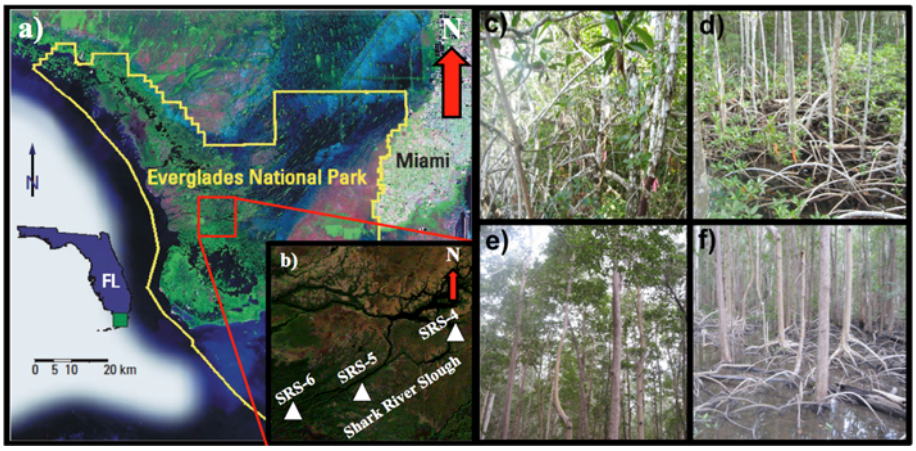

Figure 3.1. a) Location map of the Everglades National Park within the South Florida Peninsula (USGS TIME Project). b) Landsat ETM+ image showing a zoom-in view into the study sites along Shark River Slough. c) Small size mangroves in SRS-4. d) Intermediate size mangroves in SRS-5. e) Tall size mangrove canopy in SRS-6. f) Tall size mangrove prop roots in SRS-6.

Within the study area I selected three measurement sites that were located along a tidal channel of SRS. I selected these sites because they are part of the comprehensively researched Florida Coastal Everglades – Long Term Ecological Research Network (FCE-LTER). The sites differed in the stature of the mangrove community: short (< 5m) (SRS-4), intermediate (< 13m) (SRS-5) and tall (13 – 23m) (SRS-6) (Figure 3.1c - f). *R. mangle* dominates SRS-4 and SRS-5, whereas *R. mangle*, *L. racemosa* and *A. germinans* are more evenly distributed and found in SRS-6. Overall, these sites are representative of the spatial distribution of mangrove species and stature in the coastal ENP (Simard et al., 2006).

3.4. Methods

3.4.1. Terrestrial Laser Scanner Data Collection

I surveyed the three SRS sites with a TLS between March and April 2011. I used the compact and lightweight Leica ScanStation C10 TLS (Figure 3.2) because its technical and physical characteristics are suitable for forestry surveys. The Leica TLS complies with and exceeds the minimum requirements suggested for forestry studies (Maas et al., 2008). These requirements are: a minimum data acquisition range of 50 meters, a scanning rate of 10,000 points per second for field-time efficiency, an hemispheric field of view for data acquisition flexibility and a spot size of 10 millimeters to allow for adequate measurements of stem diameter. A summary of the Leica ScanStation C10 technical specifications is provided in Table 2.1.

Figure 3.2 Leica ScanStation C10 TLS in partially inundated SRS-5 site. (Feliciano et al., 2014).

At each site, I first delineated a ~50 m by 50 m area of mangroves to sample. Within this area I then placed ~15 identifiable targets and reflectors to aid in the merger of point clouds from individual scans into a single point cloud (Figure 3.3). Next, 25 scans (9 in SRS-4, 8 in SRS-5 and 8 in SRS-6) were acquired from various angles to avoid possible occlusions from surrounding vegetation (Figure 3.3). Multiple common targets were needed in order to merge the scans (point clouds). After each scan, every target in the field of view was scanned at a higher resolution to precisely identify its center, in order to reduce point cloud merging uncertainty. Finally, hemispherical photos were acquired and automatically assembled using Leica's proprietary software Cyclone v7.4 (Leica, 2013), which were useful for bark and tree identification (Figure 3.4). The scanning resolution or point spacing for every site was approximately 1 cm at a distance of 10 m. I selected this scanning resolution because it was sufficient to distinguish small

vegetation features such as leaves and small branches, and efficient enough to be acquired in approximately 7 minutes per scan.

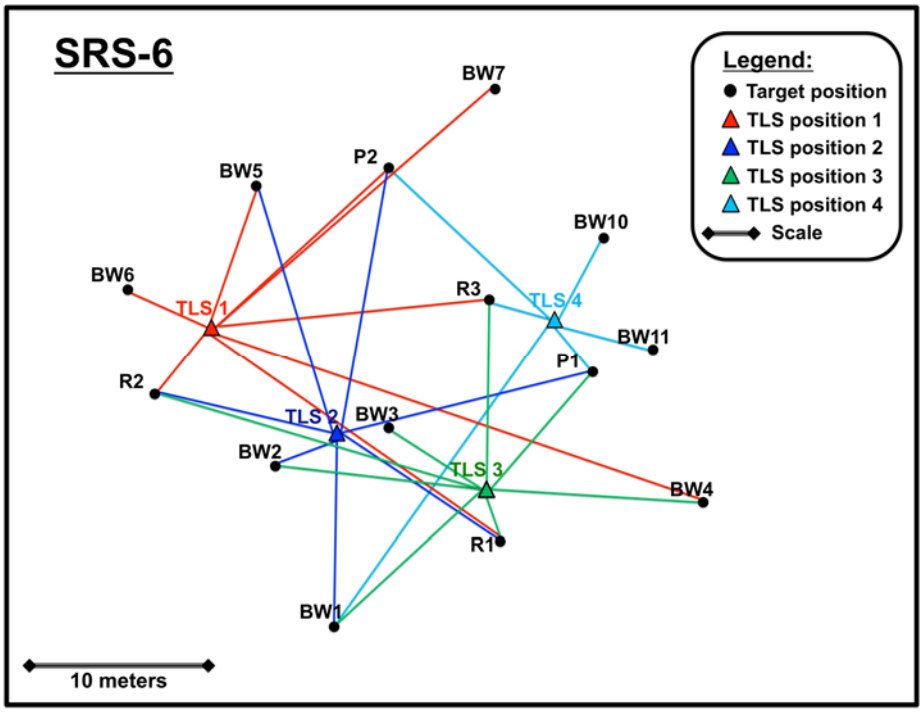

Figure 3.3 Map of main target and TLS position network in SRS-6 site. The actual survey included additional targets and scan positions that were omitted from the plot for clarity.

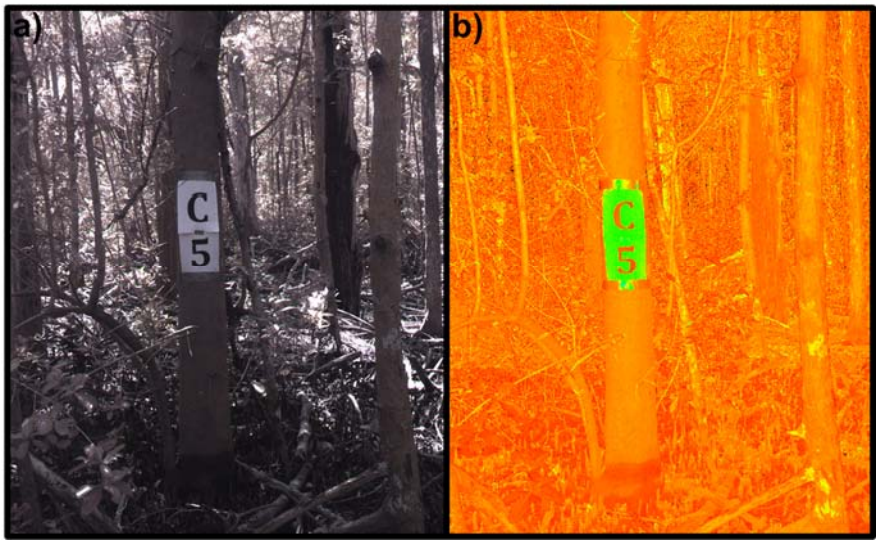

Figure 3.4 Lettered tag in an SRS-6 Black mangrove (Avicennia germinans). a) Photograph taken by the TLS. b) Intensity point cloud acquired by the TLS. Lettered tag visible in the point cloud can be used to help identify a specific mangrove species.

3.4.2. TLS Data Processing

The TLS point cloud data were processed using Leica's proprietary software Cyclone v7.4 (Leica, 2013). The steps for processing the 3-D point cloud data in Cyclone were: target registration, target registration analysis, and point cloud merging. The target registration step consisted of selecting and merging the targets that were common in every single scan. The target registration analysis consisted of a quality control assessment of the root mean square error (RMSE) of the distance between common targets. A low RMSE (e.g. 0.08 meters) is expected for a registered and merged target. Finally, the various point cloud acquisitions were merged and converted into a single point cloud for each site. Usually, a DEM is produced for a TLS study. Due to the extremely flat topography of the ENP a DEM was not necessary for this study.

3.4.3. TLS Data Post-Processing (Tree Volume Geometry Modelling)

Post-processing or secondary processing after basic data processing (merged point cloud) is an important step towards the use of the point cloud for many applications, including calculating tree volume, which I did in this study. The post-processing of the registered and merged point cloud for each site revealed that mangrove stems could be best modelled as a combination of geometric surfaces called frustums (Figure 3.5), as previously suggested by (Husch et al., 2002). A frustum is a portion of any geometric solid with the top part severed. However, frustums were not appropriate to model the curved geometry of prop roots. Therefore, I used a combination of two 3-D geometrical solids; toroids and cylinders, in order to model prop roots associated with the Red

mangrove species. A toroid or torus is a 3-D doughnut shaped solid, which is created by rotating a circle around curved line (Figure 3.6).

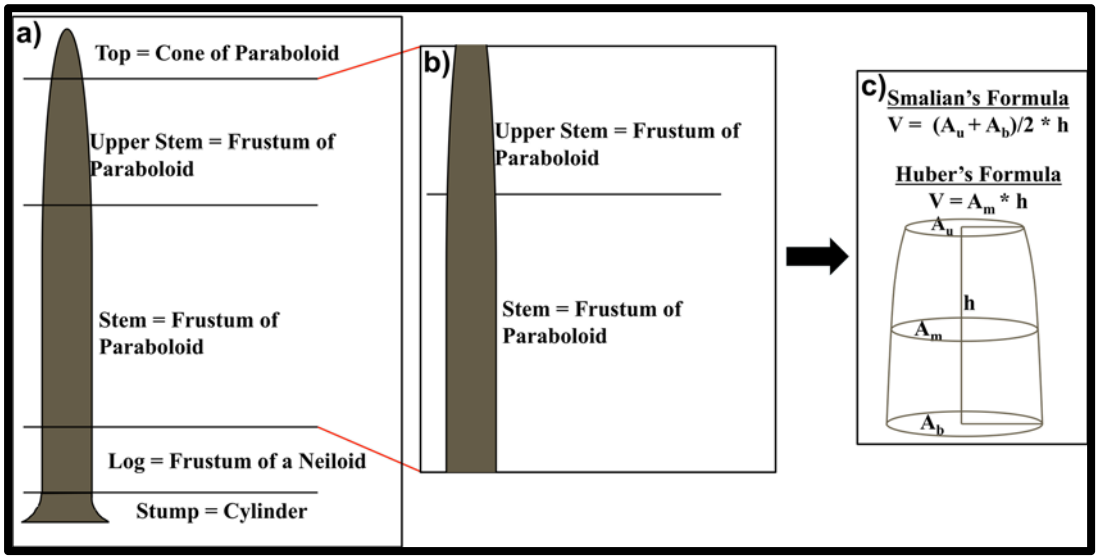

Figure 3.5 a) Suggested frustums by portion of the stem after (Husch et al., 2002). b) Zoom-in towards the frustums used in this study. c) Frustum of a paraboloid volume.

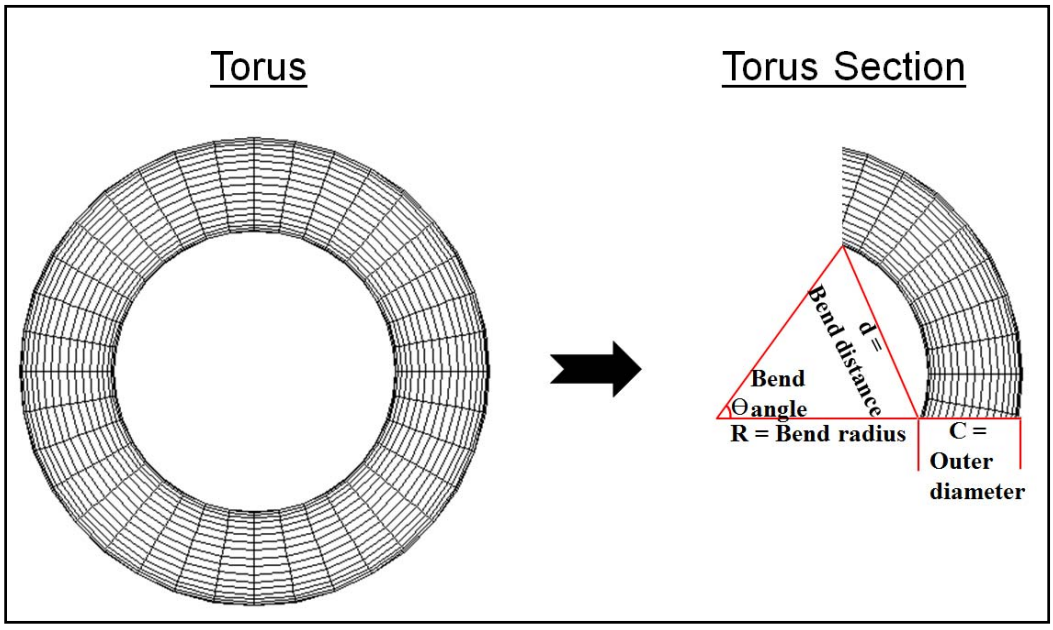

Figure 3.6 Toroidal section parameters.

3.4.3.1. Volume and AGB Estimation of Main Stem

Mangrove stem volume estimation was accomplished by modelling the stem as multiple frustums of paraboloids (Figure 3.5b). I used the Smalian's formula to estimate the parabolic frustum volume (Husch et al., 2002). The Smalian's formula calculates volume by multiplying the average cross-sectional area of a stem section by the stem section's length. The Smalian's volume is given by:

$$V = (A_T + A_B)/2 * h = (\pi D_T^2/4 + \pi D_B^2/4)/2 * h \quad \textbf{(6)}$$

where V is the volume of the stem section, A_T and A_B are the cross-sectional areas of the upper and bottom sections respectively, h is the length of the stem section and D_T and D_B are the diameters of the upper and bottom sections respectively (Figure 3.5c). The first step towards estimating stem volume was dividing the stem into smaller sections (frustums). Using Cyclone software, various cylinders were created at different heights in order to divide the stem into multiple frustums (Figure 3.7). The advanced Cyclone software automatically created best-fit cylinders from the point cloud in locations determined by the operator. I defined a frustum as the region between two created cylinders. In Cyclone, the two end diameters and the section length were then measured for each frustum. Next, these parameters were incorporated into the Smalian's formula to calculate each frustum volume. Finally, the total stem volume was obtained by summing all of the frustum volumes (Figure 3.7).

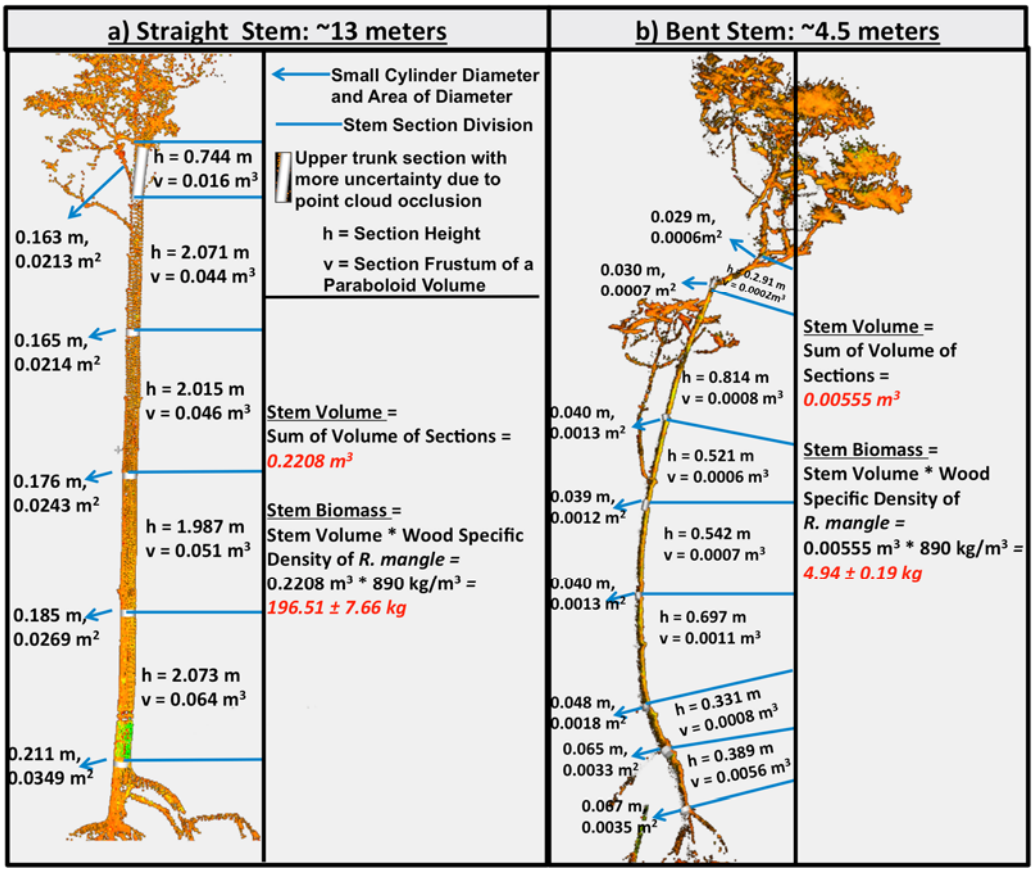

Figure 3.7 Volume estimation example for two types of stem shapes. This method is applicable for the three mangrove species. a) Straight stem volume and AGB estimation. b) Bent stem volume and AGB estimation. Multiple frustums are required where the stem is bent.

For *L. racemosa* and *A. germinans* species the main stem was measured from the ground to the first canopy branch in the point cloud. However, for the *R. mangle* species the main stem was measured from the first prop root up to the first canopy branch. I estimated AGB by multiplying my estimated volume by an estimated species-specific WSD. WSD is usually determined by taking wood cores from trees and weighing them before and after oven drying to determine water content. In lieu of doing this, I compiled a list of published WSD measurements of same mangrove species developed in other neotropical locations (Saenger, 2003; Chave et al., 2009; Zanne et al., 2009; WAC, 2013). For each species I estimated the following WSD values and an uncertainty range:

890 ± 33 kg/m^3 for *R. mangle*, 770 ± 42 kg/m^3 for *A. germinans* and 620 ± 51 kg/m^3 for *L. racemosa*. A median value was used instead of the average, because the WSD sample size for each species in the previous studies was small and the distributions were not normal.

3.4.3.2. Volume and AGB Estimation of Prop Roots (*R. mangle*)

Prop root volume estimation was accomplished by modelling them as a combination of toroidal sections (Figures 3.6, 3.8). I used the toric volume formula to estimate the volume of the roots. The toric volume formula is given by:

$$V = (\pi^2/4) * ((C+R)^2 - R)^2) * (C) * (\theta/360); \quad \textbf{(7)}$$

where C is the outer diameter, R is the bend radius and θ is the bend angle in degrees. For each single prop root, the volume estimation was done in Cyclone (Figure 3.8). Although the majority of prop roots resembled toroidal sections, secondary or smaller prop roots mostly located in the SRS-4 and SRS-5 sites, resembled cylinders. The volume of these cylinder-type prop roots was estimated using a simple cylinder volume formula given by:

$$V = \pi R^2 * h; \quad \textbf{(8)}$$

where R is the radius of the circular cross-section of the cylinder and h is the height of the cylinder.

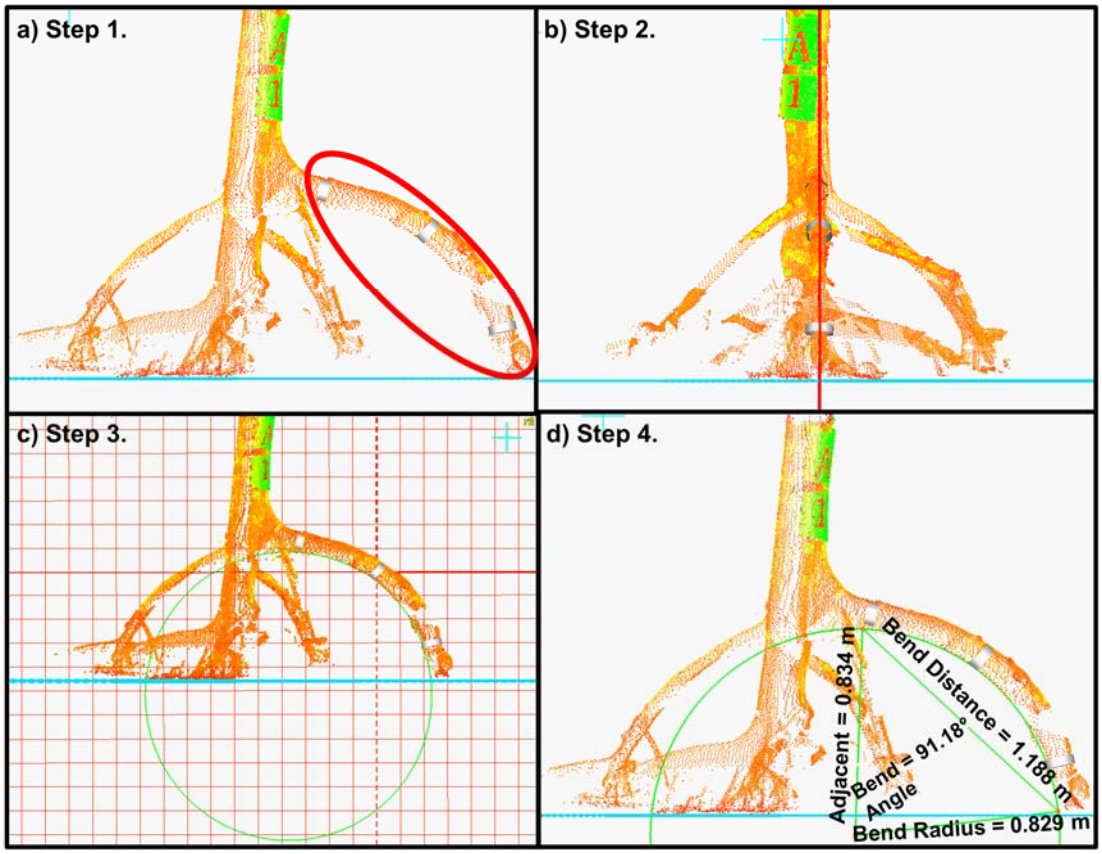

Figure 3.8 Root parameters acquisition for using the toric volume estimation technique for a single root: a) Creation of cylinders to acquire and average prop root diameter in the Y plane. b) Vertical rotation of the point cloud by 90° to the left and creation of a plane (blue line) which cuts the root of interest. This plane is used to create and fit a circle into the root bend. c) Point cloud rotated 90° to the right. A circle is fitted into the root bend. d) A triangle with three known sides is created with the circle in order to estimate the root bend angle.

The volume estimation of the prop roots consisted of the following four steps (Figure 3.8). Step 1: Selecting a prop root with sufficient point cloud data. Step 2: Defining a plane that intersects the prop root of interest. Step 3: Rotating the point cloud by 90° and defining a circle that fits the angular bend of the prop root. Step 4: Defining a triangle with three known sides: bend distance, bend radius and adjacent side. I then applied the Law of Cosines to solve the Side-Side-Side (SSS) triangle and estimate the prop root bend angle. Subsequently, I estimated the toric volume with all of the

parameters that were acquired from the prop root point cloud. These four steps were repeated for every prop root. Finally, I estimated the total prop root volume by adding each single prop root volume. I estimated the total prop root AGB by multiplying the total prop root volume by the *R. mangle* WSD (890 ± 33 kg/m^3).

3.4.4. Canopy Correction

The canopy structure and tree height were not accurately acquired by my TLS survey, because (1) the top sections of canopies cannot be imaged from the ground, and (2) there were line-of-sight obstructions between the TLS and the canopies. In order to be able to compare my results with published mangrove allometry, a canopy estimate was needed. Mangrove canopy AGB allocation estimates range approximately from 10 – 30 % of the total AGB (Clough et al., 1997; Fromard et al., 1998; Komiyama et al., 2005). For this reason I applied a proposed canopy correction (20 ± 10%) to my TLS-based AGB results. I thus multiplied my estimated TLS-based AGB (stem + prop roots) by 1.25 yielding a canopy allocation of 20% of the total AGB every single tree. As a real example from a mangrove in SRS-5, I obtained a TLS-based estimate (stem + prop roots) of 200.2 kg for a specific tree. Multiplying its AGB by a factor of 1.25 would give a total AGB estimate of 250.2. Thus, in this case, the canopy AGB estimate would be 50 kg, which represents 20% of the total AGB. The ± 10% canopy biomass uncertainty was included in the total uncertainty calculation for every tree. I applied my suggested canopy correction (1.25) to every processed mangrove.

3.4.5. Mangrove Allometry from TLS Data

I created two regressions with my TLS-based results (Figure 3.9) in order to generate allometric equations for their use on ENP mangroves. The goal of my regressions was the creation of a common allometric equation (all data points from the three species) and the creation of a *R. mangle* allometric equation, which is the most abundant species. my proposed allometric equations are based on fitting my data with the power function equation. White and Gould (1965) proposed and demonstrated that the power equation has a relationship with allometry. The power relationship is given by:

$$F(x) = a*x^{b}; \quad \textbf{(9)}$$

where $F(x)$ or y is AGB, x is DBH, a represents the allometry coefficient and b represents the proportionality between cumulated variables.

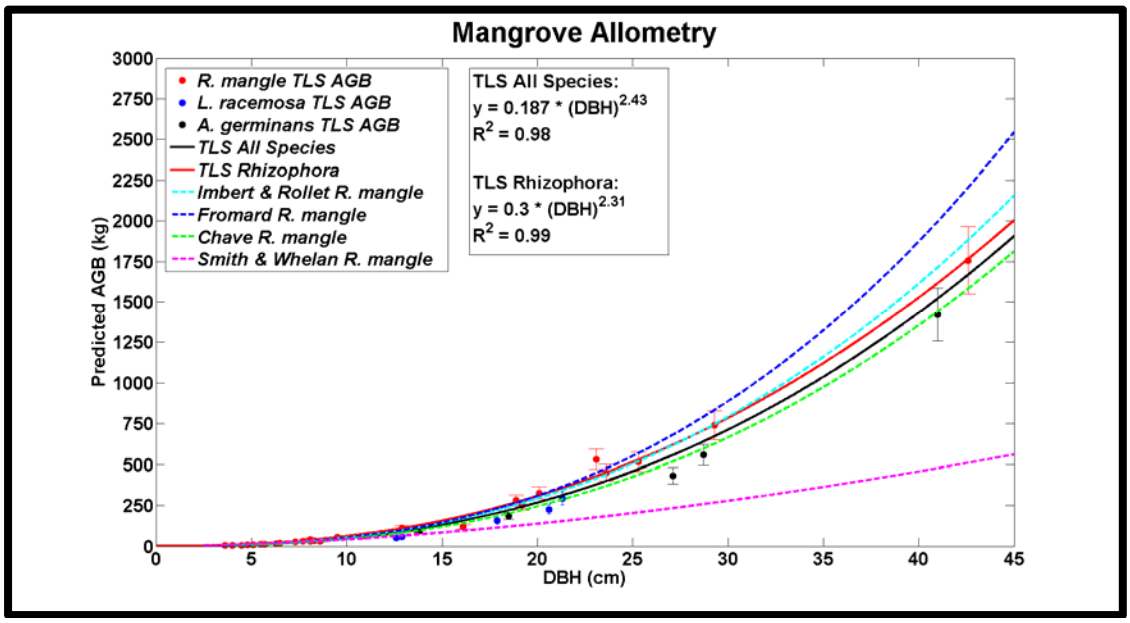

Figure 3.9 Mangrove allometry between DBH and AGB. Data points with uncertainty are derived from my TLS estimates. The regressions calculated in this study are shown in black and red solid lines and published regressions (Imbert and Rollet, 1989; Fromard et al., 1998; Chave et al., 2005; Smith and Whelan, 2006) are shown for comparison purposes.

3.4.6. Mangrove Allometry Comparison

In order to test the reliability of the TLS-based AGB estimations, I compared my results with published mangrove allometric equations. As there are no published allometry for the SRS ENP sites, I used tropical mangrove allometric equations that predict AGB from DBH (Imbert and Rollet, 1989; Fromard et al., 1998), to compare my AGB results. Furthermore, I used allometric equations from Smith and Whelan (2006), which were developed for three different ENP sites (Black Forest: ~27 km from SRS, Mud Bay: ~13 km from SRS and Highland Beach: ~20 km from SRS). These published studies include site-specific allometric equations for the three mangrove species studied in this investigation and use DBH as an AGB predictor. Additionally, I compared my TLS-based AGB results with the mangrove common equation established by Chave et al. (2005), which uses DBH and WSD to predict AGB and can be applied to any mangrove species. I used DBH measurements acquired from my TLS dataset as input for the various allometric equations.

3.5. Uncertainty Analysis

My AGB estimates were calculated by multiplying the TLS-derived tree volume by WSD and then correcting for the unobserved canopy. The calculation components (volume, WSD, and canopy corrections) are known with a range of uncertainties. In order to evaluate the combined contribution of the uncertainties on the AGB estimates, I used an uncertainty propagation analysis. Sources of uncertainties are: TLS measurement error, geometrical parameters of the stem volume (eq. 6) and prop root volume (eq. 7), WSD, and the canopy correction.

3.5.1. Parameter Uncertainties

3.5.1.1. TLS Measurement Errors – The point spacing or resolution of the TLS was set to 1 cm per 10 m, which has an uncertainty of 0.01 divided by √3 (standard uncertainty for a digital device); the resulting uncertainty in very small (~0.5%). As TLS is a high precision tool, point spacing or resolution resulted in a very small uncertainty, which is negligible with respect to the other parameter uncertainties and, hence, omitted from the calculations.

3.5.1.2. Geometrical Parameters - Repeatedly estimating the geometric parameters provides a measure of repeatability and uncertainty. As an example, the fitting of cylinders for the acquisition of diameter measurements into the point cloud was essential in order to estimate the paraboloidal volume of the mangrove stems and toroidal volume of prop roots. The repeated diameter fit analysis revealed the following uncertainties: 0.51-1.32%, depending on vertical location of the cylinder along the stem with an average stem uncertainty of 0.84%. I conducted the same repeatability uncertainty analysis for every parameter involved in the volumetric calculations. For the frustum of paraboloidal/stem volume parameters, the uncertainties were: 0.84% for the diameter (average stem diameter uncertainty) and 0.65% for the paraboloid's height. For the toroidal/prop root volume parameters the uncertainties were: 2.0% for the prop root outer diameter, 0.96% for the bend radius and 1.5% for the bend angle.

3.5.1.3. Wood Specific Density - For each species I estimated, based on literature values (section 3.3.1), the following median WSD value and an uncertainty range: 890 ± 3.7%

kg/m^3 for *R. mangle*, 770 ± 5.5% kg/m^3 for *A. germinans* and 620 ± 8.2% kg/m^3 for *L. racemosa*.

3.5.1.4. Canopy Correction - A canopy correction with an uncertainty of 10% (Section 3.4) was applied to the AGB estimations as the TLS in not able to acquire the entire canopy structure.

3.5.2. Estimation of Uncertainty Propagation

My uncertainty propagation analysis approach is based on my method for estimating total AGB. For *L. racemosa* and *A. germinans*, AGB is defined as:

$$AGB_{Total} = AGB_{stem} + AGB_{canopy}; \quad \textbf{(10)}$$

where AGB_{stem} is stems's AGB calculated as a product of the paraboloidal volume (6) and WSD and AGB_{canopy} is the canopy correction. For *R. mangle*, the total AGB is defined as:

$$AGB_{Total} = AGB_{proproot} + AGB_{stem} + AGB_{canopy}; \quad \textbf{(11)}$$

where the additional $AGB_{proproot}$ is a product of the toroidal volume (7) and WSD.

The stem AGB (AGB_{stem}) for the three species and prop root AGB ($AGB_{proproot}$) for *R. mangle* are product of several volumetric parameters and WSD. Calculating the uncertainty for a frustum of a paraboloid can be complicated, as the volume equation contains both multiplication and addition products (6). However, I can simplify the calculations by assuming that both diameters are identical ($D_T \approx D_B$) and calculate the uncertainty of a cylinder. In this case the stem biomass uncertainty ratio is found by

applying the multiplication uncertainty propagation equation (Taylor, 1997), which for a cylinder is:

$$\frac{\delta AGB_{stem}}{|AGB_{stem}|} = \sqrt{2\left(\frac{\delta D}{D}\right)^2 + \left(\frac{\delta H}{H}\right)^2 + \left(\frac{\delta WSD}{WSD}\right)^2} \quad \textbf{(12)}$$

where $\frac{\delta D}{D}$, $\frac{\delta H}{H}$ and $\frac{\delta WSD}{WSD}$ represent the uncertainty ratio of the diameter, height and WSD respectively.

Similarly, uncertainty propagation for the toroidal volume calculations (12) was estimated by assuming that the prop root's outer diameter is much smaller than the prop root radius (C << R). This assumption reduces the prop root uncertainty AGB ratio calculations to:

$$\frac{\delta AGB_{proproot}}{|AGB_{proproot}|} = \sqrt{2\left(\frac{\delta C}{C}\right)^2 + \left(\frac{\delta R}{R}\right)^2 + \left(\frac{\delta \theta}{\theta}\right)^2} \quad \textbf{(13)}$$

where $\frac{\delta C}{C}$, $\frac{\delta R}{R}$ and $\frac{\delta \theta}{\theta}$ represent the uncertainty ratio of the outer diameter, the bend radius and the bend angle, respectively.

3.6. Results

3.6.1. AGB Estimation and Allocation

My results included 40 processed mangroves (10 *R. mangle* per site, 5 *L. racemosa* in SRS-6 and 5 *A. germinans* in SRS-6). Examples of my TLS- based mangrove stem volume estimations along with AGB results are presented in Table 3.1 for a sub-sample (3 from each site) of *R. mangle* individuals. My calculations of the stem

AGB ranged between 2.68 ± 0.1 kg in an SRS-4 small mangrove up to 1295.35 ± 50.52 kg in a tall mangrove located in SRS-6 (Table 3.1). Another objective of this study was estimating prop root volume and AGB. Table 3.1 also shows examples of total prop root volume and AGB estimations for the same sub-sample (3 from each site) of *R. mangle* individuals. Prop root AGB ranged from 0.47 ± 0.02 kg in a small mangrove located at SRS-4 up to 109.87 ± 5.5 kg in a tall mangrove located at SRS-6 (Table 3.1). Canopy AGB estimations from the proposed canopy correction explained in section 3.4.4 are presented in Table 3.1 for this sub-sample.

Site	TLS-based Main Stem Volume (m^3)	Main Stem AGB (kg)	TLS-based Prop Root Volume (m^3)	Prop Root AGB (kg)	Canopy AGB from Canopy Correction (kg)
SRS-4	0.00301	2.68 ± 0.10	0.000528	0.47 ± 0.02	0.79 ± 0.08
	0.00555	4.94 ± 0.19	0.000640	0.57 ± 0.03	1.38 ± 0.14
	0.00864	7.69 ± 0.30	0.001888	1.68 ± 0.08	2.34 ± 0.23
SRS-5	0.07634	67.98 ± 2.65	0.01417	12.62 ± 0.06	20.15 ± 2.06
	0.07304	65.01 ± 2.54	0.02269	20.19 ± 1.01	21.30 ± 2.13
	0.09016	80.24 ± 3.13	0.01687	15.01 ± 0.75	23.81 ± 2.38
SRS-6	0.22080	196.51 ± 7.66	0.03140	27.96 ± 1.40	56.12 ± 5.6
	0.41680	370.95 ± 14.47	0.06187	55.06 ± 2.75	106.50 ± 10.70
	1.45400	1295.35 ± 50.52	0.12340	109.87 ± 5.50	351.31 ± 35.13

Table 3.1 Mangrove stem/prop root volume, stem/prop root AGB and canopy AGB estimations for a sub-sample of 9 of the 30 processed Rhizophora mangle trees (WSD = 890 ± 33 kg/m^3).

Accounting for prop root, stem and canopy AGB, my TLS-based results for the SRS sites were in the AGB range of 3.9 ± 0.4 to 31.3 ± 3.4 kg per tree in the short mangrove site, 27.4 ± 3.0 to 119.1 ± 12.9 kg per tree in the intermediate site and 52.1 ± 6.7 to 1756.5 ± 189.7 kg per tree in the tall mangrove site (Table 3.2). AGB allocation results were estimated by comparing the proportion of prop root, stem and estimated canopy AGB in the 30 *R. mangle* individuals (10 per site). Overall, prop root allocation

ranged from 10 – 20%, stem allocation was in the range of 60 – 70 %, and based on literature's values, canopy allocation was estimated in the range of 10 – 30%. Comparing the AGB allocation among the sites did not yield systematics trends.

Mangrove Species	TLS-based DBH (cm)	TLS-based AGB (kg); with Canopy Correction	AGB (kg); (Imbert & Rollet, 1989)	AGB (kg); (Fromard et al., 1998)	AGB (kg); (Chave et al., 2001)	AGB (kg); (Smith & Whelan, 2006)
R. mangle	11.0	**61.20** ± 6.61	66.48	65.29	55.84	49.05
	12.9	**112.21** ± 12.12	98.53	98.80	82.77	64.63
	18.9	**280.60** ± 30.30	253.09	266.69	212.60	125.19
	19.2	**250.20** ± 27.02	263.13	277.84	221.03	128.65
	20.1	**326.61** ± 35.27	294.66	312.98	247.51	139.26
	23.1	**532.51** ± 57.51	415.47	449.37	349.0	177.18
	23.6	**450.86** ± 48.69	438.04	475.10	367.95	183.87
	25.3	**517.48** ± 55.89	520.15	569.28	436.93	207.40
	29.3	**740.63** ± 80.00	747.45	833.81	627.86	267.39
	42.6	**1756.53** ± 189.71	1883.92	2206.35	1582.49	511.10
L. racemosa	12.6	**52.08** ± 6.72	60.95	57.48	66.60	48.16
	12.9	**58.34** ± 7.53	64.25	60.96	70.58	50.40
	17.9	**156.55** ± 20.19	133.82	138.27	158.53	94.84
	20.6	**227.09** ± 29.29	183.32	196.46	224.29	124.38
	21.3	**293.29** ± 37.83	197.57	213.57	243.58	132.67
A. germinans	13.8	**95.38** ± 10.97	74.02	76.18	95.35	64.50
	18.5	**187.55** ± 21.57	155.84	153.94	196.67	113.69
	27.1	**432.45** ± 49.73	410.95	384.82	504.97	237.88
	28.7	**560.0** ± 64.40	475.41	441.62	581.83	265.79
	41.0	**1421.55** ± 163.48	1176.31	1039.46	1404.12	529.81

Table 3.2 SRS–6 TLS-based mangrove AGB compared with published mangrove allometry (10 Rhizophora mangle - WSD = 890 ± 33 kg/m^3, 5 Laguncuria racemosa - WSD = 620 ± 51 kg/m^3, 5 Avicennia germinans - WSD = 770 ± 42 kg/m^3).

3.6.2. AGB Uncertainty

The total AGB uncertainty (δAGB_{Total}) for the three species was calculated as the summation of the individual uncertainties of the mangrove segments. Thus, I used the addition uncertainty propagation equation (Taylor, 1997). In my study, it is defined as:

$$\delta AGB_{Total} = \sqrt{\left(\delta AGB_{stem}\right)^2 + \left(\delta AGB_{proproot}\right)^2 + \left(\delta AGB_{canopy}\right)^2} \quad \textbf{(14)}$$

where δAGB_{stem}, $\delta AGB_{proproot}$ and δAGB_{canopy} represent the uncertainty values (in kilograms) of AGB_{stem}, $AGB_{proproot}$ *(R.mangle)*, and AGB_{canopy}, respectively. In order to use the uncertainty ratio, values were calculated in equations (12) and (13), I then scaled them by multiplying them with the calculated AGB for each tree. This scaling is accurate for the *L. racemosa* and *A. germinans*. However, for *R. mangle* the scaling of $\delta AGB_{proproot}$ was conducted, for simplicity, using one third of AGB_{stem}, because the ratio of $AGB_{proproot}/AGB_{stem}$ was smaller than a third (Table 3.3). The total AGB uncertainty for each species was calculated using (eq. 14), which revealed the following uncertainties: 10.8% for *R. mangle*, 12.9% for *L. racemosa* and 11.5% for *A. germinans* (Table 3.4).

Mangrove AGB Segment	**Parameter**	**Uncertainty (%)**	**Uncertainty Propagation (%) Eq. (12) for Stem, Eq. (13) for Prop Root**
L. racemosa **AGB_{stem}**	Height (*H*)	0.65	**8.3**
	Diameter (*D*)	0.84	
	WSD	8.2	
A. germinans **AGB_{stem}**	Height (*H*)	0.65	**5.7**
	Diameter (*D*)	0.84	
	WSD	5.6	
R. mangle **AGB_{stem}**	Height (*H*)	0.65	**3.9**
	Diameter (*D*)	0.84	
	WSD	3.7	
R. mangle **$AGB_{proproot}$**	Outer Diameter (*C*)	2.0	**5.0**
	Bend Radius (*R*)	0.96	
	Bend Angle (°)	1.5	
	WSD	3.7	

Table 3.3 Parameter uncertainty estimates for the three mangrove species in the ENP.

Total AGB Uncertainty (%) for Each Species using Eq. (14)			
Mangrove Species	**Mangrove AGB Segment Uncertainty (%)**		**Total AGB Uncertainty (%)**
L. racemosa	AGB_{stem}	8.3	**12.9**
	AGB_{canopy}	10	
A. germinans	AGB_{stem}	5.6	**11.5**
	AGB_{canopy}	10	
R. mangle	AGB_{stem}	3.9	**10.8**
	$AGB_{proproot}$	1.3*	
	AGB_{canopy}	10	

Table 3.4 Total AGB uncertainty estimates (%) for the three mangrove species in the ENP.

*** For *R. mangle* the scaling of $\delta AGB_{proproot}$ in Eq. (13) is conducted, for simplicity, using one third of AGB_{stem}, because the ratio of $AGB_{proproot}/AGB_{stem}$ is smaller than a third (Table 3.3).**

3.7. Discussion

3.7.1. Mangrove Allometry from TLS Data

I created two regressions with my TLS-based results (Figure 3.9) in order to generate allometric equations for their use on ENP mangroves. my estimated individual AGB values versus DBH measurements, along with my TLS-based regressions are shown in Figure 3.9. For comparison purposes, the regressions from the other compared studies were plotted. The goal of my regressions was the creation of a common allometric equation (all data points from the three species) and the creation of a *R. mangle* allometric equation, which is the most abundant species. My *R. mangle* regression (AGB = $0.3 * x^{2.31}$) is more similar to the Imbert and Rollet (1989) regression (Figure 3.9). My proposed common (three species) mangrove regression (AGB = $0.187 * x^{2.43}$) resembles that of Chave et al. (2005), which is also a common mangrove regression. Overall, my SRS-4, SRS-5 and SRS-6 AGB results were inside or close to the range of the estimations obtained from the three published allometric studies, suggesting the potential

of TLS as an AGB estimation tool. A trend of stem height and AGB was noticed in my study; however, as the focus of the paper was to compare allometry of published studies that predict AGB from DBH this information was not included.

3.7.2. Mangrove Allometry Comparison

A visual comparison between my results and the published mangrove allometry in the form of regressions is presented in Figure 3.9. Below a 20 cm DBH, my data fit all of the *R. mangle* regressions except Smith and Whelan (2006). Above 20 cm, my data fit the Imbert and Rollet (1989) and Chave et al. (2005) regressions, whereas Fromard et al. (1998) does not. The non-fitting of Fromard's regression above 20 cm could be due to the fact that it was created for a limited DBH range (up to 32 cm for *R. mangle*). The closest fit to my results is presented by Imbert and Rollet's regression. Interestingly, the ENP study by Smith and Whelan (2006) predicts lower AGB values when compared to all of the regressions. However, as their study suggested, environmental factors such as the hydrology, salinity, nutrient availability of a specific region or site could yield different and variable AGB values. Although not presented in Figure 3.9 as regressions (not enough points), my *L. racemosa* and *A. germinans* mangrove results were highly comparable to the common equation developed by Chave et al. (2005). This resemblance could be due to the fact that the common equation uses WSD in addition to DBH (up to 50 cm) to constrain the AGB estimation. On the other hand, the *L. racemosa* and *A. germinans* mangroves equations developed by Fromard et al. (1998) and Imbert and Rollet (1989) use only DBH for a more limited range and yielded more dissimilar results when compared to my estimates and the Chave et al. (2005) equation results. Although I

extrapolated predicted values from the published studies (Figure 3.9) for comparison purposes, it is of upmost importance to understand that using DBHs larger than those specified by the allometric equations might give more AGB uncertainties. Furthermore, site-specific variations in mangrove architecture between my study areas and those published, including the ENP study by Smith and Whelan (2006) could also yield AGB differences.

3.7.3. TLS Data Analysis

In my TLS data analysis, for fairly straight stems (Figure 3.7a) I found that the creation of four frustum sections best approximated the true volume of the stem, as the creation of more sections did not change the estimated volume by a significant quantity. This was the case for most of the stems of the more mature mangroves located in SRS-6, which can reach up to ~23m in canopy height. I suggest that this method is applicable for the three species in the ENP. On the other hand, special consideration had to be taken to estimate the volume of bent stems (Figure 3.7b). The 3-D point cloud showed that small to intermediate size mangroves (up to ~13 m) located in SRS-4 and SRS-5 tended to have a more bent stem structure. My approach for the volume calculation of a bent stem consisted of starting with a frustum section at approximately every bending point in order to create smaller straight stem sections (Figure 3.7b). For prop roots, whether they resemble toroidal sections or cylinders, I estimated the total prop root volume of a particular tree as the sum of every singular prop root volume (Figure 3.8).

My methodology and analysis was focused on the AGB estimation of the main stem and prop roots as a substantial amount of the above-ground carbon is stored in these

areas. It is important to understand AGB allocation in these two structures, as they are the foundation of biomass replacement for branches, leaves and twigs which are shed and converted to litterfall (detritus and deadwood) throughout the year (Clough, 1992). Although my prop root and stem TLS-based AGB allocation estimations are comparable with published mangrove studies (Clough et al., 1997), biogeographic dissimilarities and site-specific environmental factors could result in different AGB values and allocation for different regions (Smith and Whelan, 2006).

3.8. Conclusion

I used TLS data to estimate mangrove stem and prop root volume and AGB in various mangrove individuals located in the ENP. The use of TLS data in addition to the proposed canopy correction proved to be successful in estimating mangrove AGB and showed comparable results with published mangrove allometry. I suggest that the methodology presented in this paper could be nearly as accurate as destructive techniques, as tree volume is analyzed and processed as a tree-by-tree basis with a state-of-the-art tool. TLS data presents a unique opportunity to evaluate and analyze prop root AGB and structure, which has not been done in much detail. In addition, TLS presents the advantage of acquiring and analyzing tall mangroves, which is not possible with traditional methods, as it would encompass an enormous task to harvest and sample such mangroves. Furthermore, mangrove harvesting is prohibited in protected ecosystems such as the ENP. The results of this case study revealed that although mangrove structure could be complex (bent structures) there is potential for the use of TLS in this kind of wetland environment.

I suggest that the use of TLS could be a substitute tool to destructive sampling and harvesting, towards the creation of allometric equations. For this reason I proposed ENP mangrove allometric equations with the data acquired and analyzed in this study. Sources of discrepancies between my estimations and the published allometry may have arisen from uncertainty or from the allometric equations themselves, which were developed for specific mangrove forest locations. Future research should seek the integration of Airborne LiDAR data with TLS data in order to acquire the full canopy structure, enhance the total AGB estimation and expand the study area. The use of TLS presents the advantage of estimating various sources of uncertainties, which is not common for this type of study. It is of upmost importance to mention that my TLS methodology is not limited to AGB studies. There is potential to apply these methods to quantify structural damage after storms, hurricanes and fires, or to monitor stand development along different sites. This is the first reported TLS study for a mangrove ecosystem.

Chapter 4: Estimating Mangrove Canopy Height and Above-Ground Biomass in Everglades National Park with Airborne LiDAR and TanDEM-X Data

4.1. Summary

Mangrove forests are difficult to monitor from the ground, due to their large spatial extent and restricted accessibility. The coastal mangroves forests of the ENP are well protected from development. However, climate change and other anthropogenic disturbances have affected these intertidal ecosystems. Monitoring forest structure parameters (canopy height and AGB) is important for the establishment of an historical database for past, present and future ecosystem comparisons. It is possible to study the vertical structure of forests (canopy height) using remote sensing sensors from air- or spaceborne LiDAR/Laser Scanning or spaceborne SAR systems such as SRTM and TanDEM-X. In this study, I estimated mangrove canopy height in the ENP using an Airborne LiDAR dataset and TanDEM-X data acquired during the years 2011-2014. Analysis of the Airborne LiDAR and TanDEM-X datasets showed that mangrove canopy height can reach up to ~25 m close to the coastal ENP waters and the mean canopy height in the whole mangrove forest is located around ~9.7 m. The comparison of the Airborne LiDAR and the TanDEM-X data yielded an $R^2 = 0.85$ and RMSE = 1.96 m. To estimate AGB at the plot-scale I used ground-based LiDAR a.k.a TLS. The AGB TLS-based results indicate values ranging from 197.5 ± 22 Mg/ha for short mangroves, to 460 ± 60 Mg/ha for tall mangroves. The TLS-based results suggest that there might be higher AGB/carbon content in the ENP than previously thought.

4.2. Overview

Mangrove forests are difficult to monitor, due to their large spatial extent and limited accessibility. Although the coastal mangrove forests of ENP are well protected from development, climate change, sea level rise and other anthropogenic disturbances have affected these intertidal ecosystems (Alongi, 2002). Monitoring changes in the vertical structure (canopy height) and AGB is vital for the establishment of an historical database for past, present and future ecosystem comparison, especially on mangroves as they provide beneficial ecosystems goods and services (Alongi, 2002; Giri et al., 2011). High-resolution remote sensing technology represents a useful tool for quantifying forests structural parameters such as canopy height and AGB from local up to global scales.

The vertical structure of forests have been studied using multi-spatial remote sensing sensors including Airborne LiDAR/Laser Scanning (Airborne LiDAR) (Hyyppä et al., 2004; Simard et al., 2006), SRTM (Simard et al., 2006; Fatoyinbo et al., 2008) and TanDEM-X (Hajnsek et al., 2009; Sadeghi et al., 2014). A previous study of the canopy height and AGB in the ENP mangroves was conducted a decade ago based on Airborne LiDAR data acquired in 2004 in conjunction with SRTM data acquired in 2000 (Simard et al. 2006). Although Airborne LiDAR data is very useful and accurate for forestry applications, its acquisition is expensive and cover relatively small regions, representing an enormous disadvantage when compared with space-based SAR remote sensing sensors such as SRTM and TanDEM-X. The TanDEM-X mission represents a great opportunity to estimate mangrove canopy height over wide areas using data with no temporal decorrelation (Krieger et al., 2007), an important element in the processing of a canopy height map, also known as DCM, derived from InSAR data.

In this study, I introduce the use of higher spatial resolution Airborne LiDAR data in addition to TanDEM-X data with higher horizontal (12 m) and relative vertical (< 2 m) resolutions than SRTM data. I use DCMs derived from Airborne LiDAR and TanDEM-X data to validate and estimate mangrove canopy height in the ENP. Additionally, I use ENP site-specific AGB measurements derived from TLS (Feliciano et al., 2014) to estimate mangrove AGB. My study explores the use of three high-resolution multi-spatial techniques: TLS, Airborne LiDAR and SAR in a coastal mangrove ecosystem. The main goal of this study is to produce forest structure maps that includes canopy height and AGB in the ENP mangrove ecosystem using the aforementioned multi-sensor and multi-scale datasets. These maps could become a framework for past and future ecosystem comparison, including the quantification of mangrove habitat growth or destruction, and biomass distribution.

4.3. Study Area

My study area comprises the mangrove forests located along and adjacent to the coastal boundaries of the ENP (Figure 4.1) and estimated to cover an area of 144,447 ha (Simard et al., 2006). The forests are well protected and consist of various species, including: *Rhizophora mangle* (Red mangrove), *Laguncuria racemosa* (White mangrove) and *Avicennia germinans* (Black mangrove). Mangrove canopy height can reach up to 25 meters in the western boundary of the park, where SRS connects with the Gulf of Mexico (Simard et al., 2006). For this study, mangrove canopy height and AGB calibration sites were established along SRS as this region has been extensively researched by the Florida Coastal Everglades – Long Term Ecological Research Network scientific community

(FCE-LTER, 2013). The sites differed in the canopy height of the mangrove community: short (< 5 m) (SRS-4), intermediate (< 13 m) (SRS-5) and tall (13 – 23 m) (SRS-6) (Figure 4.1c - f). *R. mangle* dominates SRS-4 and SRS-5, whereas *R. mangle*, *L. racemosa* and *A. germinans* are more evenly distributed in SRS-6. The mangrove structural and environmental gradient along SRS, resembles the majority of the mangrove communities in the coastal ENP (Chen and Twilley, 1999; Castañeda-Moya et al., 2013).

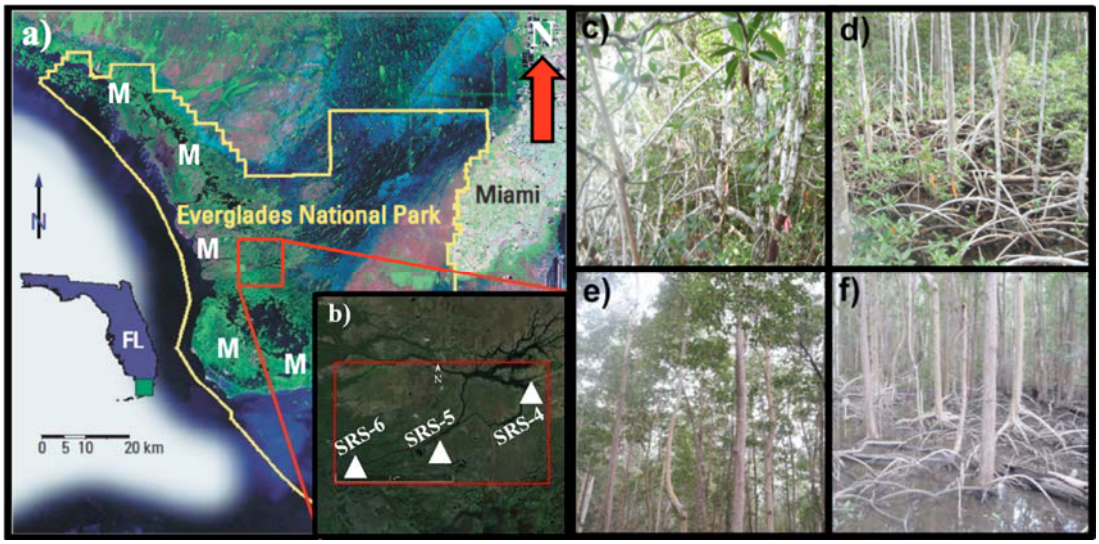

Figure 4.1 a) ENP location map within the South Florida Peninsula showing mangrove (M) forest location. b) Zoom-in to SRS area. Red polygon shows the extent of the Airborne LiDAR survey. c) SRS-4 (short size mangroves). d) SRS-5 (intermediate size mangroves) e) SRS-6 (tall size mangroves). f) SRS-6.

4.4. Datasets and Methods

In this study I acquired and processed four datasets that are described in the following sub-sections: TLS, Airborne LiDAR, Worldview-2 imagery and TanDEM-X. The TLS dataset was used to estimate site-specific AGB in the three SRS sites (SRS-4, SRS-5 and SRS-6). The Airborne LiDAR served for validating and comparing the TanDEM-X data. Airborne LiDAR observations are very precise for forest structure studies (Hyyppä et al., 2004). However, an Airborne LiDAR survey of the entire

mangrove region would be extremely expensive and would devote enormous amount of resources and field time. Thus, I used TanDEM-X data, which can be used to estimate canopy height and covers the entire ENP mangrove forest, as the Airborne LiDAR dataset only included a small portion of the total mangrove cover in the ENP. A detailed explanation of the TanDEM-X Pol-InSAR data processing is located in sub-section 2.3.2.

4.4.1. Ground Measurements

4.4.1.1. Terrestrial Laser Scanning

A very high-resolution (cm) TLS point cloud dataset was acquired for the three SRS sites between March and April 2011 (Feliciano et al., 2014). TLS survey plot sizes for the SRS sited were: 50 x 50 m for SRS-4, 50 x 50 m for SRS-5 and 100 x 50 m for SRS-6. A compact and lightweight Leica ScanStation C10 TLS (Figure 3.2) was used because of its technical and physical characteristics are best suited for forestry surveys. The TLS surveys were located inside the Airborne LiDAR sample area discussed in the next section. A very detailed explanation of the TLS processing and results can be found in Feliciano et al. (2014).

The purpose of the TLS data for this study is estimating site-specific AGB (Feliciano et al., 2014) in megagrams per hectare (Mg/ha) for the three SRS sites. The TLS data enabled us to measure DBH for trees located inside the three plots (Figures 4.2, 4.3). To obtain the total AGB in one hectare (100 x 100 m) plots, I multiplied the 50 x 50 m AGB estimates by 4.

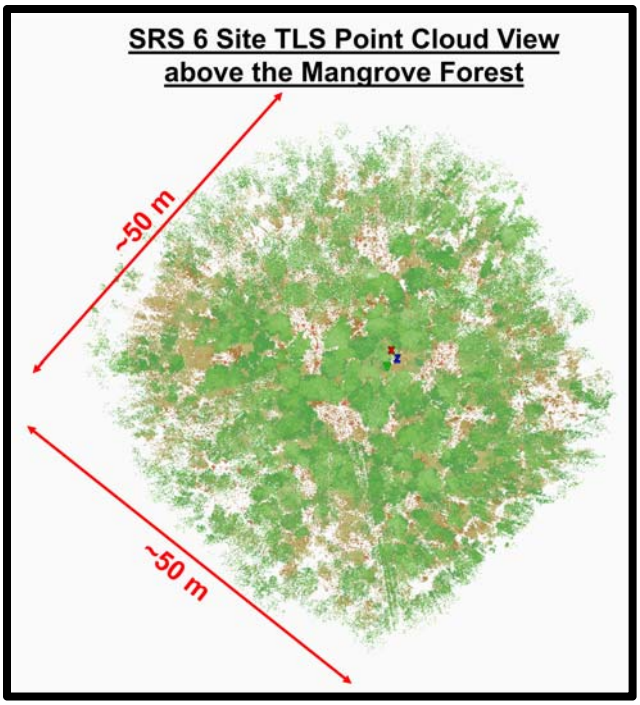

Figure 4.2 ~50 x 50 m TLS SRS-6 mangrove plot used to acquire DBH measurements. Brown color represents ground and green color represents mangrove canopies.

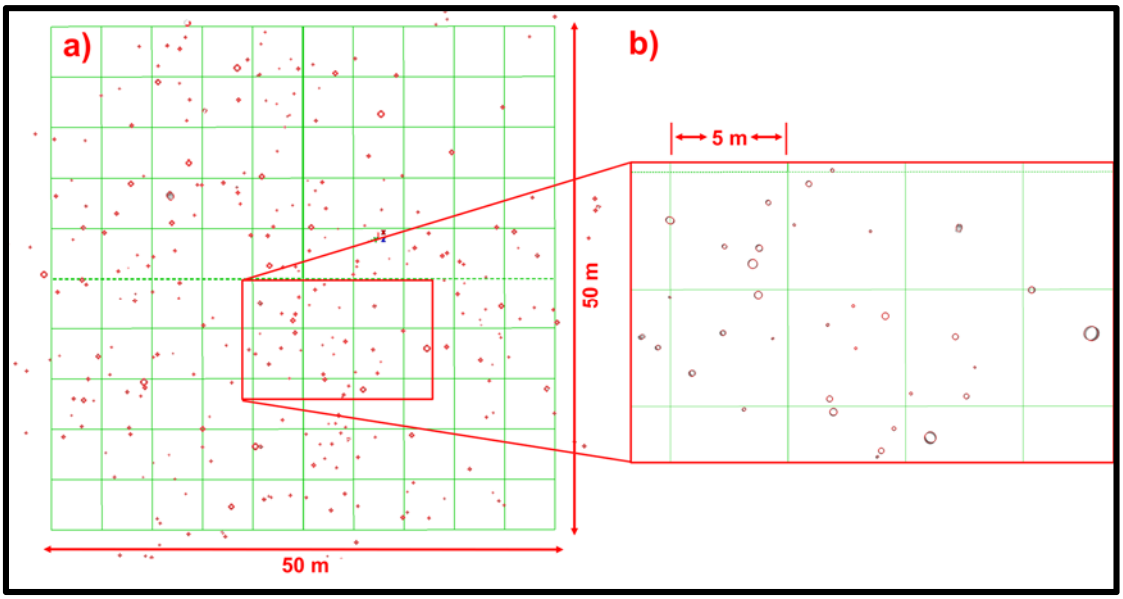

Figure 4.3 a) 50 x 50 m TLS plot in SRS 6 showing DBH measurement (cylinder) locations. b) Zoom into figure 4.3 a. In order to acquire DBH measurements the entire forest point cloud (Figure 4.2) was cut at a height of 1.3 m for the creation of cylinders where mangrove stems were located.

4.4.2. Airborne Measurements

4.4.2.1. Airborne Laser Scanning

The Airborne LiDAR data was acquired using an Optech ALTM operated by NCALM based at the University of Houston. The Airborne LiDAR survey was conducted on November 17, 2012 and comprised an approximate 30 km^2 transect that covered the mangrove height gradient across SRS (Figure 4.1b). Technical specifications for this survey are provided in Table 2.2. The data was processed using for retrieving first and last laser returns. The first returns, which mark the location of three canopies, were used to generate a DSM (Figure 4.4a). The last returns, which mark the location of the ground surface, were used to generate a DTM (Figure 4.4b). A 1 m DCM (Figure 4.4c) was produced by subtracting the DTM created with the bare ground points from the DSM created with the top of the canopy points. The Airborne LiDAR DCM was georeferenced into a NAD83 datum and UTM 17N projection.

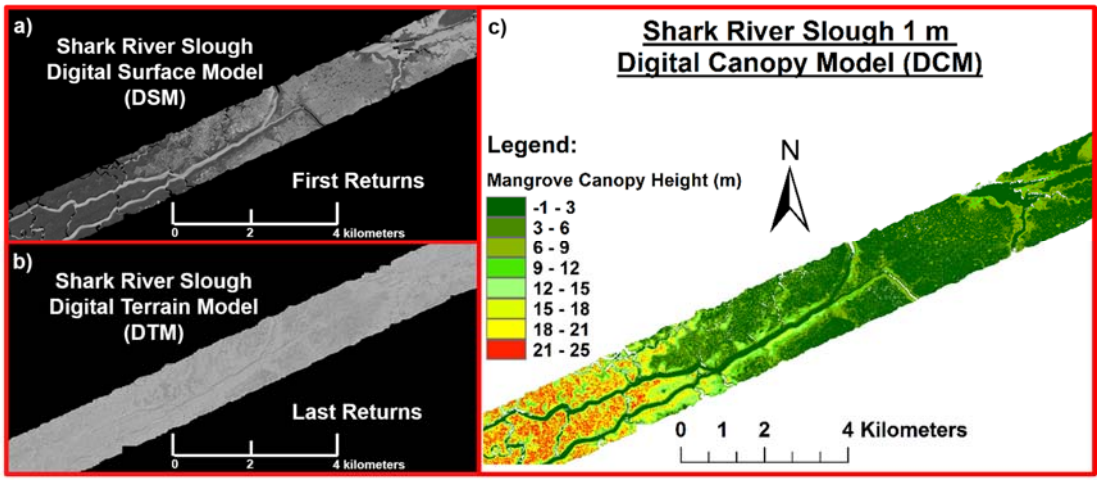

Figure 4.4 Airborne LiDAR derived elevation products of the SRS swath. a) Digital Surface Model hillshade. b) Digital Terrain Model hillshade. c) Digital Canopy Model created by subtracting the DTM from the DSM.

4.4.3. Space-based Measurements

4.4.3.1. WorldView-2 Mangrove Cover Map

Seven optical images acquired by WorldView-2 satellite from November 2010 to December 2012 were used for updating mangrove cover map of the ENP (Figure 4.5b), as the most recent vegetation map was created in 1999 (Welch and Madden, 1999). The high-resolution (1.84 m Multispectral, 0.46 m Panchromatic) imagery was provided by Digital Globe Foundation as part of a graduate student imagery grant. The images were atmospherically corrected, mosaicked and classified. In order to improve the accuracy of the classification, an atmospheric correction was applied in ENVI software to retrieve the surface reflectance by removing atmospheric effects (atmospheric particles that are absorbed or scattered from the earth surface radiation). The classification step consisted on performing a supervised classification, using training points of mangrove versus non-mangrove regions, clustering pixels of similar spectral signature into various classes. Mangroves have a distinct bright reddish spectral signature color that is very noticeable in the infrared spectrum (False Color Composite: Bands 7-5-3) (Figure 4.5a). To validate and train the mangrove versus non-mangrove classification, high-resolution geo-tagged helicopter photography and videography was acquired in June 2014 (Figure 4.6). The purpose of this map was to constrain the study area to the mangrove region inside the park and mask this region from the TanDEM-X dataset as the focus of this study are the mangrove forests.

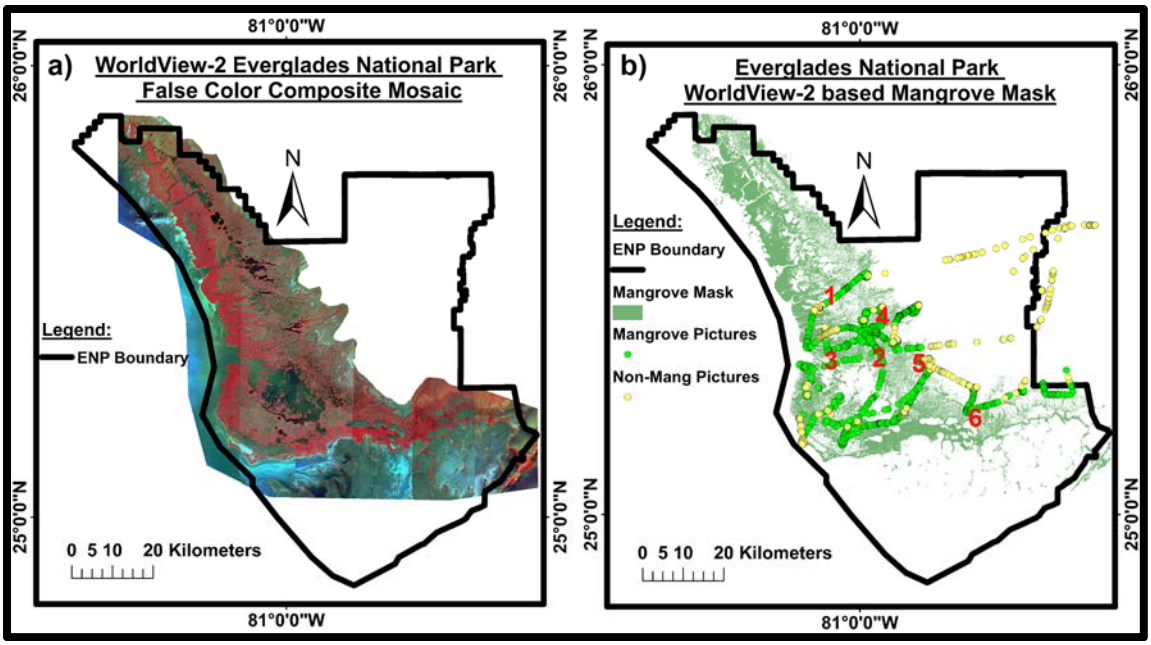

Figure 4.5 a) WorldView-2 imagery (7 scenes) used to classify mangrove cover. Mangrove cover shows a bright red spectral signature, mostly located at the Western and Southwestern areas of the map. b) Mangrove cover mask created with WorldView-2 and validation points obtained from high-resolution geo-tagged airborne photography. Red numbers show the locations of photos shown in Figure 4.6.

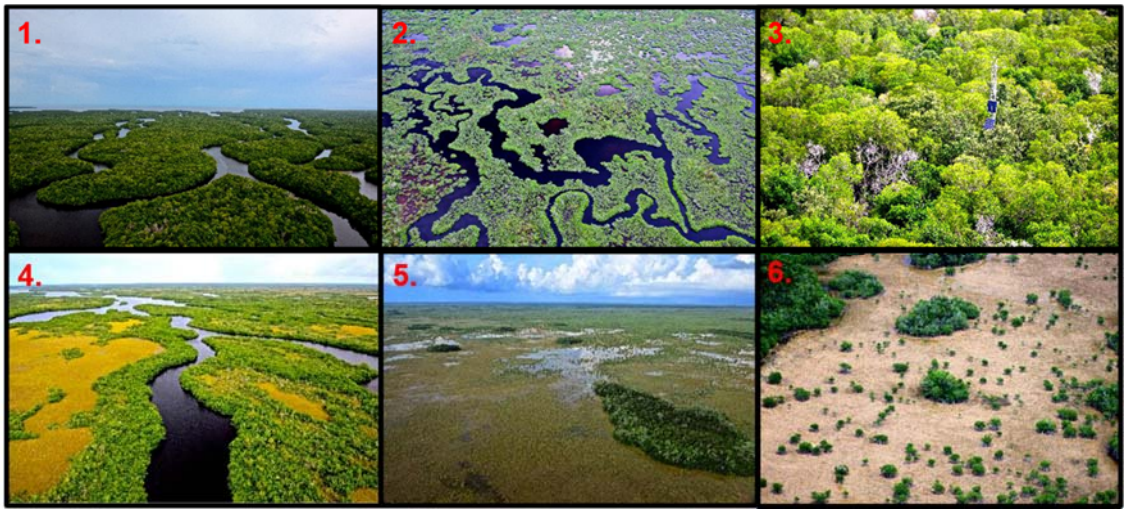

Figure 4.6 Example of geo-tagged photography acquired inside the ENP: 1. Mangroves at the mouth of Shark River Slough, 2. Short mangroves, 3. Tall mangroves in SRS-6 site. 4 Short mangroves and sawgrass located at the Northwestern region of Shark River Slough, 5. Tree islands and mangroves near the boundary of the mangrove transition zone. 6. Mixture of tree islands and short mangroves.

4.4.3.2. TanDEM-X Data

The TanDEM-X mission was launched in June 2010 and its main mission objective is the production of a worldwide high resolution (< 2 m relative vertical accuracy and 12 m horizontal raster spacing) DEM using radar interferometry with its twin satellite TerraSAR-X (Krieger et al., 2007). In contrast, the highest resolution of the current globally available DEM generated by the SRTM mission is 30 m (horizontal raster spacing) (Kellndorfer et al., 2004).

A total of 4 TanDEM-X scenes were used to cover all of the ENP mangrove forests (Table 4.1). The scenes were single-pol (HH) and were acquired in bistatic stripmap mode, in which one satellite emits the signal and both satellites receive the backscattered signal nearly at the same time with no temporal decorrelation (Krieger et al., 2007). The single-pol scenes were retrieved from the German Aerospace Center (DLR) global DEM acquisition archive.

Acquisition Date	UTC Time (hh:mm:ss)	Polarization	Incidence Angle (°)	Height of Ambiguity	Bandwidth (MHz)	Effective Baseline (m)
2011/03/06	23:30:39	HH	46.27	39.54	100	203
2011/11/09	23:22:03	HH	33.85	-48.73	100	109
2013/05/17	23:30:45	HH	48.08	-60.86	100	140
2013/05/17	23:30:52	HH	48.08	-60.68	100	141

Table 4.1 TanDEM-X scenes used in this study.

The TanDEM-X data processing for obtaining forest height was based on the Pol-InSAR RVoG model, which consists of two independent layers: (1) volume layer of randomly oriented vegetation scatterers and (2) impenetrable bottom/ground layer (Treuhaft et al., 1996; Cloude and Papathanassiou, 2003). More details of the RVoG model and TanDEM-X Pol-InSAR data processing can be found in sub-section 2.3.2 of this dissertation. A very detailed explanation of the Pol-InSAR theory and application can

be found in Cloude and Papathanassiou (1998), Papathanassiou and Cloude (2001) and Cloude and Papathanassiou (2003). Figure 4.7 shows an example of the TanDEM-X processing results, including interferometric coherence, interferometric phase and DCM.

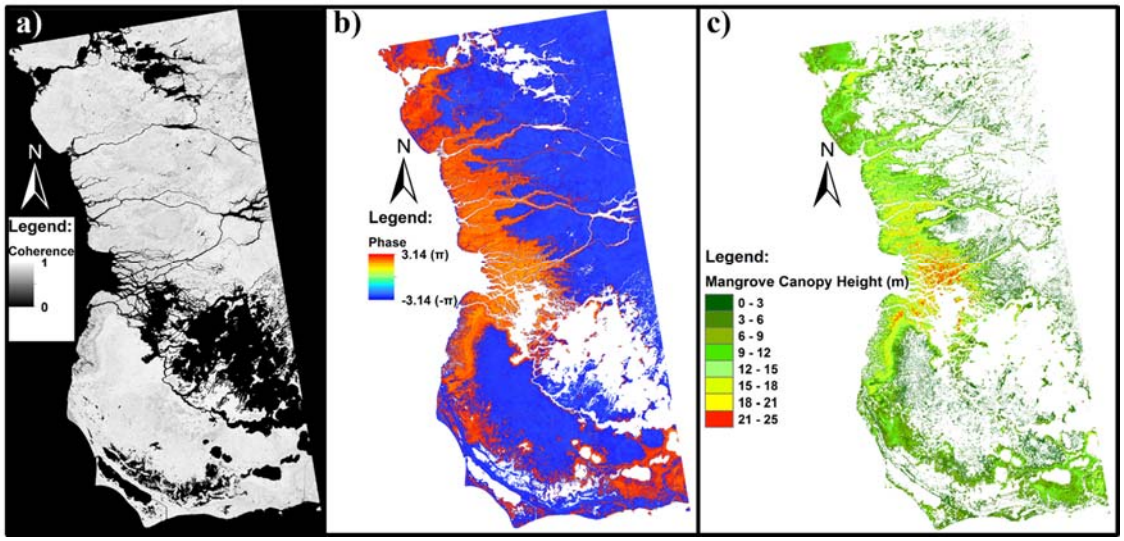

Figure 4.7 TanDEM-X scene of the Western Everglades. The data for this scene were acquired on 2013-05-17. a) Coherence. b) Phase. C) Forest height DCM after Pol-InSAR inversion.

4.6. Multi-Scale Canopy Height Data Calibration Results

The mangrove canopy height validation involved the comparison between the SRS Airborne LiDAR transect acquired in November, 2012 and a processed single-pol (HH) TanDEM-X scene acquired in May, 2013. Although the two datasets were acquired six months apart, I assume no vegetation change between the two acquisitions, as it is a very short time for significant changes in growth or mortality in mangrove forests.

4.6.1. Airborne LiDAR vs. TanDEM-X Canopy Height Validation along the Shark River Slough

The entire TanDEM-X DCM for this single-pol scene can be seen in Figure 4.7c, plotted in the range of 0 – 25 m. The TanDEM-X DCM was produced at a spatial

resolution of 10 m, whereas the Airborne LiDAR resolution is 1 m. In order to compare both datasets, I resampled (highest pixel value) the Airborne LiDAR dataset to 10 m (Figure 4.8a). Visual inspection shows a very good agreement between the Airborne LiDAR-based DCM and the SRS TanDEM-X-based DCM results (Figure 4.8).

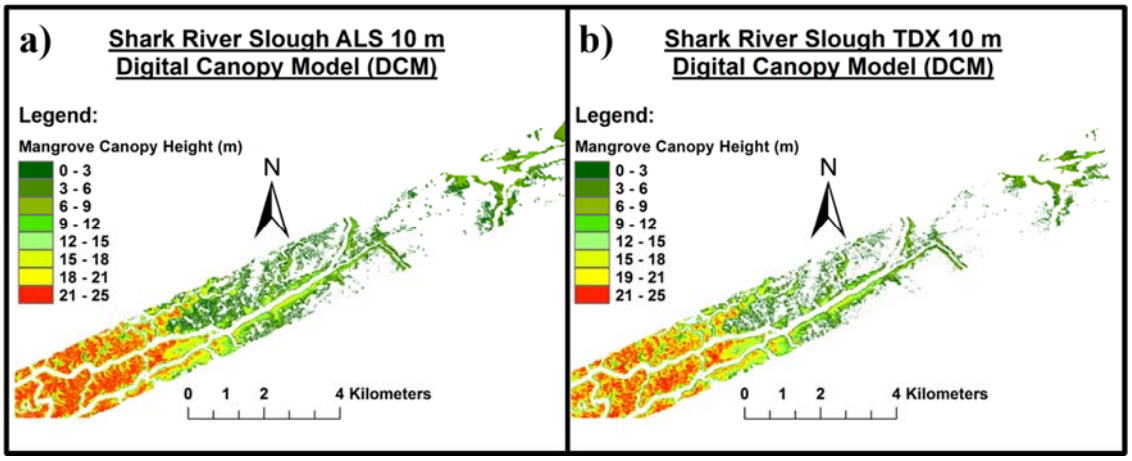

Figure 4.8 a) Airborne LiDAR -derived 10 m SRS DCM. b) TanDEM-X-derived 10 m SRS DCM.

In order to quantitatively validate the TanDEM-X results, I used the H100 model, which is extensively used in forest studies. H100 exemplifies the mean height of the 100 tallest trees per hectare. The validation plot (Figure 4.9) between the Airborne LiDAR and TanDEM-X mangrove canopy heights in SRS yielded an R^2 correlation coefficient of 0.85 and an RMSE of 1.96 m. Airborne LiDAR data is available to validate only one TanDEM-X scene. The other 3 processed scenes lie in areas where Airborne LiDAR data are not available, hence, were not validated. The validated scene covers the SRS region, which is representative of the spatial distribution of mangrove species and stature in the coastal ENP. Thus, I assume the same uncertainties can be applied to the other 3 TanDEM-X scenes.

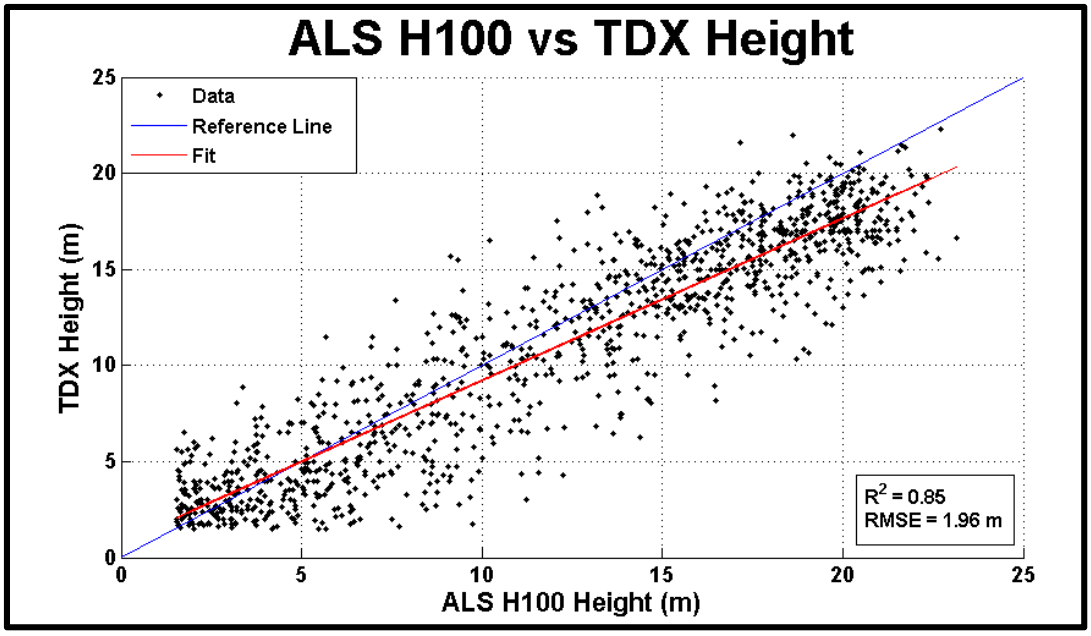

Figure 4.9 A comparison between the Airborne LiDAR H100 (ALS H100) and TanDEM-X mangrove canopy height in Shark River Slough yielding an R^2 = 0.85 and RMSE = 1.96 m.

4.6.2. Everglades National Park Mangrove Digital Canopy Model

To cover the entire ENP mangrove forests a total of 4 bistatic stripmap TanDEM-X scenes were processed, mosaicked and georeferenced into a NAD83 datum and UTM 17N projection (Table 4.1). The entire mangrove DCM (10 m horizontal resolution) derived from the TanDEM-X data is shown in Figure 4.10, including a zoomed area of the SRS region. The DCM shows that the tallest mangroves forests are located at the Western coast of the ENP, where SRS connects with the Gulf of Mexico. This overall mangrove distribution pattern agrees with the study of Simard et al. (2006), where the tallest mangroves were located in this region. Additionally, I estimated mangrove coverage (131, 813 ha) in the ENP using WorldView-2 imagery, having in consideration that some minor mangrove regions were not included in the imagery.

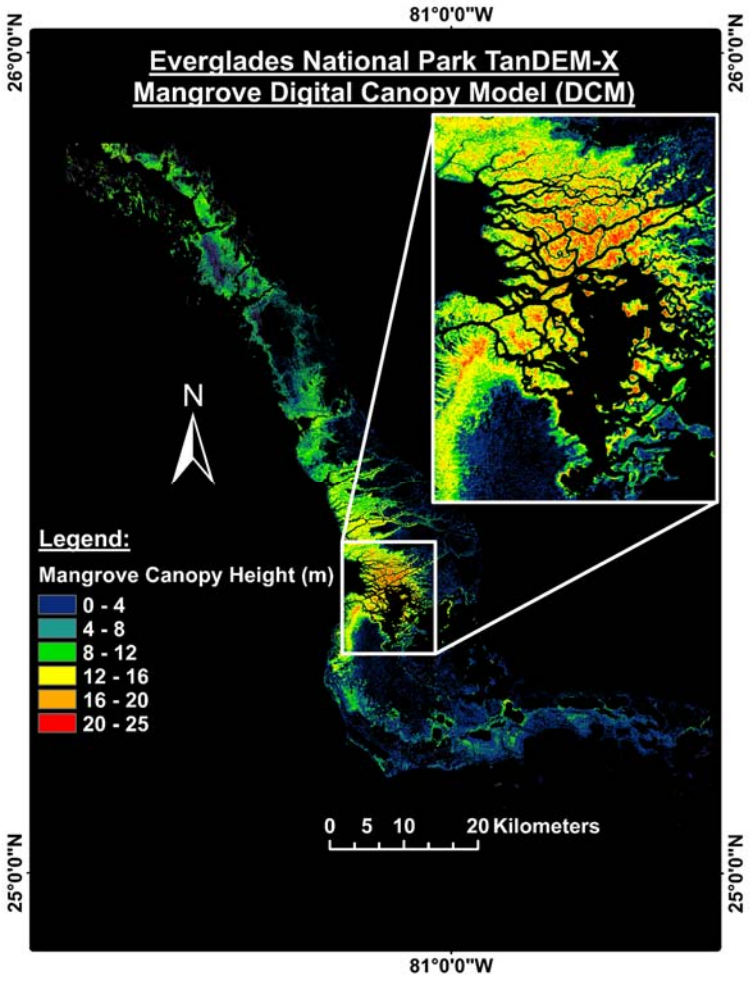

Figure 4.10 Everglades National Park TanDEM-X-based mangrove DCM with a zoomed area in the Shark River Slough region.

4.6.3. Above-Ground Biomass

I use two datasets (TLS and TanDEM-X) to estimate mangrove AGB in the ENP. The TLS dataset provides estimates at the plot-level, whereas the TanDEM-X dataset enable us to estimate AGB for the entire coastal region. Both datasets use two different proxies for estimating AGB and, hence, obtain somewhat different results. I used ENP-specific mangrove-based allometry proposed in Feliciano et al. (2014) to estimate site-specific AGB in in megagrams per hectare (Mg/ha) for the three SRS sites. The ENP mangrove AGB allometric equation is given by (15):

$$AGB = 0.187 DBH^{2.43} \quad \textbf{(15)}$$

where AGB is biomass in kilograms and DBH is Diameter-at-Breast-Height in cm. As the TLS data was acquired only in three sites, it was used as a comparison dataset for the AGB map I derived using Saenger and Snedaker (1993) global mangrove AGB equation. This equation estimates AGB using mangrove canopy height and is given by (16):

$$B = 10.8H + 34.9 \quad \textbf{(16)}$$

where B is AGB in Mg/ha and H is tree height. In this study, I used the height derived from the TanDEM-X dataset (Figure 4.10) as my final H tree heights, as it covers the entire mangrove forests. Figure 4.11 shows the AGB map derived from the global mangrove biomass equation and the TanDEM-X dataset, showing a maximum AGB value of approximately 250 Mg/ha where Shark River Slough connects with the Gulf of Mexico.

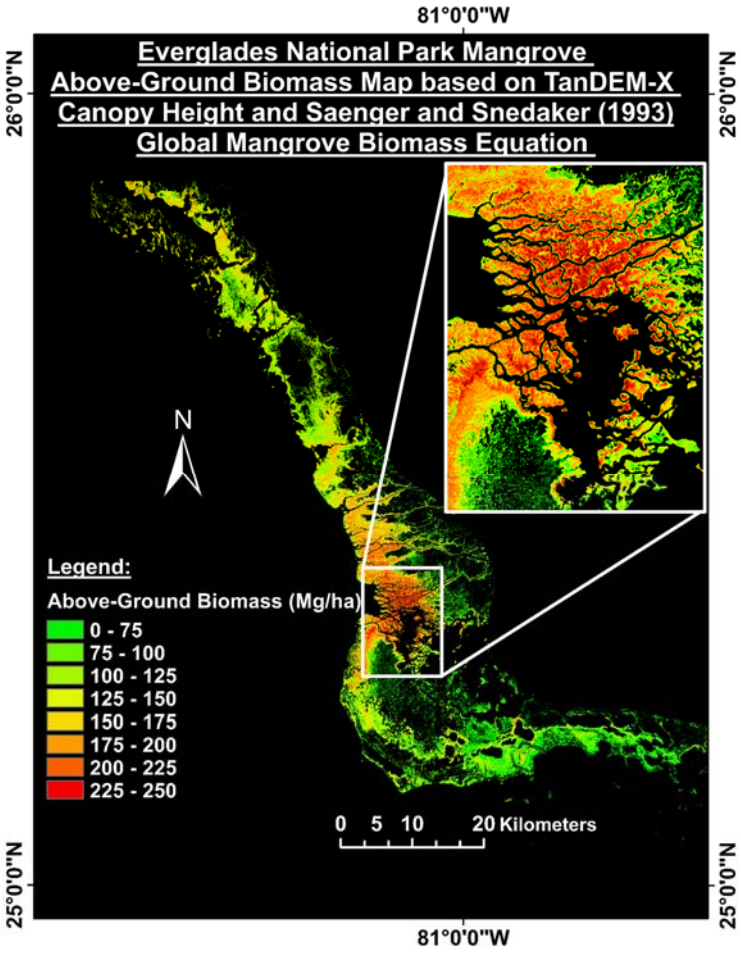

Figure 4.11 Everglades National Park mangrove AGB map based on TanDEM-X canopy height data and Saenger and Snedaker (1993) global mangrove biomass equation.

4.7. Discussion

4.7.1. Mangrove Canopy Height and Biomass

Remote sensing data products inherently include uncertainty in their estimations. For canopy height measurements Airborne LiDAR has an RMSE or underestimation that is less than 1 m (Hyyppä et al., 2004). The Airborne LiDAR versus TanDEM-X canopy height validation results in SRS (R^2 = 0.85, RMSE = 1.96 m) indicate a high potential to use TanDEM-X data for the estimation of mangrove forests canopy heights. As for TanDEM-X uncertainty my validation plot in SRS revealed an RMSE of 1.96 m. This low RMSE suggests a good agreement between the Airborne LiDAR and TanDEM-X

data. The Airborne LiDAR data covered a relatively small area (30 km^2) along SRS in only one TanDEM-X scene, meaning that the estimated RMSE is only valid for this area, not for the entire TanDEM-X mangrove map. However, I assumed that the same uncertainties can be applied to all of the TanDEM-X scenes as the validated area is representative of mangrove stature in the entire ENP mangrove forests.

At first glance, the TanDEM-X-based mangrove DCM (10 m horizontal resolution) (Figure 12b) yields similar results when visually compared with Simard et al. (2006) SRTM-based mangrove DCM (30 m horizontal resolution) (Figure 4.12a). The tallest mangrove forests (> 20 m) on both DCMs (Figure 4.12) are located at the Western ENP coast, where the Gulf of Mexico connects with SRS. Intermediate size (12 – 20 m) mangroves are located above and below SRS, and in the mid-region of SRS where SRS-5 site is located. The rest of the mangrove forests are dominated by small to intermediate stature mangroves ranging from 4 – 12 m. Differences between both DCMs are more noticeable in the SRS area, where my study shows dominance of mangroves taller than 18 m and Simard et al. (2006) shows domination of mangroves ranging in stature from 16 – 18 m. This difference could represent mangrove growth in this area as approximately one decade has passed between both studies. Taking in consideration the entire mangrove forests, my study yields a mean canopy height of 9.7 m.

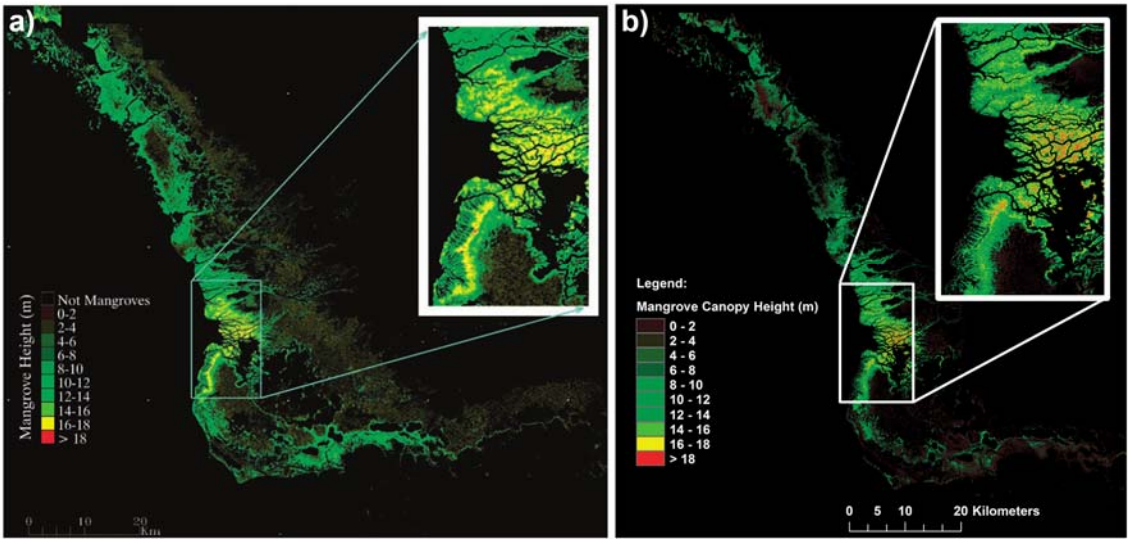

Figure 4.12 a) Simard et al. (2006) ENP mangrove Digital Canopy Model. b) Digital Canopy Model produced in this study.

The AGB TLS-based results: 197.5 ± 22 Mg/ha in SRS-4, to 251.2 ± 28 Mg/ha in SRS-5 and 460 ± 60 Mg/ha in SRS-6 seem very high when compared with the results seen on the ENP AGB map from Simard et al. (2006) (Figure 4.13) where the maximum AGB value is 200 Mg/ha. Nevertheless, as TLS measurements are very accurate, I suggest they represent the AGB of the sites. Additional TLS surveys would be needed to have a better idea of the AGB distribution at the plot-level. Additionally, one have to take in consideration that the methodology to acquire AGB on both studies, Simard et al. (2006) and Feliciano et al. (2014) are different. Furthermore, I suggest that georeferenced TLS surveys would be vital in order to create a canopy height-AGB regression with Airborne LiDAR data, which can be applied to the whole mangrove forest using TanDEM-X mangrove canopy height.

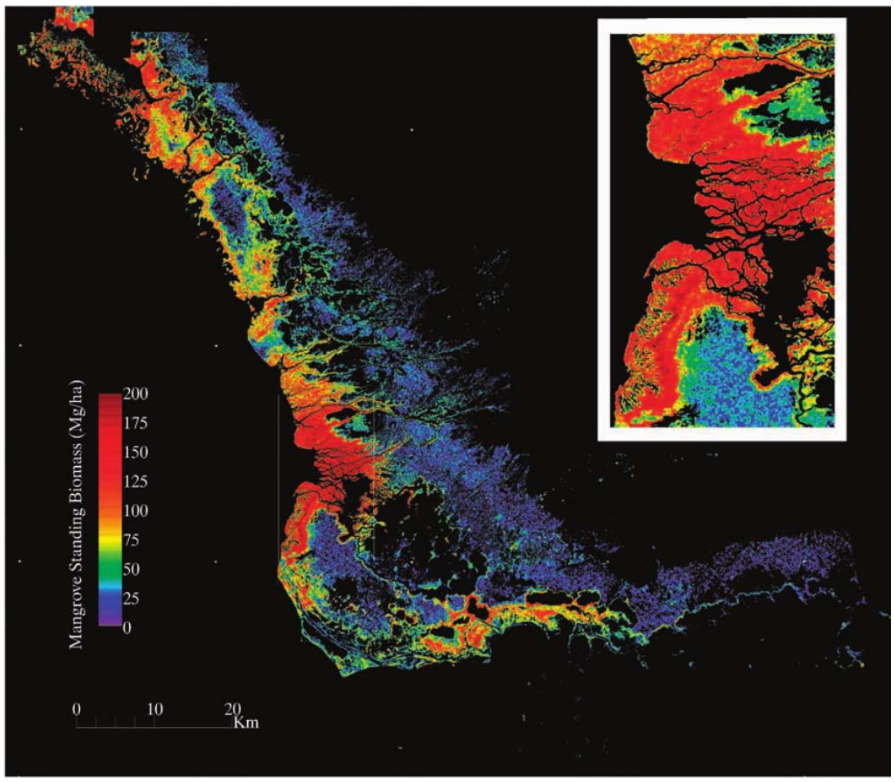

Figure 4.13 Simard et al. (2006) Everglades National Park AGB map.

4.8. Conclusion

I used TanDEM-X data to estimate canopy height and TLS data to estimate site-specific AGB in the ENP mangrove forests. Global TanDEM-X DEM acquisitions are based on single-pol (HH) data and this study successfully suggests the use of single-pol data for this kind of wetland forestry application. To validate the canopy height results of the TanDEM-X data I used Airborne LiDAR data acquired across the mangrove forests located across SRS, inside the ENP boundaries. This study showed the potential of using TanDEM-X data for the estimation of mangrove canopy height and updates the previous map (Simard et al., 2006), which serves as a potential mangrove ecosystem comparison tool. However, to further validate the entire ENP TanDEM-X-derived mangrove DCM,

additional Airborne LiDAR data is needed in order to validate locations in the northeastern and southwestern mangrove forests.

TLS data were used to estimate an assess AGB across the three SRS sites. AGB results yielded higher values 460 Mg/ha when compared to previous studies (200 Mg/ha) (Simard et al., 2006). These new AGB results, suggest that there might be higher AGB and carbon content in the ENP than previously thought. Additional georeferenced TLS surveys are needed in order to create an ENP-specific canopy height-AGB regression in conjunction with Airborne LiDAR data.

Chapter 5: Assessing the Vegetation Structure of Non-Mangrove Vegetation Communities in the Everglades National Park using Multi-Spatial Remote Sensing Techniques

5.1. Overview

The South Florida Everglades is home to various sub-tropical wetland forest communities including rockland pines, bald cypresses tropical hardwood hammocks and mangroves. Although these species are well protected inside the Everglades National Park boundaries, they are under a lot of pressure due to historical habitat loss, invasion of exotic species and external anthropogenic activities (DeCoster et al., 1999; O'Hare and Dalrymple, 2006; Lodge, 2010). Mangrove forests inside the ENP have been heavily studied as they cover a larger extent and more prone and sensitive to ecosystem changes. However, there is a need to monitor and quantify the actual status of the vegetation structure of the other major communities as together they form one wetland ecosystem interconnected by water.

Previous studies have use remote sensing techniques to quantify vegetation structure in the rockland pine and mangrove forests of the ENP. Airborne Laser/LiDAR Scanning has been used to assess the landscape and vegetation structure of the ENP rockland pine forests (Houle et al., 2006). Airborne LiDAR and InSAR were used to quantify mangrove canopy height in the ENP (Simard et al., 2006). TLS, Airborne LiDAR and InSAR were successfully used and integrated to quantify mangrove canopy height and AGB in the ENP mangrove forests (Chapter 4). However the ENP bald cypress and tropical hardwood hammocks have not been extensively studied using remote sensing techniques. Multi-spatial remote sensing is the tool needed to quantify and monitor the status of these wetland vegetation communities.

The main objective of this study is to assess the vegetation structure (canopy height) and AGB of three wetland forest ecosystems: rockland pine, bald cypress and tropical hardwood hammock, all located within the boundaries of the ENP. Improved AGB ground estimates are possible with ground-based remote sensing techniques such as TLS. Feliciano et al. (2014) showed the potential to used TLS to improve ground-based AGB estimates. The goal is to use remote sensing techniques (TLS, Airborne LiDAR and InSAR) to assess these sites at multiple scales.

5.2. Study Area

My study area comprises a pine forest (25.390° N, 080.625° W), a cypress forest (25.434° N, 080.762° W) and a hammock forest (25.386° N, 080.622° W) located inside the boundaries of the ENP (Figure 5.1). The rockland pine also known as slash pine and the tropical hammock forests are located in the ENP Long Pine Key region on top of a geological formation named the Miami Rock Ridge (Miami Limestone). The dwarf cypress forest site is located in an ENP scenic location named Rock Reef Pass. Ground elevation above sea level for the three sites ranges from 3 to 4 ft. The Airborne LiDAR data acquired for this study provided canopy height estimates up to 26.5 m for the pine forests, approximately up to 9 – 12 m for the cypress forests and up to 20 m in the hammock forests. These three sites were particularly selected because of their easy road access inside the ENP. The following sub-sections provide additional information about these three wetland vegetation communities.

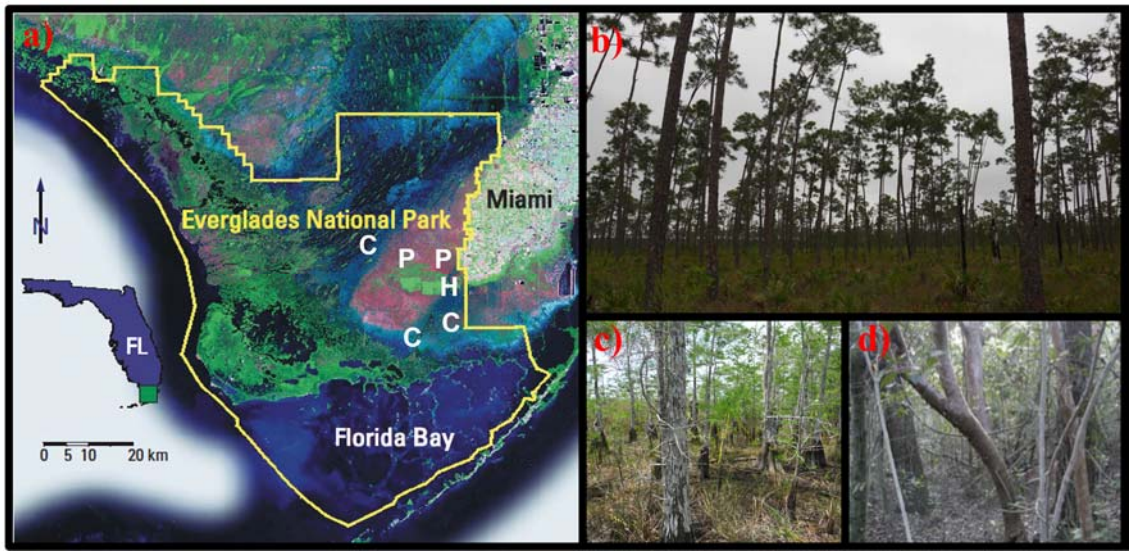

Figure 5.1 a) Location map of the Everglades National Park, including the vegetation communities and sites of this study. P = Pine, C = Cypress, H = Hammock. b) Pine site. c) Cypress site. d) Hammock site.

5.2.1. Rockland Pine

Of the original 65,450 ha of pine forests in South Florida, less than 10 % (5,220 ha) exist, with 4,300 ha located inside the ENP (O'Hare and Dalrymple, 2006). The largest area of rockland pines inside the ENP is Long Pine Key (Doren et al., 1993). In August of 1992 Hurricane Andrew severely damage these pine stands showing their vulnerability (DeCoster et al., 1999). Furthermore, exotic and invasive species such as the Burma reed and the Brazilian pepper currently threaten these pine forests (Lodge, 2010). As only a small amount of slash pine stands remain intact, there is a need to monitor and manage these forests (Doren et al., 1993). Controlled fire is a necessary technique used for the survival (invasive species) and preservation of this ecosystem, however it is dangerous as it represents a health risk (smoke) to surrounding residential communities. Nevertheless, it is a technique that has been used for decades inside the ENP for the protection, maintenance and seedling dispersion of this habitat.

5.2.2. Bald Cypress and Tropical Hardwood Hammock

Bald cypress and tropical hardwood hammock communities also comprise an important part of the ENP ecosystem, although they are less threatened than pine stands. Bald cypresses are flood tolerant species as they are covered with water for long periods of time. Additionally, they provide habitat for native fauna such as the American alligator, leopard and grass frogs, beavers, otters and endangered species such as the Florida panther and nesting birds (Lodge, 2010). Cypress stands are less susceptible to fires as they are covered with water and saturated soils. Nevertheless, during dry seasons natural fires can damage cypress roots, killing its stands. However, natural fires protect their ecosystem as they exterminate invasive species that could potentially damage or change their environment. Similar to the bald cypresses, tropical hardwood hammocks are less threatened than rockland pines. However, hammock communities are very susceptible to fires which can destroy them, particularly in very dry years (Lodge, 2010). Nevertheless, controlled fire or maintenance is not done in these communities. Tropical hardwood hammock is a general term, as approximately 30 tree species constitute this terminology (Lodge, 2010). Tropical hardwood hammock communities can be found around the rockland pines of the Miami Rock Ridge, have a close canopy (dense vegetation) and provide habitat for a variety of fauna such as wading birds (Lodge, 2010) the endangered Florida tree snail (Deisler, 1982), the endangered Florida mastiff bat (Belwood, 1992), the endangered rim rock crowned snake (Campbell and Moler, 1992) and others.

As important as rockland slash pine, bald cypress and tropical hardwood communities are for the well-being of the ENP ecosystem, detailed studies concerning

the distribution, vertical structure and AGB are barely reported. LiDAR and SAR airborne and space-based remote sensing sensors are needed to characterize vegetation structure AGB. There is a need to quantify the structure and AGB of these non-mangrove species with high-resolution remote sensing data in order to assess their current status. This approach could potentially serve as a monitoring mechanism of their health and distribution inside the ENP, especially for the threatened slash pine stands.

5.3. Methods

In this study I acquired and processed various datasets at multiple scales (TLS data [ground], Airborne LiDAR data [airborne] and InSAR-based TanDEM-X data [spaceborne]). TLS data was used to assess site-specific AGB. Airborne LiDAR data was used to estimate vegetation canopy height at each site and served as a validation and comparison dataset for the Pol-InSAR TanDEM-X data. The TanDEM-X data was explored to assess its applicability to estimate canopy height in various ecosystems ranging from less dense (pine, cypress) to more dense (hammock).

5.3.1. Datasets

5.3.1.1. TLS Data

TLS datasets were acquired in April 2010 for the rockland pine, bald cypress and tropical hardwood hammock sites. A Leica ScanStation C10 TLS was used for the surveys (Figure 5.2). Table 2.1 summarizes the TLS technical specifications. My approach to obtain stem AGB was multiplying the TLS-derived tree volume by species-specific WSD (Chapter 3). The pine site TLS survey covered approximately a ~100 m by

100 m plot and the cypress and hammock sites covered approximately ~ 50 m by 50 m plots. Multiple targets were place in the surveys in order to merge point cloud scans acquired from various positions (7 in pine site, 5 in cypress site and 17 in hammock site). Hemispherical photos were automatically acquired by the TLS after each scan. The TLS scanning resolution for every site was approximately 1 cm at a distance of 10 m, as it was sufficient to distinguish small vegetation features such as leaves and small branches, and efficient enough to be acquired in 7 minutes.

Figure 5.2 Leica ScanStation C10 TLS in ENP bald cypress site. Three targets can be seen scattered in the cypress forest.

5.3.1.2. Airborne LiDAR Data

Airborne LiDAR data was acquired using an Optech Gemini ALTM operated by the NCALM, which is funded by the NSF. The Airborne LiDAR survey was conducted on November 17, 2012 and comprised 2 regions (Pine-Hammock and Cypress) comprising 24 km^2 in area (Figure 2.6). Table 2.2 summarizes the Airborne LiDAR

sensor technical specifications. The goal of the Airborne LiDAR data was to estimate site-specific canopy height in addition of validating the TanDEM-X data.

5.3.1.3. TanDEM-X Data

TanDEM-X data was acquired in this study to cover and assess the vertical structure of the pine, cypress and hammock forests (Table 5.1). The acquired scene was single-polarized (HH) and acquired in bistatic stripmap mode, where one satellite emits the signal and both satellites receive reflected signal at the same time with no temporal decorrelation.

Acquisition Date	UTC Time (hh:mm:ss)	Polarization	Incidence Angle (°)	Height of Ambiguity	Bandwidth (MHz)	Effective Baseline (m)
2011/10/18	23:22:10	HH	36.24	-46.73	100	123

Table 5.1 TanDEM-X scene used in this study.

5.3.2. Data Processing

5.3.2.1 TLS Data Processing

The TLS data were processed using Leica's Cyclone v9.0 software. The processing of the TLS data consisted on merging and converting the multiple scans into a single point cloud for each site. Stable targets are needed in order to merge single scans. A target registration analysis was needed to assess the quality control of the root mean square error (RMS) of the distance between common targets. A low RMS (e.g. 0.08 meters) is expected for a registered and merged target (Feliciano et al., 2014). More details of the TLS data processing can be found on Chapter 3.

5.3.2.1.1. Stem Volume and AGB Estimation

Post-processing of the TLS data consisted on modeling vegetation stems in order to estimate stem volume. As tree stems are tapered, they could be modeled as geometric surfaces named frustums of paraboloids, (Husch et al., 2002; Feliciano et al., 2014). As suggested in (Feliciano et al., 2014), Smalian's formula was used to estimate the stem parabolic frustum volume (Husch et al., 2002). The Smalian's formula estimates volume by multiplying the average cross-sectional area of a stem section by the stem section's length (Figure 3.5). The Smalian's volume is given by equation (6). The first step towards estimating stem volume consisted in dividing the stem into smaller sections. Cylinders were created at different heights in order to divide the stem into multiple frustums. Cyclone software automatically created best-fit cylinders from the point cloud in locations determined by the user. I defined a frustum section as the region between two cylinders. The two end diameters and the section length were then measured for each frustum. These parameters were incorporated into the Smalian's formula (equation 6) to calculate each frustum volume. The total stem frustum volume was obtained by summing all of the smaller frustum volumes. More details about TLS processing for vegetation volume can be found in Feliciano et al. (2014). AGB was estimated by multiplying my TLS-derived volume by an estimated species-specific WSD.

5.3.2.2. Airborne LiDAR Data Processing

The Airborne LiDAR data were processed with LAStools and ENVI software for retrieving first and last laser returns. The first returns, which mark the location of three canopies, were used to generate a DSM for each site. The last returns, which mark the

location of the ground surface, were used to generate a DTM for each site. A 1 m DCM (Figure 5.3 [Cypress], Figure 5.4 [Pine and Hammock]) was produced for each site by subtracting the DTM created with the bare ground points from the DSM created with the top of the canopy points. The Airborne LiDAR DCMs were georeferenced into a NAD83 datum and UTM 17N projection.

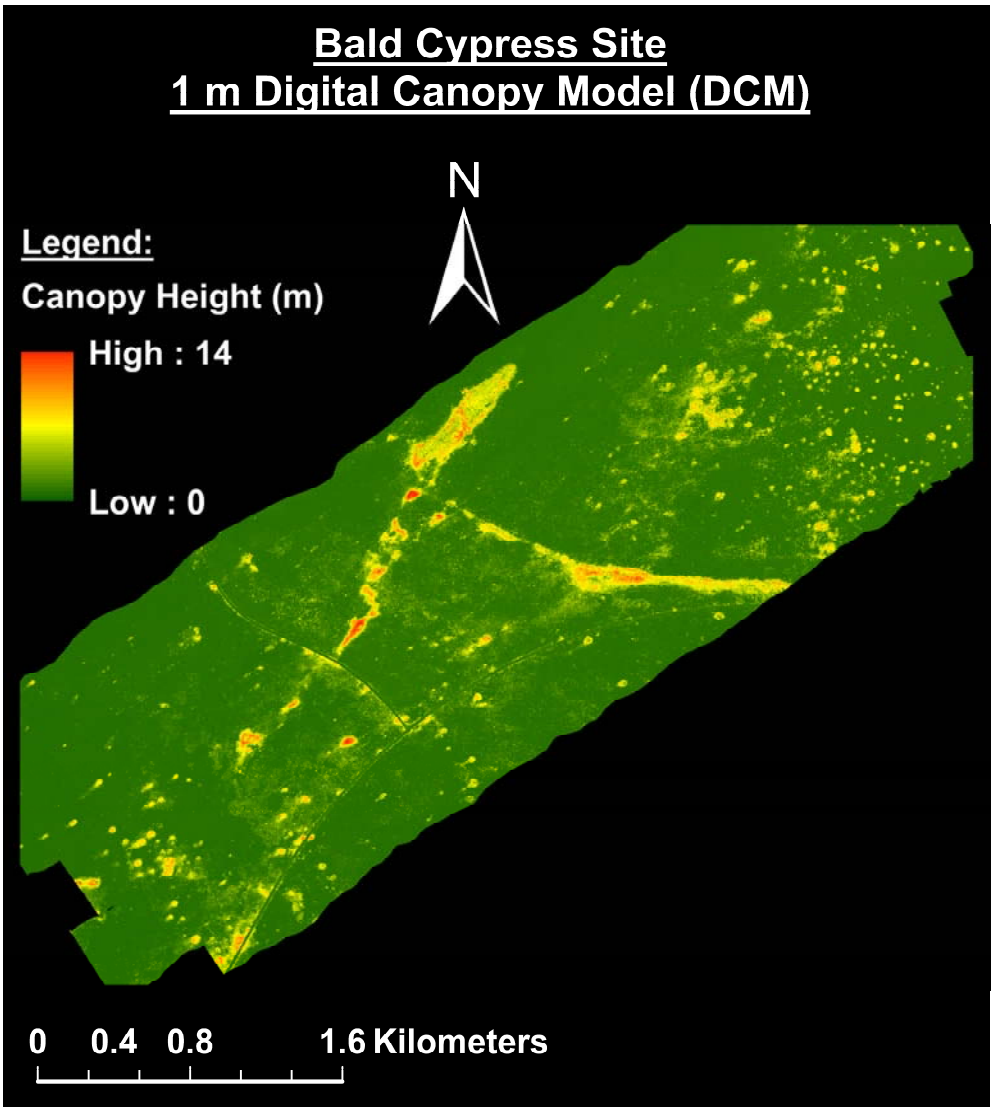

Figure 5.3 DCM of cypress site created by subtracting last laser returns (DTM) from top of the canopy height returns (DSM).

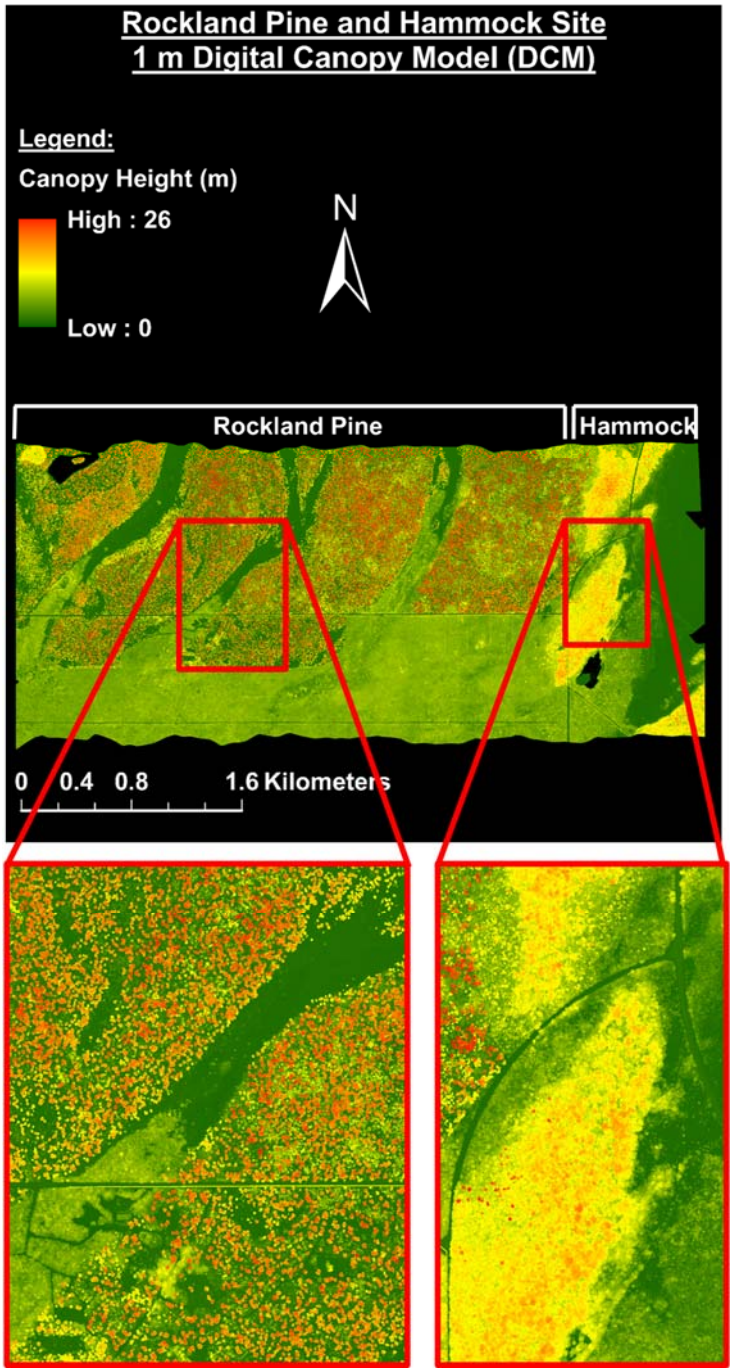

Figure 5.4 DCM of rockland pine and hammock sites created by subtracting last laser returns (DTM) from top of the canopy height returns (DSM). Bottom figures show zoom-ins into each forest.

5.3.2.3. TanDEM-X Data Processing

The processing of the TanDEM-X data to obtain canopy heightheight was based on the Pol-InSAR RVoG model. More details of the RVoG model and TanDEM-X Pol-InSAR data processing can be found in sub-section 2.3.2 of this dissertation. Additional explanations concerning the Pol-InSAR theory and application can be found in (Cloude and Papathanassiou, 1998; Papathanassiou and Cloude, 2001; Cloude and Papathanassiou, 2003).

5.4. Airborne LiDAR and TanDEM-X Canopy Height Results

The canopy height validation involved the comparison between the Airborne LiDAR data acquired in November, 2012 and a processed single-pol (HH) TanDEM-X scene acquired in October, 2011 for the rockland pine, hammock and bald cypress sites. Even though the two datasets were acquired one year apart, I assume no drastic vegetation change between the two acquisitions.

5.4.1. Airborne LiDAR vs. TanDEM-X Canopy Height Comparison in the Rockland Pine, Tropical Hardwood Hammock and Bald Cypress Sites

The final Airborne LiDAR DCM for the pine and hammock sites can be seen in Figure 5.4, scaled from 0 – 26 m. From the Airborne LiDAR data, it can be seen that the rockland pine canopy height reaches up to 26 m, while the hammock forests reach up to 18 m. In order to assess the usefulness of TanDEM-X to estimate pine and hammock canopy height I produced a DCM shown in Figure 5.5, scaled from 0 – 25 m. Although some pine canopies can be seen in the TanDEM-X DCM, the pine forests cannot be

distinguished completely, when compared to the Airborne LiDAR data (Figure 5.4). On the contrary, the hammock forests can be clearly seen in the TanDEM-X DCM. For this reason, I only compared the Airborne LiDAR and TanDEM-X datasets for the hammock forests. In order to make this comparison possible, I masked out the pine forests from both datasets (Figure 5.6).

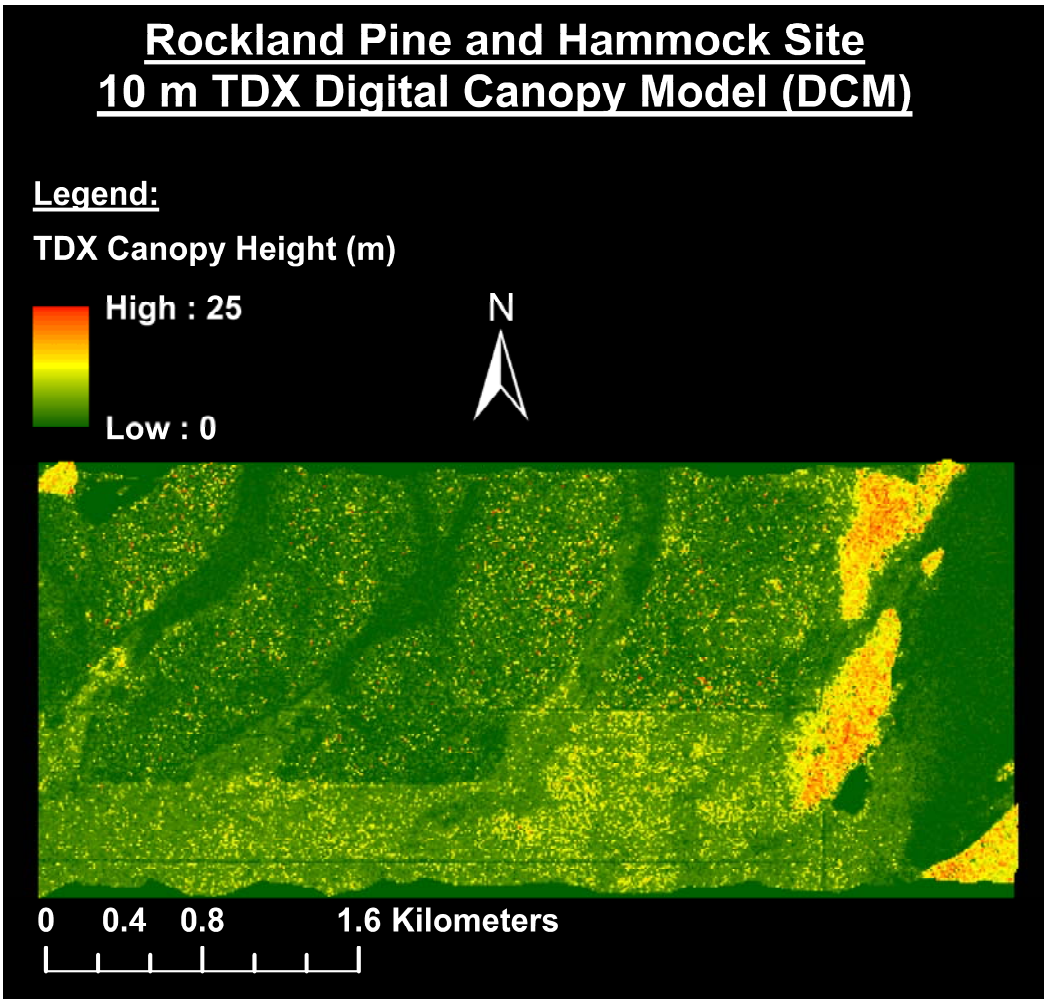

Figure 5.5 DCM of rockland pine and tropical hardwood hammock sites created with TanDEM-X data.

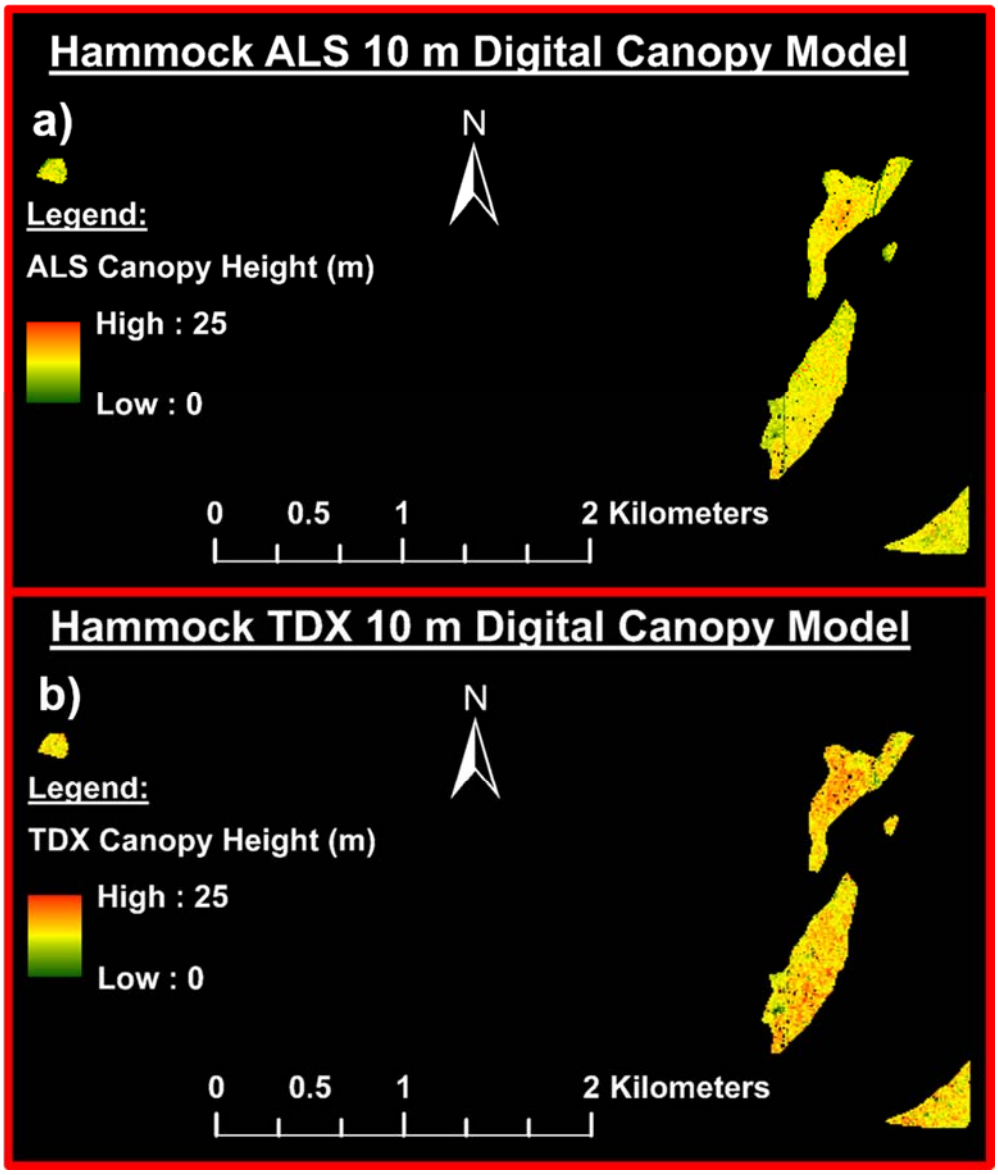

Figure 5.6 a) Airborne LiDAR -derived 10 m hammock forest DCM. b) TanDEM-X-derived 10 m hammock forest DCM.

The hammock TanDEM-X DCM was produced at a spatial resolution of 10 m, whereas the Airborne LiDAR resolution is 1 m. In order to compare both datasets, I resampled (highest pixel value) the Airborne LiDAR dataset to 10 m. Figure 5.6 a) shows the Airborne LiDAR DCM of the hammock forest, while Figure 5.6 b) shows the TanDEM-X DCM for the hammock forest. To validate and compare the TanDEM-X results I used the H100 model, which represents the mean height of the 100 tallest tress

per hectare. The hammock forest validation plot (Figure 5.7) between the Airborne LiDAR and TanDEM-X canopy heights in yielded an R^2 correlation coefficient of 0.33 and an RMSE of 1.73 m. The bald cypress Airborne LiDAR DCM shows that canopy height can reach up to 14 m in its region (Figure 5.3). However, the TanDEM-X DCM showed a similar behavior to the rockland pine TanDEM-X results, where almost no associated vegetation can be seen in the area. Therefore, no comparison between the Airborne LiDAR and the TanDEM-X for this site was plausible.

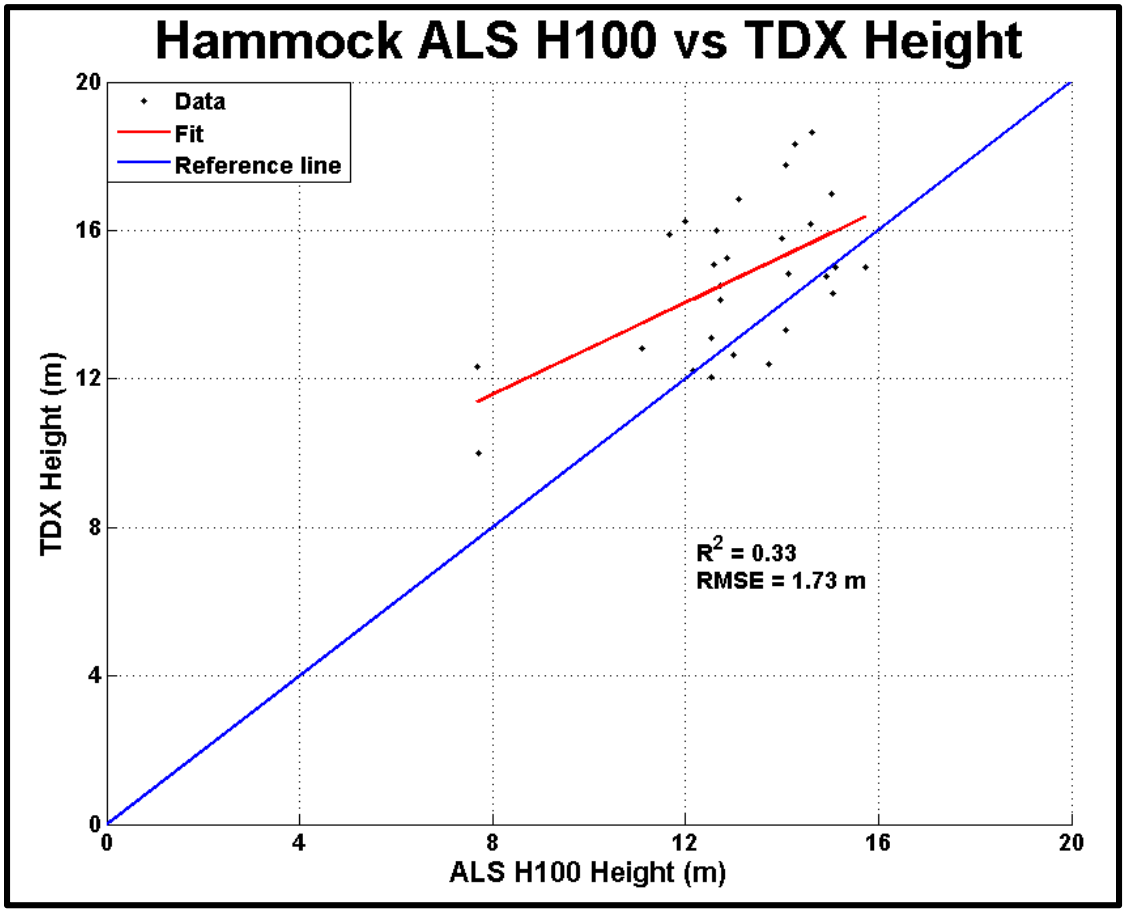

Figure 5.7 A comparison between the Airborne LiDAR H100 (ALS H100) and TanDEM-X hammock forest canopy height yielding an $R^2 = 0.33$ and RMSE = 1.73 m.

5.5. Above-Ground Biomass Examples

Following the methodology of Chapter 3 I tested the TLS technique in a pine and cypress stand (Figure 5.8). For a pine tree (Figure 5.8 a) I estimated its total AGB to be 312 kg and for a bald cypress tree (Figure 5.8 b) I estimated its total AGB to be 106.5 kg, showing the large difference in biomass/carbon content between rockland pine and bald cypress stands.

Figure 5.8 AGB estimation example in a) rockland pine tree and b) bald cypress tree, following Feliciano et al. (2014).

5.6. Canopy Height Implications

Remote sensing datasets are not extent of uncertainty in their data products. As an example, Airborne LiDAR canopy height measurements have an RMSE that is less than 1 m (Hyyppä et al., 2004). The Airborne LiDAR versus TanDEM-X canopy height validation in the hammock forest yielded and $R^2 = 0.33$ and RMSE = 1.73 m, which is

very low. The TanDEM-X canopy height estimations from the rockland pine and bald cypress did not yielded significant results, as the forest cannot be completely distinguishable. Therefore, I did not compare the Airborne LiDAR and TanDEM-X datasets in these sites. Structurally comparing the three forest communities, it is clear that the hammock forests have very dense canopy and vegetation. In contrast, the rockland pine and bald cypress forests have less dense and sparse vegetation. I suggest that the lack of vegetation density could be affecting the InSAR scattering mechanism (volume scattering) in the RVoG model, thus affecting the final results. I suggest that another TanDEM-X data processing scheme or model should be applied in these sites, in order to have more significant results.

Chapter 6: Conclusion

Wetlands provide multiple benefits to human society due to their ecosystem services and biodiversity. Wetland environments sequester and store high amounts of atmospheric carbon, which is one of their most important ecosystem services. However, wetland ecosystems are under severe pressure due to anthropogenic activities, climate change and sea level rise. There is a need to monitor these ecosystems as they are very susceptible to subtle changes. Remote sensing techniques are proven tools for continuous monitoring of wetland forests at different scales. This study investigates the use of various remote sensing techniques (TLS, Airborne LiDAR and Pol-InSAR TanDEM-X), which operate at multiple scales, from individual tree level to the entire coastal region. I applied these techniques in the South Florida Everglades wetland ecosystem, more specifically in the ENP in order to study the vegetation structure of various vegetation communities.

One of the key objectives of the Everglades restoration plan involves the conservation of the main vegetation ecosystems. In order to monitor the current status and future recovery of the various vegetation ecosystems, it is imperative to assess and quantify vegetation species changes and vegetation structural changes including canopy height and above-ground biomass as a function of time. I focus on four wetland vegetation communities; mangroves, rockland pines, tropical hardwood hammocks and bald cypresses. I assessed the use of the multi-spatial remote sensing techniques in these four forest communities.

Chapter 3 consisted in the application of TLS to estimate mangrove stem volume, prop root volume and AGB. I proved that TLS is a high-resolution remote sensing tool

that can be used as a substitute to destructive sampling in order to create mangrove allometry. The results of this study revealed that although mangrove structure could be complex, there is potential for the use of TLS in this kind of wetland environment. TLS presents the advantage of analyzing large trees with high AGB, which is not possible with traditional hand-based forestry methods. I was able to create ENP-specific mangrove allometry in addition of quantifying measurements uncertainties and successfully comparing my results with published mangrove allometry. This TLS study is the first ever reported for a mangrove environment.

Chapter 4 covered the use and integration of TLS, Airborne LiDAR and TanDEM-X (Pol-InSAR) data to quantify canopy height and AGB across the entire ENP mangrove forests. Although Airborne LiDAR is a well-established technique for the estimation of canopy height, it is very expensive and it only covers small areas. Alternatively, TanDEM-X presents the opportunity to estimate canopy height for large regions at a fraction of the cost. Because TanDEM-X Pol-InSAR is not as well established as Airborne LiDAR, I used Airborne LiDAR data to compare and validate TanDEM-X results. The canopy height validation results between Airborne LIDAR and TanDEM-X yielded and $R^2 = 0.85$ and RMSE = 1.96 m, showing the potential of using TanDEM-X data for the estimation of mangrove canopy height. Mangrove canopy height can go up to 25 m, although most of the canopy height is concentrated across 9.7 m (intermediate size mangroves). Additionally, I were able to estimate mangrove cover area with WorldView-2 data (131, 813 ha), although there were small mangrove patches not covered in the imagery. Finally, I were able to estimate site-specific AGB in the SRS sites using Chapter 3 TLS methodology. AGB ranged from 197 ± 22 Mg/ha in SRS-4, to

251 ± 28 Mg/ha in SRS-5 and 460 ± 60 Mg/ha in SRS-6, suggesting higher AGB values than previously estimated.

Chapter 5 comprised the assessment and test of TLS, Airborne LiDAR and TanDEM-X (Pol-InSAR) data to quantify canopy height and AGB across three major vegetation ecosystems located inside the ENP (rockland pines, bald cypresses and tropical hardwood hammocks). To assess and validate the usefulness of TanDEM-X data for canopy height estimations I used Airborne LiDAR data. Of the three forests communities studied, only the tropical hardwood hammock forests yielded potential and promising TanDEM-X results (R^2 = 0.33 and RMSE = 1.73 m). The rockland pine and bald cypress sites did not yielded good results, because the RVoG model is not a good representation of the sparse tree distribution of these two forest types.

In summary, this dissertation showed that the integration of remote sensing techniques is fundamental for forestry studies. TLS can be used to estimate site-specific AGB. Airborne LiDAR can be used to estimate canopy height with high accuracy and to validate TanDEM-X-based canopy height. TanDEM-X data can be used to estimate and study canopy height of forests at a very large scale. Together, these remote sensing tools can overcome their disadvantages and enhance the accuracy of vegetation structure estimations.

6.1. Future Directions

Although this dissertation showed the usefulness of studying wetland vegetation structure using various remote sensing techniques, additional work should seek the acquisition of additional data at all scales. More Airborne LiDAR data are needed for

adding validation areas to the TanDEM-X data. Additional TLS surveys are needed for estimating canopy height-AGB regressions beyond the three sites used in this dissertation. I suggest that upcoming forest height TanDEM-X studies should explore the use of multi-baseline and multi-polarimetry Pol-InSAR data to evaluate and understand the volume scattering mechanisms differences in dense and non-dense forests. To fully compare the extent of my results, there is a need to use the techniques developed in this dissertation to study other wetland ecosystems.

Future work should focus on improving biomass and carbon estimations. As the need of estimating biomass and carbon is becoming more and more urgent, missions such as the European Space Agency BIOMASS (P-band satellite) mission will provide high-accuracy measurements needed at the national scale. The integration of techniques such as TLS, Airborne LiDAR and TanDEM-X with upcoming missions such as the BIOMASS satellite will enhance canopy height and biomass estimations from the individual tree up to a continental scale, as well as reducing uncertainty.

Blibliography

Ahmed R, Siqueira P, Hensley S, Bergen K (2013) Uncertainty of forest biomass estimates in north temperate forests due to allometry: implications for remote sensing. Remote Sensing 5(6):3007-3036.

Alongi DM (2002) Present state and future of the world's mangrove forests. Environmental Conservation 29(03):331-349.

Alongi DM (2012) Carbon sequestration in mangrove forests. Carbon Management 3(3):313-322.

Amelung F, Galloway DL, Bell JW, Zebker HA, Laczniak RJ (1999) Sensing the ups and downs of Las Vegas: InSAR reveals structural control of land subsidence and aquifer-system deformation. Geology 27(6):483-486.

Amelung F, Jónsson S, Zebker H, Segall P (2000) Widespread uplift and 'trapdoor'faulting on Galapagos volcanoes observed with radar interferometry. Nature 407(6807):993-996.

Barr JG, Fuentes JD, Engel V, Zieman JC (2009) Physiological responses of red mangroves to the climate in the Florida Everglades. Journal of Geophysical Research-Biogeosciences 114.

Belwood J (1992) Florida mastiff bat, Eumops glaucinus floridanus. Rare and endangered biota of Florida 1:216-223.

Campbell H, Moler P (1992) Rim rock crowned snake, Tantilla oolitica Telford. Rare and endangered biota of Florida 3:158-161.

Castañeda-Moya E, Twilley RR, Rivera-Monroy VH (2013) Allocation of biomass and net primary productivity of mangrove forests along environmental gradients in the Florida Coastal Everglades, USA. Forest Ecology and Management 307(0):226-241.

Castaneda-Moya E, Twilley RR, Rivera-Monroy VH, Marx BD, Coronado-Molina C, Ewe SML (2011) Patterns of root dynamics in mangrove forests along environmental gradients in the Florida coastal Everglades, USA. Ecosystems 14(7):1178-1195.

CEPP (2011) Central Everglades Planning Project, U.S. Army Corps of Enginners and South Florida Water Management District, Florida. Last accessed: October 10 2013. From: http://www.sfrestore.org/cepp/cepp.html

CERP (2000) Comprehensive Everglades Restoration Plan, U.S. Army Corps of Enginners and South Florida Water Management District, Florida. Last accessed: October 10 2013. From: http://everglades.plan.org

Chave J, Andalo C, Brown S, Cairns MA, Chambers JQ, Eamus D, Folster H, Fromard F, Higuchi N, Kira T, Lescure JP, Nelson BW, Ogawa H, Puig H, Riera B, Yamakura T (2005) Tree allometry and improved estimation of carbon stocks and balance in tropical forests. Oecologia 145(1):87-99.

Chave J, Condit R, Aguilar S, Hernandez A, Lao S, Perez R (2004) Error propagation and scaling for tropical forest biomass estimates. Philosophical Transactions of the Royal Society of London. Series B: Biological Sciences 359(1443):409-420.

Chave J, Coomes D, Jansen S, Lewis SL, Swenson NG, Zanne AE (2009) Towards a worldwide wood economics spectrum. Ecology Letters 12(4):351-366.

Chen R, Twilley RR (1999) Patterns of mangrove forest structure and soil nutrient dynamics along the Shark River estuary, Florida. Estuaries 22(4):955-970.

Clawges R, Vierling L, Calhoon M, Toomey M (2007) Use of a ground-based scanning lidar for estimation of biophysical properties of western larch (Larix occidentalis). International Journal of Remote Sensing 28(19):4331-4344.

Cloude S, Papathanassiou K (2003) Three-stage inversion process for polarimetric SAR interferometry. IEE Proceedings-Radar, Sonar and Navigation 150(3):125-134.

Cloude SR, Papathanassiou KP (1998) Polarimetric SAR interferometry. Geoscience and Remote Sensing, IEEE Transactions on 36(5):1551-1565.

Clough BF (1992). Primary productivity and growth of mangrove forests, Tropical mangrove ecosystems. Coastal and Estuarine Studies. AGU Washington, DC, pp 225-249.

Clough BF, Dixon P, Dalhaus O (1997) Allometric relationships for estimating biomass in multi-stemmed mangrove trees. Australian Journal of Botany 45(6):1023-1031.

Coronado-Molina C, Day JW, Reyes E, Perez BC (2004) Standing crop and aboveground biomass partitioning of a dwarf mangrove forest in Taylor River Slough, Florida. Wetlands Ecology and Management 12(3):157-164.

Davies J, Claridge G, Bureau AW (1993) Wetland benefits: the potential for wetlands to support and maintain development. Asian Wetland Bureau.

DeCoster JK, Platt WJ, Riley SA (1999) Pine Savannas of Everglades National Park³ An Endangered Ecosystem.

Deisler J (1982) Florida tree snail. Pritchard, PCH Rare and Endangered Biota of Florida: Invertebrates 6:15-18.

Dixon TH, Amelung F, Ferretti A, Novali F, Rocca F, Dokka R, Sella G, Kim S-W, Wdowinski S, Whitman D (2006) Space geodesy: Subsidence and flooding in New Orleans. Nature 441(7093):587-588.

Donato DC, Kauffman JB, Murdiyarso D, Kurnianto S, Stidham M, Kanninen M (2011) Mangroves among the most carbon-rich forests in the tropics. Nature Geoscience 4(5):293-297.

Doren RF, Platt WJ, Whiteaker LD (1993) Density and size structure of slash pine stands in the everglades region of south Florida. Forest Ecology and Management 59(3):295-311.

Erwin KL (2009) Wetlands and global climate change: the role of wetland restoration in a changing world. Wetlands Ecology and Management 17(1):71-84.

Fatoyinbo TE, Simard M, Washington-Allen RA, Shugart HH (2008) Landscape-scale extent, height, biomass, and carbon estimation of Mozambique's mangrove forests with Landsat ETM+ and Shuttle Radar Topography Mission elevation data. Journal of Geophysical Research-Biogeosciences 113(G2).

FCE-LTER (2013) Florida Coastal Everglades - Long Term Ecological Research. Last accessed: January 2014. From: http://fce.lternet.edu

Feliciano E, Wdowinski S, Potts M (2014) Assessing mangrove above-ground biomass and structure using Terrestrial Laser Scanning: a case study in the Everglades National Park. Wetlands:1-14. doi: 10.1007/s13157-014-0558-6.

Ferretti A, Prati C, Rocca F (1999) Multibaseline InSAR DEM reconstruction: The wavelet approach. Geoscience and Remote Sensing, IEEE Transactions on 37(2):705-715.

Fröhlich C, Mettenleiter M (2004) Terrestrial laser scanning–new perspectives in 3D surveying. International archives of photogrammetry, remote sensing and spatial information sciences 36(Part 8):W2.

Fromard F, Puig H, Mougin E, Marty G, Betoulle JL, Cadamuro L (1998) Structure, above-ground biomass and dynamics of mangrove ecosystems: new data from French Guiana. Oecologia 115(1-2):39-53.

Gibbs JP (2000) Wetland loss and biodiversity conservation. Conservation Biology 14(1):314-317.

Giri C, Ochieng E, Tieszen LL, Zhu Z, Singh A, Loveland T, Masek J, Duke N (2011) Status and distribution of mangrove forests of the world using earth observation satellite data. Global Ecology and Biogeography 20(1):154-159.

Gong WK, Ong JE (1990) Plant biomass and nutrient flux in a managed mangrove forest in Malaysia. Estuarine Coastal and Shelf Science 31(5):519-530.

Hajnsek I, Kugler F, Lee S-K, Papathanassiou KP (2009) Tropical-forest-parameter estimation by means of Pol-InSAR: The INDREX-II campaign. Geoscience and Remote Sensing, IEEE Transactions on 47(2):481-493.

Hajnsek I, Papathanassiou K, Cloude S, 2001. Removal of additive noise in polarimetric eigenvalue processing, Geoscience and Remote Sensing Symposium, 2001. IGARSS'01. IEEE 2001 International. IEEE, pp. 2778-2780.

Hopkinson C, Chasmer L, Young-Pow C, Treitz P (2004) Assessing forest metrics with a ground-based scanning lidar. Canadian Journal of Forest Research 34(3):573-583.

Houle P, Zhang K, Ross MS, Simard M, 2006. Use of airborne lidar for the assessment of landscape structure in the pine forests of Everglades national park, Geoscience and Remote Sensing Symposium, 2006. IGARSS 2006. IEEE International Conference on. IEEE, pp. 1960-1963.

Husch B, Beers TW, Kershaw Jr JA (2002) Forest mensuration. Wiley.

Hyyppä J, Hyyppä H, Litkey P, Yu X, Haggrén H, Rönnholm P, Pyysalo U, Pitkänen J, Maltamo M (2004) Algorithms and methods of airborne laser scanning for forest measurements. International Archives of Photogrammetry, Remote Sensing and Spatial Information Sciences 36(8/W2):82-89.

Imbert D, Rollet B (1989) Phytmassaerienne et production primaire dans la mangrove du Grand Cul-de-sac Marine (Guadeloupe, Antilles francaises). Bulletin D Ecologie 20:27-39.

Jacobsen K (2003) DEM generation from satellite data. EARSeL Ghent:273-276.

Jennerjahn TC, Ittekkot V (2002) Relevance of mangroves for the production and deposition of organic matter along tropical continental margins. Naturwissenschaften 89(1):23-30.

Kauffman JB, Heider C, Cole TG, Dwire KA, Donato DC (2011) Ecosystem carbon stocks of Micronesian mangrove forests. Wetlands 31(2):343-352.

Kellndorfer J, Walker W, Pierce L, Dobson C, Fites JA, Hunsaker C, Vona J, Clutter M (2004) Vegetation height estimation from shuttle radar topography mission and national elevation datasets. Remote Sensing of Environment 93(3):339-358.

Ketterings QM, Coe R, van Noordwijk M, Ambagau' Y, Palm CA (2001) Reducing uncertainty in the use of allometric biomass equations for predicting above-ground tree biomass in mixed secondary forests. Forest Ecology and Management 146(1–3):199-209.

Komiyama A, Ong JE, Poungparn S (2008) Allometry, biomass, and productivity of mangrove forests: A review. Aquatic Botany 89(2):128-137.

Komiyama A, Poungparn S, Kato S (2005) Common allometric equations for estimating the tree weight of mangroves. Journal of Tropical Ecology 21:471-477.

Krieger G, Moreira A, Fiedler H, Hajnsek I, Werner M, Younis M, Zink M (2007) TanDEM-X: A satellite formation for high-resolution SAR interferometry. Geoscience and Remote Sensing, IEEE Transactions on 45(11):3317-3341.

Kugler F, Schulze D, Hajnsek I, Pretzsch H, Papathanassiou KP (2013) TanDEM-X Pol-InSAR performance for forest height estimation.

Lefsky MA, Harding DJ, Keller M, Cohen WB, Carabajal CC, Espirito-Santo FDB, Hunter MO, de Oliveira Jr R (2005) Estimates of forest canopy height and aboveground biomass using ICESat. Geophysical Research Letters 32(22):L22S02.

Leica (2013) Cyclone 3D Point Cloud Processing Software. Last accessed: July 2013. From: http://hds.leica-geosystems.com/en/Leica-Cyclone_6515.htm

Liang XL, Litkey P, Hyyppa J, Kaartinen H, Vastaranta M, Holopainen M (2012) Automatic stem mapping using single-scan terrestrial laser scanning. IEEE Transactions on Geoscience and Remote Sensing 50(2):661-670.

Lodge TE (2010) The Everglades Handbook: Understanding the Ecosystem. Taylor and Francis Group.

Lugo AE, Snedaker SC (1974) The ecology of mangroves. Annual Review of Ecology and Systematics 5(1):39-64.

Maas H-G, Bienert A, Scheller S, Keane E (2008) Automatic forest inventory parameter determination from terrestrial laser scanner data. International Journal of Remote Sensing 29(5):1579-1593.

Mcleod E, Chmura GL, Bouillon S, Salm R, Björk M, Duarte CM, Lovelock CE, Schlesinger WH, Silliman BR (2011) A blueprint for blue carbon: toward an improved understanding of the role of vegetated coastal habitats in sequestering CO2. Frontiers in Ecology and the Environment 9(10):552-560.

Mitchell AH (2001) Wise use of wetlands, the Ramsar Convention on wetlands, and the need for an Asian Regional Wetlands Training Initiative. Aquatic Ecosystem Health & Management 4(3):235-242.

Mitsch WJ, Bernal B, Nahlik AM, Mander Ü, Zhang L, Anderson CJ, Jørgensen SE, Brix H (2013) Wetlands, carbon, and climate change. Landscape Ecology 28(4):583-597.

Mitsch WJ, Gosselink JG, 2007. Wetlands. Hoboken. NJ: Wiley.

O'Hare NK, Dalrymple GH (2006) Growth and survival of South Florida slash pine (Pinus elliottii var. densa) on restored farmlands in Everglades National Park. Ecological Restoration 24(4):242-249.

Papathanassiou K, Cloude SR, 2003. The effect of temporal decorrelation on the inversion of forest parameters from PoI-InSAR data, International Geoscience and Remote Sensing Symposium, pp. III: 1429-1431.

Papathanassiou KP, Cloude SR (2001) Single-baseline polarimetric SAR interferometry. Geoscience and Remote Sensing, IEEE Transactions on 39(11):2352-2363.

Rivera-Monroy VH, Castañeda-Moya E, Barr JG, Engel V, Fuentes JD, Troxler TG, Twilley RR, Bouillon S, Smith TJ, O'Halloran TL (2013) Current methods to evaluate net primary production and carbon budgets in mangrove forests. Methods in Biogeochemistry of Wetlands(methodsinbiogeo):243-288.

Rivera-Monroy VH, de Mutsert K, Twilley RR, Castaneda-Moya E, Romigh MM, Davis SE (2007) Patterns of nutrient exchange in a riverine mangrove forest in the Shark River Estuary, Florida, USA. Hidrobiologica 17(2):169-178.

Ross M, Ruiz P, Telesnicki G, Meeder J (2001) Estimating above-ground biomass and production in mangrove communities of Biscayne National Park, Florida (U.S.A.). Wetlands Ecology and Management 9(1):27-37.

Sadeghi Y, St-Onge B, Leblon B, Simard M, Papathanassiou K, 2014. Mapping forest canopy height using TanDEM-X DSM and airborne LiDAR DTM, Geoscience and Remote Sensing Symposium (IGARSS), 2014 IEEE International. IEEE, pp. 76-79.

Saenger P (1982). Morphological, anatomical and reproductive adaptations of Australian mangroves. In: B.F. Clough, Mangroves ecosystems in Australia. Australia National University Press, Canberra pp 153 - 191.

Saenger P (2003) Mangrove ecology, silviculture and conservation. Springer SBM.

Saenger P, Snedaker SC (1993) Pantropical trends in mangrove above-ground biomass and annual litterfall. Oecologia 96(3):293-299.

Sánchez BG, (2005). Belowground productivity of mangrove forests in southwest Florida, Faculty of Louisiana State University and Agricultural and Mechanical College in partial fulfillment of the requirements for the degree of Doctor of Philosophy in The Department of Oceanography and Coastal Sciences by Beatriz Giraldo Sánchez BS, Universidad Del Valle.

Santoro M, Shvidenko A, McCallum I, Askne J, Schmullius C (2007) Properties of ERS-1/2 coherence in the Siberian boreal forest and implications for stem volume retrieval. Remote Sensing of Environment 106(2):154-172.

Schlesinger WH, Bernhardt ES (2013) Biogeochemistry: An analysis of global change 3th Edition. Access Online via Elsevier, 2013.

Seidel D, Beyer F, Hertel D, Fleck S, Leuschner C (2011) 3D-laser scanning: A non-destructive method for studying above- ground biomass and growth of juvenile trees. Agricultural and Forest Meteorology 151(10):1305-1311.

Simard M, Zhang K, Rivera-Monroy VH, Ross MS, Ruiz PL, Castañeda-Moya E, Twilley RR, Rodriguez E (2006) Mapping height and biomass of mangrove forests in Everglades National Park with SRTM elevation data. Photogrammetric Engineering and Remote Sensing 72(3):299-311.

Smith TJ, III, Whelan KRT (2006) Development of allometric relations for three mangrove species in South Florida for use in the Greater Everglades Ecosystem restoration. Wetlands Ecology and Management 14(5):409-419.

Tansey K, Selmes N, Anstee A, Tate NJ, Denniss A (2009) Estimating tree and stand variables in a Corsican Pine woodland from terrestrial laser scanner data. International Journal of Remote Sensing 30(19):5195-5209.

Taylor JR (1997) An introduction to error analysis: The study of uncertainties in physical measurements. University Science Books.

Treuhaft RN, Madsen SN, Moghaddam M, Zyl JJ (1996) Vegetation characteristics and underlying topography from interferometric radar. Radio Science 31(6):1449-1485.

Twilley R, Chen R, Hargis T (1992) Carbon sinks in mangroves and their implications to carbon budget of tropical coastal ecosystems. Water, Air, and Soil Pollution 64(1-2):265-288.

WAC (2013) World of Agroforestry Centre - Wood Density Database. Last accessed: July 2013. From: http://worldagroforestry.org/sea/products/afdbases/wd

Watt PJ, Donoghue DNM (2005) Measuring forest structure with terrestrial laser scanning. International Journal of Remote Sensing 26(7):1437-1446.

Wdowinski S, Kim S-W, Amelung F, Dixon TH, Miralles-Wilhelm F, Sonenshein R (2008) Space-based detection of wetlands' surface water level changes from L-band SAR interferometry. Remote Sensing of Environment 112(3):681-696.

Welch R, Madden M (1999) Vegetation map and digital database of south Florida's National Park Service lands. Final Report to the US Department of the Interior, National Park Service, Cooperative Agreement Number 5280–4 9006.

Welch R, Madden M, Doren RF (1999) Mapping the everglades. Photogrammetric Engineering and Remote Sensing 65(2):163-170.

White JF, Gould SJ (1965) Interpretation of the coefficient in the allometric equation. American Naturalist 99(904):5-18.

Zanne AE, Lopez-Gonzalez G, Coomes DA, Ilic J, Jansen S, Lewis SL, Miller RB, Swenson NG, Wiemann MC, Chave J, 2009. Data from: Towards a worldwide wood economics spectrum. Dryad Data Repository.